M-PM-Sym-1

STRUCTURE AND FUNCTION OF SMALL ICOSAHEDRAL RNA AND DNA VIRUSES. Jun Tsao, Michael S. Chapman, Mavis Agbandje, Walter Keller, Hao Wu and Michael G. Rossmann

Structural studies of picornaviruses have shown that in general: (1) the different viral capsid proteins are based on a unique eight-stranded antiparallel folding motif; (2) they possess a depression ("canyon") which is the binding site of the host cell receptor; (3) they possess surface protrusions which are the site of epitopes where neutralizing antibodies can bind; and (4) in some cases there is a pocket within one of the viral capsid proteins which may be a functional necessity for assembly and uncoating. This pocket can bind certain antiviral agents which can inhibit both attachment and uncoating.

We have recently solved the structure of canine parvovirus (CPV), a ssDNA virus. This has many of the features found also in picornaviruses. Infectious virions contain 60 proteins that are VP2 and VP3 with some copies of VP1, while empty capsids contain primarily VP2 (the precursor of VP3) and VP1. Electron density along the fivefold axes shows that some of the amino termini run to the exterior, consistent with the observation that some VP2's in full particles can be cleaved by trypsin. The fivefold axes are surrounded by an unusual cylindrical structure formed by five β-ribbons. The central structural motif of VP2 has the same topology as found in other icosahedral RNA viruses. There is a 22 Å long spike on the threefold axes, a 15 Å deep canyon circulating about each of the five cylindrical structures at the fivefold axes and a 15 Å deep depression at the twofold axes on the viral surface. By analogy, the canyon may be the site of receptor attachment. Residues related to the antigenic properties of the virus are on the threefold spikes. A substantial volume of electron density is shown to correspond to at least 10 DNA nucleotides or (taking account of the icosahedral symmetry imposed on the nucleic acid) about 12% of the total genome.

M-PM-Sym-2

PATHWAY OF ICOSAHEDRAL CAPSID ASSEMBLY
Peter Prevelige & Jonathan King, Dept of Biol., MIT (Supported by NIH GM17,980)

The product of coat subunit polymerization for many DNA viruses is not the mature capsid, but a procapsid precursor shell composed of a shell of coat protein with an internal core of scaffolding protein. In DNA phage the viral-genome is packaged into the procapsid, with concomitant removal of the scaffolding protein.

In contrast to TMV, the pathway of subunit polymerization for spherical viruses is ill-defined, but presumably includes initiation, elongation, and termination stages. The gene 5 coat and gene 8 scaffolding subunits of the icosahedral Salmonella phage P22 can be assembled into procapsids in vitro, exhibiting the regulated polymerization observed in vivo. The predominant state of scaffolding subunits alone is elongated 2.5s monomers; in the absence of scaffolding subunits coat subunits remain as 3.2s monomers. Addition of scaffolding subunits results in mutual subunit activation and copolymerization into closed double shells with a $t_{1/2}$ of 5min at 20°C (1mg/ml). The reaction kinetics suggest rate-limiting formation of an initiation complex, followed by a rapid shell growth phase. Addition of small numbers of the gene 16 pilot protein increases the rate of assembly, probably by binding to the initiation complex. Growing shell intermediates have been identified by electron microscopy, indicating that growth proceeds by the sequential addition of subunits or small oligomers to the edge of the growing structure. The formation of closed shells from similar subunits requires that the same polypeptide chain adopt different conformations at appropriate locations in the lattice. Activation of subunits for assembly, and position dependent conformational switching may be coupled, both occurring at the active growing edge.

M-PM-Sym-3

CRYSTALLOGRAPHY OF INTACT RIBOSOMAL PARTICLES
A. Yonath, Z. Berkovitch-Yellin W.S. Bennett, H.A.S. Hansen, U. Evers, S. Weinstein & F. Franceschi; Weizmann Inst., Rehovot, Israel, Max-Planck-Research-Unit, Hamburg & Max-Planck-Inst. for Mol. Genetics, Berlin.

Diffracting crystals have been grown from active bacterial ribosomal particles. Crystallographic data are currently being collected with synchrotron radiation at cryo-temperature from the following systems: whole 70S ribosomes; intact 30S and 50S subunits; 50S subunits of mutated bacteria; chemically modified 50S subunits with multi-metal-clusters and complexes, mimicking distinct funtional states, of ribosomal particles together with components of protein biosynthesis: tRNA and short nascent protein chains. These crystals diffract to various resolution limits, at best to 4.5Å, and X-ray crystallographic data have been collected using intense synchrotron radiation, at cryo-temperature. Monofunctional reagents have been prepared from dense heavy-atom-clusters. These proved to be useful for phasing of the crystallographic data. The mode of binding of these clusters to the ribosomal particles and to components or inhibitors of protein biosynthesis will be discussed. Models have been reconstructed at 30 and 47Å from two-dimensional sheets of 50S and 70S particles. These show the overall shape of the ribosome as well as the separation between the two subunits; a void which may be the location of the process of protein biosynthesis; a possible binding site for m-RNA and t-RNA and a tunnel which may be the exit path of the nascent protein chain. These models were used for low-resolution phasing of the X-ray crystallographic data, and found to correlate well with density maps, obtained from low resolution neutron-diffraction data, phased by direct methods.

M-PM-Sym-4

THE ROLE OF RIBOSOMAL RNA IN THE STRUCTURE AND FUNCTION OF THE RIBOSOME. James Ofengand, Philip R. Cunningham, Paul Popieniek, Carl Weitzmann, and Kelvin Nurse. Roche Institute of Molecular Biology, Nutley, NJ 07110, USA.

Ribosomes of all species consist of two unequally sized subunits, each containing a single large RNA molecule, numerous proteins, and in the larger subunit of many species, two small RNAs. The large RNAs (in *E. coli*, 16S and 23S), originally thought to be merely a scaffold upon which the functionally active ribosomal proteins were arranged, are now believed to play an active and perhaps even a major role in ribosome function. In this regard, the existence of long sequence-conserved segments (LSCS) in ribosomal RNAs is particularly interesting. Several LSCS occur in 16S RNA, one of which was shown by us in earlier studies to be at the ribosomal decoding site. The significance of these LSCS has been probed by making single site mutants in the LSCS and studying the function of the mutant ribosomes so created. This was done by site-specific mutation of the ribosomal RNA gene, *in vitro* transcription, *in vitro* reconstitution of the RNA into 30S ribosomes, and *in vitro* analysis of the ability of the mutant ribosomes to carry out specific partial reactions of the ribosomal protein synthesis cycle. Nucleotide substitutions of conserved residues induced four classes of effects on ribosomal activity. Some had little or no effect, some caused a partial loss of activity in all the assays, some were "killer" substitutions and inactivated all ribosomal functions, and others specifically inactivated certain activities. The existence of a functionally important tertiary base pair connecting two of the LSCS was also detected by these studies.

M-PM-A1

INVESTIGATION OF A D-HELIX SYMMETRIZED REACTION CENTER MUTANT OF *RHODOBACTER CAPSULATUS*. Jonathan W. Stocker, Steven G. Boxer. Department of Chemistry, Stanford University, Stanford, CA 94305. Neal W. Woodbury, Aileen K. Taguchi. Department of Chemistry, Arizona State Univeristy, Tempe, AZ 85287-1604.

A *Rhodobacter capsulatus* RC mutant in which residues M187 through M203 have been replaced by a homologous region of the L subunit (L160 through L176) was constructed, expressed, and shown to grow photosynthetically. This construction was specifically chosen in order to produce an RC in which the protein environment in the vicinity of the special pair (SP) is considerably more symmetric than that in the wild-type. The mutant shows interesting spectroscopic, kinetic, and redox characteristics. The SP of this mutant has a broader Q_y absorption band than that of wild-type and shows evidence of a shoulder at 1.5K. The minimum of the Stark effect for this band is red-shifted by 200 cm^{-1} relative to the absorption maximum. This suggests that there is more than one band present in the 880 nm to 830 nm region. The oxidation potential of the mutant SP increases by over 100 mV as compared to that of wild-type. Delayed fluorescence measurements confirm that the ΔG for the initial charge separation is reduced to only about 60 mV. The initial electron transfer rate has been measured as $k = (11\ ps)^{-1}$ compared to $(3\ ps)^{-1}$ for wild-type at room temperature. At the present time, there is no evidence in the Q_x region of the spectrum for electron transfer occurring down the M-side. At room temperature, the $P^+Q_A^-$ quantum yield is about 85% for the mutant and the $P^+Q_A^-$ recombination rate is measured as $(140\ ms)^{-1}$. The P^+ EPR linewidth is found to be greater than that of wild-type but smaller than that of the heterodimer (MH200L) mutant [1]. Pigment extraction assays indicate a ratio of 4 BChl: 2 BPheo for this RC. Interestingly, it appears symmeterization of the protein around the SP gives an RC which has several characteristics similar to those of the heterodimer RC [1]. These observations suggest that the modified characteristics of this RC may arise not only from direct interactions between the chromophores and the altered residues, but also from a structural change in the RC which perturbs the geometery of the special pair.

[1] Bylina, E.J. *et.al.*, P.N.A.S., 85, 7726-7230 (1988)

M-PM-A2

TIME-DEPENDENT SPECTRA AS A TOOL FOR THE ANALYSIS OF $P^+Q_A^-$ CHARGE RECOMBINATION IN BACTERIAL REACTION CENTERS Stefan Franzen and Steven Boxer Department of Chemistry, Stanford University, Stanford CA 94305

Spectra of the $P^+Q_A^-$ charge recombination reaction in Rb. sphaeroides RCs in 50% glycerol buffer solution as a function of time were obtained at 280 K and 77 K. The regions of the spectrum investigated were 400-460 nm and 700-960 nm. The data analysis employed singular value decomposition (SVD) followed by global fitting of the basis time courses obtained from SVD. This method allows one to distinguish between sequential and parallel models for multi-exponential processes. The decays were found to be biexponential at both temperatures, and no evidence was found for conformational changes on the time scale of the reaction. A parallel model in which there are two populations of RCs is consistent with the data. At 77 K, this is in agreement with previous reports, while at 280 K the $P^+Q_A^-$ recombination reaction is usually taken to be a single exponential ($k = 10\ s^{-1}$). The improved signal-to-noise ratio obtained by the SVD and global fitting procedure reveals that at 280 K there are two components which have quite similar rate constants ($k_1 = 6\ s^{-1}$ and $k_2 = 13\ s^{-1}$). It has been observed that RCs frozen in the presence of a saturating light have three times slower kinetics than RCs frozen in the dark [1]. The spectral changes are nearly identical for RCs frozen in the light and dark. Time dependent spectra for RCs frozen in the light are also well fit by a model in which there are two populations of RCs where the two rates are slower than for RCs frozen in the dark, but the amplitudes are the same. Analysis of the spectra suggests that the effect on the recombination reaction of freezing RCs in the light is to change the energetics but not necessarily the distance of electron transfer. This analysis is quite different from that in [1] and stresses that solvation of the $P^+Q_A^-$ dipole is an important factor in the differences between the two populations and between RCs frozen in the light and the dark. Data will also be reported for a number of Rb. capsulatus and Rb. sphaeroides mutants. These provide further evidence for two populations of RCs and for superexchange mediation of the recombination reaction.

1. Kleinfeld et al. Biochemistry 1984, 23, 5780

M-PM-A3

ENERGY TRANSFER AND CHARGE SEPARATION KINETICS IN THE REACTION CENTER OF *Chloroflexus aurantiacus* STUDIED BY PICOSECOND TIME--RESOLVED FLUORESCENCE SPECTROSCOPY

Alfred R. Holzwarth, Marc G. Müller and Kai Griebenow
Max-Planck-Institut für Strahlenchemie,
Stiftstraße 34 - 36, D-4330 Mülheim/Ruhr, F.R.G.

The kinetics of the primary processes in the reaction centers of Chloroflexus aurantiacus has been studied by time-resolved fluorescence spectra with picosecond resolution. We find lifetimes of $\tau_1 \sim 3$ ps, $\tau_2 = 12 - 15$ ps and $\tau_3 = 150 - 300$ ps in global target analysis at 50°C. At r.t. the τ_2-component is in the range 19 - 22 ps. The time-resolved fluorescence spectra provide clear evidence for an energy transfer process occuring with the τ_1-lifetime of ~ 3 ps most probably from the primarily excited accessory BChl a to the special pair P866. The species-associated emission spectra of the two excited states are presented. The τ_2-lifetime is attributed to charge separation while the τ_3-component reflects the electron stabilization on Q_A. We have also determined the free energy difference between P^* and the primary radical pair state to be $\Delta G = -170 \pm 25$ meV. No evidence was found for a significant heterogeneity in the electron transfer rates. The possible consequences of this data, in particular for the interpretation of the corresponding processes in purple bacterial reaction centers are discussed.

M-PM-A4

BLEACHING OF THE BACTERIOCHLOROPHYLL MONOMER BAND: CAN ABSORPTION KINETICS DISTINGUISH VIRTUAL FROM TWO-STEP ELECTRON TRANSFER IN BACTERIAL PHOTOSYNTHESIS?, Julian S. Joseph, William Bruno, and William Bialek, Departments of Physics and Molecular and Cell Biology, University of California at Berkeley, 94720.

The significance of absorption kinetics data in distinguishing between two-step and virtual mechanisms for the primary charge separation in reaction centers of photosynthetic bacteria is examined. A simple class of models is presented in which the transfer may occur predominantly by a virtual process, and in which the intermediate state develops some small, but non-zero, transient population. The simplicity of the model allows both the virtual and two-step contributions to the intermediate state population to be easily calculated. The behavior in various regimes is discussed. We find that the peak intermediate state population can be either close to 1 or very small (< 0.01), depending on the system parameters such as electronic matrix elements, the energy denominator, and the lifetimes and dephasing rates in the electronic states. These calculations imply that observation of a small amount of bleaching in the bacteriochlorophyll monomer band does not necessarily rule out a virtual transfer process.

This work was funded by the Regents of the University of California, the Department of Education, the National Science Foundation, Cray Research Inc., Sun Microsystems, and the NEC Research Institute.

M-PM-A5

FTIR SPECTROSCOPY OF THE HIS^{M200} → LEU HETERODIMER MUTANT OF *RB. CAPSULATUS*.

J. Breton[1], E.J. Bylina[2], S.J. Robles[3], D.C. Youvan[3] & E. Nabedryk[1],
[1]DBCM, C.E.N. Saclay, 91191 Gif-sur-Yvette Cedex, France.
[2]Pacific Biomedical Research Center, University of Hawaii at Manoa, Honolulu, HI 96822. [3]Department of Chemistry, M.I.T., Cambridge, MA 02139.

Light-induced FTIR difference spectroscopy has been performed on chromatophores from *Rb. capsulatus* wild type (WT) and the genetically-modified system His^{M200} → Leu in which the primary donor P consists of a BChl-BPh heterodimer. Large differences are found between light-induced FTIR P+Q-/PQ spectra of WT (a) and mutant (b) at 275K as well as at 100K. The most striking of these is the sharpening and upshift of a negative band at 1696 cm^{-1} in the mutant. In WT, the corresponding 1682 cm^{-1} signal is larger and most probably results from the overlap of the 9keto C=O of each $BChl_L$ and $BChl_M$ of P. These data imply that the 9keto of $BChl_L$ is free from interactions with the protein, at least in the heterodimer. Furthermore, the positive signals in the heterodimer at 1545 cm^{-1}, 1525 cm^{-1} and 1504 cm^{-1} closely correspond to those observed for C-C vibrations of the BChl *a* cation generated electrochemically *in vitro*. Thus, these FTIR spectra suggest, in agreement with recent EPR data, that the cation state of P is localized on a monomeric BChl in the heterodimer. In contrast, the large positive signals observed in WT at ≈1300 cm^{-1} and in part at 1480-1430 cm^{-1} and 1580-1530 cm^{-1}, appear characteristic for a BChl dimer state of P+. In both WT and mutant, a comparable absorption change at 1751 cm^{-1} is observed and is assigned to the 10a ester C=O of $BChl_L$ in P+. The positive signals at 1478 cm^{-1} and 1460 cm^{-1}, as well as the negative one at 1264 cm^{-1}, are characteristic for the semiquinone anion formation in both WT and mutant.

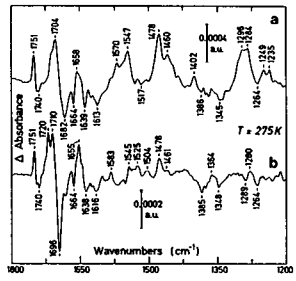

M-PM-A6

HEME PHOTOREDUCTION IN SPINACH CYTOCHROME b6f COMPLEXES STUDIED BY RESONANCE RAMAN SPECTROSCOPY

J. D. Hobbs [1], D. J. Nunez [1], R. M. Wynn [2], R. Malkin [2] and M. R. Ondrias [1].
1. University of New Mexico, Department of Chemistry, Albuquerque, NM 87131.
2. Division of Molecular Plant Biology, University of California at Berkeley, Berkeley, CA 94720.

We have investigated laser-induced photoreduction occuring in the spinach cytochrome b_6f complex and the isolated turnip cytochrome f using transient and time-resolved resonance Raman spectroscopy. The transient photoreduction behavior of these proteins suggest that heme reduction occurs within the laser pulse-width and is both power and wavelength dependent. In the presence of ferricyanide, heme photoreduction is reversible; however, in the absence of ferricyanide the higher potential heme of the b_6f complex remains reduced. Further, when cytochrome f of the complex is reduced using sodium ascorbate, no additional photoreduction is observed. Time-resolved resonance Raman experiments indicate that the rapidly photoreduced cytochrome f is reoxidized within 1.2 us of the laser-initiated reduction. These results will be addressed in terms of electronic and structural properties of heme proteins. This work is supported by the NIH (GM33300 to MRO).

M-PM-A7

SPIN-POLARIZED RADICAL ION PAIRS IN PHOTOSYNTHETIC MODEL SYSTEMS. A NEW STRUCTURAL PROBE OF PS I AND PS II REACTION CENTERS.

M. R. Wasielewski* and G. L. Gaines, III, Chemistry Division* and Biological and Medical Research Division, Argonne National Laboratory, Argonne, IL 60439

Photoinduced, multi-step charge separation in bacterial photosynthetic reaction centers proceeds from the lowest excited singlet state of the dimeric bacteriochlorophyll electron donor in two steps to yield a weakly interacting dimer cation - quinone anion radical pair, P^+-Q^-, separated by 28 Å. The chromophores within the reaction center are positioned at precise distances and orientations to insure that the electronic coupling between P^+ and Q^- is sufficiently weak to allow P^+-Q^- to live for about 100 ms. At long distances the electron-electron exchange interaction, *J*, between radicals within a charge separated ion pair is sufficiently weak that differences in local magnetic fields surrounding each radical result in S-T_0 mixing of the radical pair spin sublevels This mixing produces a non-Boltzmann population of the spin sublevels of the radical pair and may result in the appearance of spin-polarized EPR spectra. Such spectra have been reported extensively for both bacterial and green plant reaction centers, but have not been observed previously in rigid model systems. We have synthesized several molecules, which undergo two-step, sequential charge separation at 5 K to yield stable radical ion pairs which possess overall 16-25 Å center-to-center distances, a variety of fixed donor-acceptor orientations, *lifetimes in the ms range*, and *spin-polarization* as indicated by EPR. Since both the distance and orientation of the two radicals within the pair are known, the spin-polarized EPR spectra can be modeled using reasonable values for the exchange and dipolar interactions, in addition to the anisotropic *g*-tensors of the radicals. Thus, spin-polarized EPR spectra can be used to predict unknown structures with increased confidence based on successful predictions with model systems of known structure. These results can be used to predict structural features of both PS I and PSII reaction centers.

(This work was supported by the Division of Chemical Sciences, Office of Basic Energy Sciences of the Dept. of Energy under contract W-31-109-Eng-38.)

M-PM-A8

CAROTENOID ELECTRONIC STATE DYNAMICS AND PHOTOSYNTHETIC CAROTENOID-TO-CHLOROPHYLL ENERGY TRANSFER

A.P. Shreve*, J.K. Trautman*, T.G. Owens# and A.C. Albrecht*;
*Department of Chemistry and #Section of Plant Biology, Cornell University, Ithaca, NY 14853

Femtosecond time-resolved experiments of *in vitro* and *in vivo* carotenoid excited state dynamics and measurements of the quantum yields for carotenoid emission have been used to determine the S_2 (B-state) lifetime for some carotenoids of photosynthetic importance. Both types of measurements give an S_2 lifetime for β-carotene of ≈ 200 fsec. No evidence of emission from S_1 (A-state), with its 10 psec lifetime, is observed from β-carotene. In contrast, fucoxanthin (the major light-harvesting carotenoid in brown algae) has a somewhat shorter S_2 lifetime of about 100 fsec, and in addition to the S_2 emission, a relatively strong S_1 emission is observed. From the directly measured S_1 lifetime of 40 psec and the S_1 emission yield of 8 x 10^{-4}, the integrated oscillator strength for the $S_1 \rightarrow S_0$ transition in fucoxanthin is found to be a few percent of the strongly allowed $S_0 \rightarrow S_2$ transition. These results, together with previous time-resolved measurements of *in vivo* carotenoid-to-chlorophyll energy transfer times, are used to propose that Coulombic (transition dipole) coupling, from either the carotenoid B-state or, in some cases, the A-state, is important as a mechanism of carotenoid-to-chlorophyll singlet energy transfer.

M-PM-A9

ENERGY TRANSFER PROCESSES IN ALLOPHYCOCYANIN.

Warren F. Beck and Kenneth Sauer, Department of Chemistry and Chemical Biodynamics Division, Lawrence Berkeley Laboratory, University of California, Berkeley, California 94720.

Allophycocyanin is a light-harvesting protein that is found in the core of the phycobilisome in cyanobacteria. It directs excitation energy received from *C*-phycocyanin towards the photosystem II reaction center. As it is found in the phycobilisome, allophycocyanin is organized as a ring-like homotrimer; each monomeric subunit is composed of an α and a β subunit, each of which binds a single phycocyanobilin chromophore via a thioether linkage to a cysteine residue at amino acid position 84. Interactions between the chromophores in adjacent monomers are thought to lead to a large bathochromic shift of the electronic absorption spectrum upon aggregation of monomers into trimers. We have characterized the energy transfer paths in allophycocyanin with a one- or two-color picosecond transient absorption/linear dichroism spectrometer. Allophycocyanin monomers exhibit a long-distance $\alpha 84 \leftrightarrow \beta 84$ energy-transfer path; the $\alpha 84$ and $\beta 84$ chromophores behave as inequivalent chromophores. Allophycocyanin trimers, in contrast, contain a system of three equivalent strongly-coupled chromophore dimers arranged with C_3 symmetry. The rapid (< 2 ps time constant) radiationless transition from the upper to the lower exciton state of the intersubunit $\alpha 84$–$\beta 84$ chromophore dimer occurs with a polarization change that is consistent with a transition between two orthogonal electronic states. Thus, excitation energy is rapidly trapped in the lower exciton state of allophycocyanin following excitation of the upper exciton state. This behavior suggests that dimers of chromophores in light-harvesting proteins can act as excitation traps by virtue of radiationless transitions between exciton states. [Supported by the Director, Office of Energy Research, Division of Energy Biosciences, of the U.S. Department of Energy (contract DE-AC03-76SF-00098). W.F.B. is the recipient of a postdoctoral fellowship from the Miller Institute for Basic Research in Science (University of California, Berkeley).]

M-PM-B1

SITE-DIRECTED MUTAGENESIS ALTERS AGONIST SENSITIVITY OF THE NICOTINIC ACETYLCHOLINE RECEPTOR. Gordon F. Tomaselli, James T. McLaughlin, Mark Jurman, Edward Hawrot* and Gary Yellen, Howard Hughes Medical Institute and the Depts. of Neuroscience, Biophysics, and Medicine, Johns Hopkins Sch. of Med., Baltimore, MD 21205; *Molecular and Biochemical Pharmacology, Brown Univ., Providence, RI 02912.

We used site-directed mutagenesis to evaluate the importance of specific amino acids for ligand-binding and channel activation of the mouse muscle AChR. Mutations were chosen based on prior biochemical and spectroscopic data and on sequence homology.

We prepared the following mutants of the AChR α subunit and expressed them in *Xenopus* oöcytes: Y93F, H186F, P194T, Y190F, and Y198F. All mutants gave a level of expression comparable to wild-type, as judged by surface labeling with α-bungarotoxin.

Receptor affinity for agonist was evaluated by measuring the ability of ACh to compete for [^{125}I]-α-bungarotoxin binding to oöcyte membranes. Physiological function was tested by electrical recording of channel activity in outside-out patches exposed to pulses of varying agonist concentrations.

One of these mutations, Y190F, had a dramatic effect on both agonist binding and channel activation. Approximately 100-fold higher concentrations of ACh were required to compete for α-bungarotoxin binding to this mutant. Similarly, the ACh concentration required for half-maximal channel activation was increased by several orders of magnitude: no channel activation was seen at 10μM (which gives nearly maximal activation of wild-type); substantial activation occurs in the range 0.1-10mM ACh. The single-channel conductance of the mutant was unaltered.

Affinity labeling studies have also implicated the tyrosines at positions 93 and 198 in agonist binding, but changing these residues to phenylalanine produces only modest alterations in receptor function.

M-PM-B2

A PHENOTYPIC SELECTION STRATEGY FOR MUTATIONS AT THE LIGAND BINDING SITE OF THE NICOTINIC ACETYLCHOLINE RECEPTOR. Mark P.E. West, Kathleen L. Choi and Gary Yellen, Howard Hughes Med. Inst., Neuroscience, and Biophysics, Johns Hopkins Sch. of Med., Balto., MD 21205.

We have expressed functional acetylcholine receptors (AChRs) in a mammalian cell line, and have identified a strategy for using this expression system to select mutants of functional interest from a large pool of random mutants.

The four subunits of the mouse muscle nicotinic AChR have been transiently expressed in 293 cells (transformed human embryonic kidney fibroblasts) using a mammalian cell expression vector with the adenovirus major late promoter. The expressed AChRs exhibit both normal ligand binding properties and normal channel function. The nicotinic neurotoxin [^{125}I]-α-bungarotoxin specifically labels transfected cells at 24h post-transfection. Outside-out patch recording from these cells shows many channels that open in response to 1-100μM ACh. Approximately 20-50% of the treated cells express functional AChRs.

We have used the same system to express a mutant AChR with a site-directed mutation (Y190F) of the α subunit. This mutation alters the affinity of the receptor for ACh as well as the sensitivity of the channel response (G.F. Tomaselli, J.T. McLaughlin, M.E. Jurman, E. Hawrot and G. Yellen, *this volume*).

Fluorescein-labeled α-bungarotoxin provides a fluorescent tag for cells expressing AChRs, and a fluorescence-activated cell sorter can be used to analyse and to sort labeled cells. A substantial fraction of cells transfected with wild-type or mutant AChR subunits are labeled by fluorescent toxin. For the wild-type AChR, this signal is almost completely abolished when 100μM ACh is used to compete for toxin binding. As expected, though, toxin binding to the Y190F mutant is virtually unaffected by this same concentration of ACh, which is below that required for activation of the mutant. Thus, the cell sorter can be used to select for other mutants that still bind toxin but have altered affinity for agonist or antagonist molecules.

M-PM-B3

MODIFICATION OF $GABA_A$ RECEPTOR DESENSITIZATION BY SUBUNIT SUBSTITUTION. R.S. Kass, T.A. Verdoorn, P.H. Seeburg, and B. Sakmann. Max-Planck-Institut fur med. Forschung and ZMBH, Heidelberg, Germany and Department of Physiology, University of Rochester, Rochester, NY.

We have investigated desensitization of $GABA_A$ receptors expressed in mammalian fibroblasts transiently transfected with cloned subunit-specific cDNA's. Functional receptor properties were measured in isolated cells using whole cell patch clamp procedures. Extracellular solutions perfusing the cells were changed rapidly (< 100 ms) using a stepper-motor-controlled pipette. Onset of desensitization was measured during exposure of cells to 20 second pulses of GABA over a concentration range of 1 to 300 μM. Recovery from desensitization was studied by applying brief (500 ms) GABA pulses (over the same concentration range) at variable times after exposing cells to conditioning pulses of GABA. We studied cells expressing β_2 and γ_2 subunits in combination with members of the α subunit family. Exchanging α_2 for α_1 slightly increased the sensitivity of the expressed receptors to GABA but had little effect on the time course or extent of receptor desensitization. In contrast, exchange of α_3 for α_1 reduced the GABA sensitivity and significantly slowed the onset of desensitization of receptors comprised of $\alpha_3\beta_2$, $\alpha_3\gamma_2$, and $\alpha_3\beta_2\gamma_2$ combinations. The voltage-dependence of desensitization of $\alpha\beta_2$ receptors was also reversed by exchanging α_3 for α_1. However, the recovery from desensitization was not significantly altered by this subunit substitution for any of the subunit combinations investigated. Our results show that slight modification of the structure of the alpha subunit of $GABA_A$ receptors has distinct effects on receptor desensitization onset without altering recovery from desensitization. Thus these data provide evidence for independent onset and recovery pathways and suggest a molecular basis for desensitization.

M-PM-B4

ION-SELECTIVITY OF MUTATED AND WILD-TYPE NICOTINIC ACh CHANNELS. B. N. Cohen, C. Labarca, N. Davidson, and H. Lester. Division of Biology, Caltech, Pasadena, CA 91125.

We investigated the effects of site-directed mutations in the MII region and changes in subunit composition on the ion-selectivity of nicotinic acetylcholine receptor-channels (nAChRs) cloned from BC3H-1 cells (mouse) and expressed in *Xenopus* oocytes. MII was defined as the 19 residue segment begining with α:M243, β:M254, γ:C252, or δ:T257 (position 1). Oocytes were injected with 2-19 ng of mRNA per subunit and ACh-induced currents were recorded 2-5 d later using a 2-electrode voltage-clamp. The permeability of the expressed nAChRs to a variety of monovalent cations relative to Na^+ was estimated from the shift in the biionic reversal of the ACh-induced current after substituting the cation of interest for Na^+. Wild-type (WT) mouse nAChRs expressed heterologously in oocytes were relatively nonselective among the monovalent metal cations, Na^+, Li^+, K^+, and Cs^+, as are nAChRs at the frog neuromuscular junction, but were significantly more permeant than frog nAChRs to a number of large organic cations. None of the mutations had a significant effect on the relative permeabilities of the monovalent metal cations except the position 2 mutant hybrid, α:T to A and δ:S to A (α:T2A and δ:S2A), which reduced the relative Cs^+ permeability by 19%. However, several mutations did have dramatic effects on the relative permeability of the nAChR to organic cations. Deletion of mRNA for the δ-subunit from the injection mixture had the most dramatic effect and reduced the relative $TRIS^+$ permeability by 86%. Delta-less channels are thought to have two γ-subunits instead of one γ- and one δ-subunit. One notable difference between γ and δ in MII is the substitution of a negatively charged glutamate at the -1 position in δ with an uncharged glutamine in γ. This difference may explain the reduction in relative $TRIS^+$ permeability. The following 3 mutant hybrids at position 2, (1) δ:S2F, (2) α:T2A and δ:S2A, and (3) α:T2A, β:G2S, and δ:S2A, also reduced the relative permeability to $TRIS^+$ by 58-67%. The relative permeability of δ:S2F to several other large organic cations was also lower than the WT. Deletion of the γ-subunit from the injection mixture, substitution of ε for γ, and mutations at other positions in MII had no significant effect on the relative permeability to $TRIS^+$. The results support the hypothesis that that MII lines the ion pore of nAChR and are consistent with models of the nAChR which suggest that position -1 is the narrowest portion of the pore. Support: NIH #NS-11756, #GM-10991, and the Muscular Dystrophy Association.

M-PM-B5

ROLE OF LIGAND-BINDING SITE TYROSINES IN THE GATING OF THE *TORPEDO* ACh RECEPTOR

Michael E. O'Leary and Michael M. White, Dept. of Pharmacology, University of Pennsylvania School of Medicine, Philadelphia, PA 19104-6084

Affinity-labelling studies from several laboratories have identified amino acids 180-210 on the α subunit as forming part of the ligand binding site of the *Torpedo californica* acetylcholine receptor (AChR). When one compares the sequence of this region with the those of homologous regions of AChRs of species ranging from *Drosophila* to humans, several amino acids are found to be conserved throughout evolution; namely tyr-190, cys-192, cys-193, tyr-198, and asp-200. We assume/hope that this conservation is a reflection of important functional roles for these residues. Tyrosine can form hydrogen bonds with both the carbonyl and quaternary nitrogen portions of ACh. We have examined the putative role of tyr-190 and tyr-198 in ACh-mediated channel opening of the *Torpedo* AChR through the use of site-directed mutagenesis and the *Xenopus* oocyte expression system. We have been unable to detect ACh-elicited currents using 1-500 μM ACh when tyr-190 is replaced by phe. However, using cell-surface [^{125}I]α-bungarotoxin binding as an alternate way of detecting receptors, AChRs are present at levels approximately 30% of wild type, suggesting that the mutation does not abolish receptor expression. Replacement of tyr-189 by phe (which is found in all mammalian AChRs at this position) has no effect on AChR gating. Functional AChRs are expressed after substitution of tyr-198 by phe, although the midpoint of the dose-response curve is shifted to the right ($K_{1/2}$=98 μM for the mutant *vs* 24 μM for the wild-type). This mutation has no effect on the Hill coefficient for ACh activation, which was 1.6-1.7 in both cases. The shift in the dose-response curve corresponds to a weakening of the ACh-AChR interaction by 0.8 kcal/mol, which is consistent with (but by no means proves) the notion that tyr-198 forms a hydrogen bond with the carbonyl moiety of ACh. Supported by NIH grants R01 NS23885 and F32 NS08880 and the Lucille P. Markey Charitable Trust.

M-PM-B6

THE PERMEABILITY OF NEURONAL NICOTINIC RECEPTOR-CHANNELS TO MONOVALENT AND DIVALENT INORGANIC CATIONS.

Thomas J. Nutter and David J. Adams. Dept. of Molecular & Cellular Pharmacology, University of Miami Sch. Med., Miami, FL.

Nicotinic acetylcholine (ACh) receptor-channels in parasympathetic cardiac neurons mediate the postsynaptic response to ACh released from the vagus nerve. Parasympathetic intracardiac neurons were dissociated from rat atria, and the whole-cell patch clamp technique was used to determine the ionic permeability of nicotinic ACh receptor-channels to monovalent and divalent inorganic cations. Relative permeabilities were determined from changes in reversal (zero current) potential upon total replacement of $[Na^+]_o$ with osmotically equivalent concentrations of the test cations. Reversal potentials were corrected for liquid junction potentials, and ionic activities were taken into account in calculation of the relative permeabilities (P_X/P_{Na}). The following values of P_X/P_{Na} were obtained for the mono- and divalent cations tested:

X	P_x/P_{Na}	X	P_x/P_{Na}
NH_4^+	2.69	Mg^{2+}	1.10
Cs^+	1.57	Sr^{2+}	0.78
K^+	1.49	Ba^{2+}	0.72
Rb^+	1.12	Mn^{2+}	0.67
Li^+	0.87	Ca^{2+}	0.65

Reference Solution: 140 mM NaCl, 1 mM $CaCl_2$, 7.7 mM Glucose, 10 mM Histidine. Intracellular Solution: 130 NaCl, 10 mM Na_4BAPTA, 2 mM Na_2ATP, 10 mM HEPES-NaOH, pH 7.2.

The neuronal nicotinic receptor-channel exhibits weak selectivity among monovalent and divalent cations. The permeability sequence for monovalent metal cations, $Cs^+ > K^+ > Rb^+ > Na^+ > Li^+$, follows Eisenman sequence IIA, indicating that the narrow region of the channel is a low field strength site. The selectivity sequence for the divalent cations, $Mg^{2+} > Sr^{2+} > Ba^{2+} > Mn^{2+} > Ca^{2+}$, coincides with increasing hydrated radius of the divalent cations. The permeability of the neuronal nicotinic receptor-channel for divalent cations is significantly higher than that determined for the ACh receptor-channel at the frog motor endplate [Adams et al. (1980) *J. Gen.Physiol.* 75, 493-510.]. This may be attributed to fewer net negative charges associated with the neuronal α and non-α (β) subunits [see Unwin, N. (1989) *Neuron* 3, 665-676.]. (Supported by NIH grant # HL35422)

M-PM-B7

AMINO ACIDS RESPONSIBLE FOR DIFFERENCES IN CONDUCTANCE BETWEEN ADULT AND FETAL FORMS OF THE ACETYLCHOLINE RECEPTOR

Villarroel, A., Herlitze, S. and Sakmann, B.
Max-Planck-Institut für medizinische Forschung, Abteilung Zellphysiologie, Jahnstr. 29, D-6900 Heidelberg, FRG

The adult form of the rat acetylcholine receptor (AChR) differs from the fetal form in one subunit. The difference between these subunits makes the adult type channel (ε-AChR channel) high conductance and fast kinetics. The fetal channel (γ-AChR channel) on the other hand has lower conductance and slower kinetics. In order to identify amino acid residues responsible for these differences, we exchanged amino acids between γ- and ε-subunits using site directed mutagenesis. Inside-out patches from *Xenopus* oocytes previously injected with RNA encoding for the four subunits of the wild type and mutant channels were performed. Mutations at cytoplasmic and extracellular ends of the M2 segment produce a change in channel conductance. The mutant εQ292K produces a decrease, and the corresponding γK293Q an increase, of single channel conductance. Similar results were found for γK268Q and εQ267K. Several other exchange mutations between γ and ε subunits show no significant differences in conductance with respect to wild type. None of the mutations performed was able to invert the gating behaviour of these two forms of AChR channel. Thus by using "natural mutations" some amino acids responsible for the difference in conductance between the fetal and adult form of AChR channel were identified.

M-PM-C1

3-D RECONSTRUCTION FROM A SINGLE OBLIQUE SECTION THROUGH A CRYSTALLINE OBJECT

K. A. Taylor and R. A. Crowther§ Dept. of Cell Biology, Duke Univ. Med. Center, Durham, NC and §MRC Molecular Biology Lab, Cambridge, UK.

Oblique section 3-D reconstruction can produce a 3-D image of a sectioned crystal from a single electron micrograph. We call the approach crystallographic serial section 3-D reconstruction (CSSR). The procedures described were developed during studies of ~15 nm transverse sections of rigor insect flight muscle and are applicable to both 2-D and 3-D crystals. Unit cell coordinates in the oblique section are obtained by peak fitting from a low pass filtered image or a correlation map. With these coordinates, an averaged strip image is obtained that samples the 3-D density along the section gradient. A variance map and signal to noise ratio calculated during the averaging of strip images are later used in deconvoluting the section thickness. Successive cells in the averaged strip image are stacked sequentially to produce the reconstruction. Resolution perpendicular to the section plane of the CSSR can be improved by deconvolution of the section thickness using a Wiener filter. Section thickness can be determined by cross correlation with the transform of a [100] projection from an image of a thick longitudinal section. The effect of finite section thickness is modelled by multiplying the thick section transform with the point spread function for the estimated section thickness. This filtered transform is cross correlated with the CSSR projected down the [100] direction. Phase residuals and vector differences are calculated and results plotted as a function of estimated section thickness. These plots show a minimum that matches the thickness observed from folds in the section. The transform of an oblique section through a 3-D crystal reveals superlattice spots that represent structure factors on upper level planes of the 3-D crystal transform modulated by the point spread function. Section thickness in this case can be determined by plotting mean phase residuals of symmetry related spots after deconvolution over a range of estimated section thicknesses. This approach requires no model data and reveals minima in agreement with thick section cross correlation. We have evaluated variations of the Wiener filter that differ in the treatment of signal to noise ratio. In one case only the phases are corrected with no amplification. In another variant, we use the ratio of the power spectrum of the variance map to that of the CSSR to set a filter level that varies with spatial frequency. This latter variant appears preferable to using a filter level based on a single value of signal to noise ratio. Supported by NIH grant GM30598.

M-PM-C2

KINETICS OF THE STRUCTURAL CHANGE IN THE MYOSIN FILAMENTS OF RELAXED PSOAS FIBRES AFTER A MILLISECOND TEMPERATURE-JUMP.

G. Rapp, M. Schrumpf & J. S. Wray, EMBL c/o DESY, Hamburg and Dept. of Biophysics, Max Planck Institute for Medical Research, Heidelberg, Germany. (Intro. by W. Mommaerts)

The crossbridge arrangement in thick filaments of relaxed psoas muscle depends markedly on temperature between 0° and 20° C, becoming more "ordered" in the warm (Wray, J. Muscle Res. Cell Motil. 8, 62 (1987), Wakabayashi et al., Adv. Exp. Biol. Med. 226, 39 (1988)) and affecting the intensities of the equatorial X-ray reflections. We have studied the kinetics of the structural change after a temperature (T)-jump using synchrotron X-ray diffraction at the X13 and X33 beamlines at EMBL. Small bundles of skinned fibres of rabbit psoas in relaxing solution were subjected to rapid T-jumps by flashing with an erbium laser while the (10) and (11) intensities were measured. The laser delivered its energy within ca. 2.5 msec., and the temperature reached remained constant within 15% for ca. 800 msec. before starting to fall back towards the bath temperature. The (10) and (11) intensities could be followed with 1 msec. time resolution by averaging over 10 flashes. The (11)/(10) intensity ratio fell after the flash with a half-time that varied considerably with the apparent value of the post-jump temperature, from about 5 msec. (for a jump from 15° to 22°C) to 50 msec. (jump from 0° to 7 °C). These rates and the dependence on post-jump temperature are consistent with the suggestion (Wray 1987) that the conversion of structurally "disordered" to "ordered" states is related to the conversion of the species M.ATP to M.ADP.Pi). There was some evidence for a slower phase (time-scale of the order of 1 sec.), consistent with the expected fall in the number of M.ADP crossbridges (Wakabayashi et al. 1988). Preliminary results suggested that in fibres in which vanadate replaced Pi in the active site the rapid phase of conversion of "disordered" to "ordered" states was even faster. This work provides further evidence that the global conformation of detached crossbridges is related to the state of the γ-phosphate in the active site of myosin.

M-PM-C3

KINETIC AND PHYSICAL CHARACTERIZATION OF A FORCE GENERATING STEP IN MUSCLE: A LASER TEMPERATURE-JUMP AND LENGTH-STEP STUDY

Julien S. Davis & William F. Harrington
Dept. of Biology, The Johns Hopkins University, Baltimore, MD 21218

Laser T-jump and L-step experiments were performed at various temperatures between 1 and 31°C on skinned fibers of rabbit psoas muscle undergoing isometric contraction. The results of these experiments show that an endothermic force-generating transition is associated with the slowest exponential component of the Huxley-Simmons phase 2 of tension recovery. Force, therefore, appears to be generated by a single step, order-disorder (entropy driven) transition in this time domain.

Experimental records of force generation after a 1μs T-jump of 5°C can be subdivided into four distinct kinetic phases. Comparison of these data with L-step experiments (2 nm per 1/2 sarcomere step-release in 200 μs) allows the resolution of temperature sensitive and temperature insensitive mechanical states.

1) The first phase following the T-jump of a fiber consists of a small instantaneous drop in tension thought to arise from normal thermoelastic expansion of the component proteins on heating. Since the perturbation by the T-jump is small, it appears that the Hookean elements responsible for the Huxley-Simmons phase 1 are little perturbed by temperature.

2) A fast, low amplitude (6%, 11°C) increase in tension follows. Goldman *et al.*, (J. Physiol. (1987) **392**, 71), view this phase as slightly temperature dependent and kinetically equivalent to tension recovery during the H-S phase 2.

3) A temperature dependent medium speed relaxation (80-500 s^{-1}) of moderate amplitude (32%, 11°C) occurs next. Comparison of this phase with the L-step kinetics reveals a correspondence between it and the slowest exponential component of the H-S phase 2. This interpretation is based on the observation that they are of similar rate and that the two processes exhibit a similar, non Arrhenius, temperature dependence; reaction amplitudes of both decline as temperature is increased. This relegates the, less temperature sensitive, fast components of the H-S phase 2 to the small amplitude fast relaxation that follows the initial drop in tension.

4) The slow (≈10 s^{-1}) temperature independent relaxation of larger amplitude (62%, 11°C) that completes the reaction is thought to be a rate-limiting step between the temperature sensitive hydrolysis of ATP and force generation.

M-PM-C4

RAPID TENSION RECOVERY IN RESPONSE TO SHORTENING STEPS FOLLOWING A CYCLE OF RAMP SHORTENING AND LARGE RESTRETCH IN SKINNED RABBIT PSOAS FIBERS.

K. Burton. MRC Muscle and Cell Motility Unit, King's College London, London, U.K.

The mechanics of skinned rabbit psoas fibers have been studied following rapid stretch. The stretch was applied after a period of shortening and was sufficiently large (5-15%) so that cross-bridges attached at this time are expected to be forcibly detached (Brenner, 1983, Biophys. J. 41:99). The force response to the stretch was a spike of tension, followed by a minimum (T_{min}) of about 40-50% P_o, and then a slow recovery to the isometric level. Recent experiments have indicated that cross-bridges forcibly dissociated by ramp (Colomo et al., 1989, Pflügers Archiv, 414:245) or step (Brenner, 1988, Pflügers Archiv, 412:R79; Burton, 1989, J. Physiol., 418:66P) lengthening can reassociate on the timescale of the rapid stretch (< 1 ms). An important question concerning cross-bridges which have rapidly reattached following forcible detachment is whether they can still generate (not merely bear) force. In order to address this question step changes in length were applied shortly after the restretch, but before a significant change in tension during the slow recovery (< 3% P_o in 10 ms). This has the advantage of allowing the response of cross-bridges which have rapidly reattached to be separated from cross-bridges attaching during the slow recovery (≈5 s^{-1}). The step shortening (5-20 nm/hs) produced a rapid fall of force, followed by a recovery of at least three phases. The first was a rapid partial recovery requiring 1-2 ms (5°C). The amplitude of the rapid phase was 20-30% of the value for "phase 2" of an isometric tension transient. The rapid phase was followed by a pause during the period of T_{min} and then a slow recovery to the isometric value. The rapid phase of tension recovery provides evidence that the attached cross-bridges responsible for force and stiffness after a large stretch can also generate force. If a process of detachment, rapid reattachment to a new actin site, and force generation occurs during shortening (Burton & Simmons, 1990, Biophys. J. 57:548a), it could provide a mechanism whereby the sliding distance per ATP hydrolysis cycle during which a cross-bridge is in force generating states can be much greater than one cross-bridge throw.

M-PM-C5

TENSION TRANSIENTS FOLLOWING SUDDEN LENGTH CHANGES IN THE PRESENCE AND ABSENCE OF INORGANIC PHOSPHATE IN SINGLE RABBIT PSOAS MUSCLE FIBERS. J.A.Dantzig, Y.E.Goldman and V.Lombardi* Univ. of Pa., Phila. PA USA, *Univ. degli Studi Firenze, Firenze Italy

The reaction step leading to the force generating state of the cross-bridge cycle has been linked mechanically to quick recovery following length steps (Huxley & Simmons, Nature 233:533, 1971) and biochemically to P_i release from AM.ADP.P_i (Hibberd *et al.*, Science 228:1317,1985). To further characterize the relation between these two processes, we measured kinetics of tension (T) transients elicited by 150 μs step length changes imposed on isometrically activated skinned fibers in ± 10 mM P_i (10°C). Stiffness was estimated from the slope of the linear region of the T1 curve (extreme T at the end of the step *vs.* step size). P_i reduced isometric force (P_o) to 0.63 ± 0.02 and stiffness to 0.75 ± 0.02 relative to 0 P_i values (means ± sem, n = 4). In ± P_i, quick recovery was almost complete for small length changes, but decreased as step release size increased. P_i right-shifted the extrapolated intercept of the linear part of the T2 curve (T at end of quick recovery *vs.* step size). Quick recovery was faster for releases than stretches, e.g. t_i = 1.12 ± 0.20 and 0.61 ± 0.04 ms for ~0.2% L_o stretch and release, (0 P_i,n=4) and was accelerated by P_i (fig., step amplitudes are truncated and pre-step tensions are superimposed): t_i = 0.72 ± 0.03 and 0.49 ± 0.01 ms for ~0.2% stretch and release. The delayed rise after stretch and the fall after release were more prominent in P_i. Based on sinusoidal analysis, our previous data (J. Physiol. 426:39P, 1990) suggested that P_i increases the rate of cross-bridge detachment during ramp stretches. The present results suggest P_i also increases the rate constants for transitions contributing to quick recovery and shifts the distribution of states toward lower force per attachment. (MDA; NIH HL15835 to PA. Musc. Inst. & AR26846; MURS, Italy).

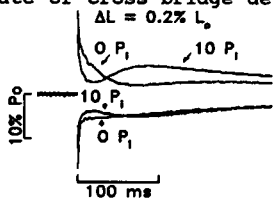

M-PM-C6

PURIFICATION OF DYSTROPHIN FROM RABBIT SKELETAL MUSCLE

James M. Ervasti, Steven D. Kahl and Kevin P. Campbell. Howard Hughes Medical Institute and Department of Physiology and Biophysics, University of Iowa College of Medicine, Iowa City, Iowa 52242.

We have recently shown that dystrophin is part of a large (18S), tightly associated oligomeric complex which also contains a 59 kDa protein and four glycoproteins (J.M. Ervasti et al. *Nature* 345:315-319, 1990). Here, we report the purification of dystrophin from rabbit skeletal muscle. Dystrophin-glycoprotein complex was first prepared from digitonin-solubilized rabbit skeletal muscle membranes by a novel two-step method involving derivatized lectin chromatography and DEAE-cellulose ion exchange chromatography. Proteins co-purifying with dystrophin were a protein triplet of 59 kDa and four glycoproteins of M_r 156 kDa, 50 kDa, 43 kDa and 35 kDa, all previously identified as components of the dystrophin-glycoprotein complex. This method thus yielded dystrophin-glycoprotein complex of the same purity and quantity as previously reported while obviating the need for the sucrose gradient step. Alkaline treatment of the dystrophin-glycoprotein complex resulted in complete dissociation of dystrophin from the other components of the complex. Alkaline-dissociated dystrophin was separated from the majority of associated proteins by sucrose density gradient centrifugation. The residual dystrophin-associated glycoproteins which contaminated peak dystrophin-containing gradient fractions were then removed by WGA-Sepharose adsorption. 98% of the pure dystrophin appeared as a single band of ~400 kDa on overloaded Coomassie Blue-stained gels while the remaining 2% was of slightly lower M_r. The predominant and minor components appear to be intact dystrophin isoforms as antisera specific for the amino- or carboxyl-terminals of human dystrophin recognized both bands on immunoblots. Immunoblots stained with peroxidase-conjugated WGA revealed no contaminating glycoproteins in the pure dystrophin. Based on previous estimates that dystrophin makes up only 0.002% of all muscle protein, this rapid method represents a 50,000-fold purification of dystrophin. This protocol required only commercially available materials and yielded protein of sufficient quantity (approximately 75-100 μg per preparation) to afford the necessary biochemical, functional and ultrastructural characterization of dystrophin. Characterization of pure dystrophin will allow confirmation of the structural predictions originating from the primary sequence deduced by recombinant DNA techniques and help to identify the component(s) of the dystrophin-glycoprotein complex which bind dystrophin directly. K.P. Campbell is Investigator of the Howard Hughes Medical Institute. J.M. Ervasti is an MDA postdoctoral fellow. This work was also supported by a grant from MDA.

M-PM-C7

DYSTROPHIN CONSTITUTES FIVE PERCENT OF MEMBRANE CYTOSKELETON IN SKELETAL MUSCLE

Kay Ohlendieck and Kevin P.Campbell. Howard Hughes Medical Institute and Department of Physiology and Biophysics, University of Iowa College of Medicine, Iowa City, Iowa 52242.

Dystrophin, the high molecular weight protein product of the human Duchenne muscular dystrophy (DMD) gene, is localized in the sarcolemma membrane in normal muscle but absent from skeletal muscle of DMD humans and mdx mice. Dystrophin represents about 0.002% of the total muscle protein and its predicted primary structure suggests that it shares many features with membrane cytoskeletal proteins. Recently, we have shown that dystrophin is associated in a large oligomeric complex with four sarcolemma glycoproteins (Ervasti et al.(1990) Nature 345: 315-319). The precise functional or structural role of dystrophin and the amount of dystrophin in the muscle cytoskeleton is still unknown. Here, we report the preparation of highly purified sarcolemma vesicles from rabbit skeletal muscle using sucrose density gradient centrifugation followed by a wheat germ agglutination procedure. Thin section electron micrographs of the isolated sarcolemma pellet show mostly round sealed vesicles of various size. Components of the dystrophin complex are highly enriched in the sarcolemma fraction and copurify with sarcolemma marker Na/K-ATPase as revealed by immunoblotting using monoclonal antibodies. Extraction with Triton X-100, which leaves the cytoskeleton fraction as an insoluble residue, demonstrates that dystrophin, along with its associated glycoproteins, is concentrated in the sarcolemmal cytoskeleton fraction. Densitometric scanning of SDS-PAGE gels of purified rabbit skeletal muscle cytoskeleton illustrates that dystrophin is a significant component of the muscle cytoskeleton constituting approximately five percent of the total cytoskeleton protein. Like other cytoskeletal elements, dystrophin is solubilized from the sarcolemma by alkaline treatment but the dystrophin-associated glycoproteins of apparent 50 kDa and 156 kDa remain with the bilayer. These results confirm the findings from the detergent extraction, that dystrophin is a component of the peripheral membrane cytoskeleton and that its characteristics are comparable to the major membrane skeleton component spectrin in other cell types. Analysis of mdx mice compared to control shows that the major difference between the isolated sarcolemma from control and mdx mice is the absence of dystrophin. Thus, our results indicate that instability of the sarcolemma membrane in DMD muscle is very likely due to the absence of one of the major constituents of the sarcolemma cytoskeleton. K.P. Campbell is an Investigator of the Howard Hughes Medical Institute.

M-PM-C8

CONTROLLED ASYMMETRIC EXTRACTION OF TROPONIN-C: FURTHER STUDIES ON THE MOLECULAR BASIS OF THE LENGTH-TENSION RELATIONSHIP

JAGDISH GULATI AND ÁRVIND BABU, *Albert Einstein College of Medicine, Bronx, NY*

Ca^{2+}-sensitivity of both cardiac and skeletal muscle increases with sarcomere length, and we have shown that length-dependence is also greater when cardiac TnC replaces skeletal TnC in either tissue (*Science* 240,74,1988; *J Physiol* 410,71P,1989). We presently examine the effect of individual TnC molecules distributed along the thin filament on the length-dependence of Ca^{2+}-sensitivity. Skinned fibers of rabbit psoas muscle were partially extracted ($0.73P_o \pm .04$ residual force) either at 2.6μm or at 1.6μm. The force ratio (P at 2.4μm/P at 1.9μm) was $0.36 \pm .03$ for extraction at long length and 0.85 ± 0.02 for extraction at short length. This indicates highly asymmetric TnC extraction for the former and symmetric extraction for the short length. The length-dependence of Ca^{2+}-sensitivity in the fibers decreased from 0.10pCa unit in the unextracted fiber to 0.05pCa unit in the symmetrically extracted fiber, for 0.5μm length change. The results suggested that the factors transmitting the length effect were cut down in this case by the uniform TnC extraction along the thin filament length. In the asymmetric case, we found that the length-dependence of Ca^{2+}-sensitivity changes in the opposite direction: it increases from 0.11pCa unit for the control to 0.18 unit in the extracted fiber. These results for the asymmetric case suggest that the TnC molecules in the overlap region act independently of those in the nonoverlap region. [Supported by NIH and NYH]

M-PM-C9

MUSCLE CONTRACTION IS NOT DUE TO THE "CONTRACTILE FORCE". Avraham Oplatka, Weizmann Institute of Science, Rehovot, Israel (intr. by D.Rao Sanadi)

It is generally taken for granted that the "contractile force" developed in an isometric contraction of muscle, which is associated with a conformational change of tightly bound complexes of myosin and actin , is also the force which causes shortening in an isotonic contraction. It is argued that shortening is the outcome of another force, generated following the dissociation of the complexes by ATP. Hence, the sliding distance i.e., the distance covered by a myosin head "coupled" with the breakdown of one ATP molecule, is determined by the (large) free energy decrease of the dissociation reaction and by the resistance to sliding. Since the latter, as well as the free energy change, might depend on temperature, ionic strength etc. the sliding distance could be a variable. On the other hand, the distance covered after the release of a muscle which had developed rigor tension, in which the proteins form a continuous three dimensional network, cannot exceed the length of a myosin head.

In conclusion: a) One type of force is responsible for tension generation and another for movement. b) There exist two different sliding distances.

M-PM-C10

GLYCOLYTIC ENZYME CONTENT IN DROSOPHILA FLIGHT MUSCLE LACKING ACTIN. **D. Maughan, J. Hurley, R. Schaaf. Dept. Physiology & Biophysics, U. Vermont, Burlington, VT 05405.**

The indirect flight muscle (IFM) is abundantly endowed with glycolytic enzymes involved in carbohydrate metabolism required for flight. The absence of an isoform of even one enzyme, glyceraldehyde 3-P dehydrogenase (GPD), results in flightlessness (D. Sullivan, pers. com.). GPD and other glycolytic enzymes appear to be located in the actin-containing I-band region of the sarcomere (e.g., Emmart et al., Exp. Cell Res. 26: 79, 1962). Here we used the genetic mutant KM88 (Okamoto et al., EMBO J 5(3): 589, 1986), an actin null allele, to investigate whether glycolytic enzyme content is reduced in the absence of actin. IFM protein content in cytosolic and cytomatrix fractions of KM88 was measured by quantitative SDS-PAGE and compared to that of wild type Canton-S. GPD was identified by western blot. Other representative glycolytic enzymes (triose P-isomerase: TIM, and phosphoglucose isomerase: PGI) were tentatively identified by their electrophoretic mobilities. IFM content of proteins known to be either associated with actin (tropomyosin: TM) or not (myosin light chain 2: MLC-2) was also measured. To adjust for sample size, protein content was measured relative to that of myosin heavy chain (MHC) whose concentration was assumed to be similar in all IFM studied. Compared to Canton-S, the GPD, TIM, PGI and MLC-2 content in KM88 IFM was simlilar; TM content, however, was considerably reduced, in agreement with the notion that TM binding to actin offers protection against proteolysis (Mahaffey et al., Cell 40: 101, 1985). Apparently a similar protective role of actin is not neccessary for the glycolytic enzymes. **[Supported by NIH RO1 AR40234]**

M-PM-D1

TRYPTOPHAN TRIPLET PHOTOPHYSICS AND PHOTOCHEMISTRY.

P. Ilich and F.G. Prendergast
Department of Biochemistry and Molecular Biology
Mayo Foundation, Rochester, Minnesota 55905

Following an excitation into the low singlet domain (260 - 290 nm) a considerable proportion of Trp residues either gets converted into an excited triplet or undergoes a photochemical decyclisation and eventual deamination of the indole ring.

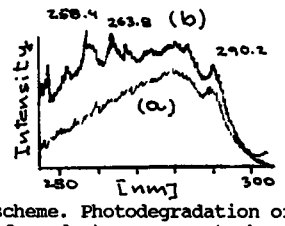

Comparison of the low temperature fluorescence (a) and phosphorescence (b) spectra in cod-fish parvalbumin, Figure, demonstrates the prominence of the ^1L_a vibronicb ands in the latter and a dominance of the ^3L_a <- ^1L_a <- ^1A, spin-state conversion scheme. Photodegradation of Trp into kynurenine chain of products appears to be autosensitized, exibits a strong indole -> kynurenine triplet-triplet energy transfer (and a weaker reverse transfer) and is characterized by a prominent array of phosphorescence bands starting at 371.8 nm (369.3 nm in indole in Ar). The latter is an invariant of indole, coumaron and benzothiophene ring. On the other hand, certain phosphorescence excitation bands are highly sensitive to temperature, embedding medium and presence of metal ions. These effects are analyzed in view of (i) the singlet band assignments and resolution of fluorescence decay curves of protein Trp residues, and in view of (ii) bioanalytical identification of Trp degradation products (e.g. the depletion of NAD in the Interferon-γ treated tumor cells, or the increase of kynurenine-type metabolites in human eye lenses). Supported by NIH grant GM34847 (F.G.P.).

M-PM-D2

DIFFUSION-DEPENDENT AND -INDEPENDENT COLLISIONAL QUENCHING OF FLUORESCENCE AND PHOSPHORESCENCE.

C. S. Owen[1] & J.M. Vanderkooi[2], Jefferson Medical College[1] & Univ. of Pennsylvania[2], Philadelphia, PA

The fluorescence or phosphorescence of large biological molecules can often be quenched by molecules which are free to diffuse in solution. The analysis of the data requires a theory that contains at least 3 rates: the intrinsic (unquenched) rate of luminescence, the reaction rate for the reaction of donor and acceptor in the limit of infinitely fast diffusion, and the rate of diffusion. If the quenching reaction is slow in comparison with the rate of diffusion, the observed quenching is independent of the diffusion constant. At the opposite extreme, in which diffusion is slow in comparison with the quenching reaction, the quenching rate becomes strictly proportional to the diffusion constant. A theory is developed to handle the range from an almost completely diffusion-limited system to one which is limited solely by the kinetics of the quenching reaction. The degree of diffusion dependence depends on the relative magnitudes of the diffusion constant and an effective interaction strength which can be calculated from the rate constant for the quenching interaction and the distance of closest approach. Three cases are considered: (1) long-range quenching by a dipolar resonant electromagnetic interaction, (2) long range quenching by an electron exchange mechanism, or (3) the quencher molecule itself can diffuse within the macromolecule. All 3 cases can give rise to diffusion-independent quenching, and they will differ in the detailed time dependence at early times after excitation. In practice, identifying the mechanism which pertains in an experimental system should involve criteria in addition to analysis of kinetic data. (Supported by NSF DCB-8718274 and NIH GM44448 and GM36392).

M-PM-D3

Time Resolved Circularly Polarized Phosphorescence

J. Schauerte, M. Model, D. Steel & A. Gafni
University of Michigan, Ann Arbor, Michigan 48109

Circularly polarized phosphorescence (CPP) measures the chirality of the excited state of a chromophore and has been used extensively to investigate structural information complimentary to circular dichroism spectroscopy for the ground state. Steady state CPP measures the time averaged chirality of the chromophore. However, the chiral environment of the chromophore may be time dependent due to various dynamical processes such as conformation changes or binding and dissociation of the chromophore to the chiral macromolecule. Time-resolved CPP (TR-CPP) will then provide unique information about the change in chromophore asymmetry during its excited state. An instrument is described for TR-CPP measurements, capable of resolving CPP decays greater than 10's of microseconds.

With the reports of room temperature phosphorescence of proteins in the millisecond to second time domain, TR-CPP has the potential to resolve contributions from individual tryptophan residues to the optical activity in multi-tryptophan phosphorescent proteins. Phosphorescence measurements are more sensitive to chromophore environment than fluorescence measurements, and TR-CPP can enhance the sensitivity of tryptophan phosphorescence studies in measuring protein dynamics in protein folding studies. Our preliminary work is based on the use of terbium luminescence which exhibits CPP signals upon coordination to proteins such as transferrin and calcium binding proteins. Irradiation of a protein in the UV results in excited state transfer from the chromophore (e.g. tyrosinate) to the terbium ion, which excentuates the bound terbium luminescence over free terbium in solution. The dissociation of terbium ion from these binding domains results in the attenuation of the CPP signal, and hence in a time resolved CPP signal corresponding to the terbium ion off rate from the protein.

M-PM-D4

TIME-RESOLVED FLUORESCENCE DATA ANALYSIS USING QUANTIFIED MAXIMUM ENTROPY METHOD (QMEM)

J.C. Brochon*, S.F. Gull+, J. Skilling+, B. Valeur×
(*)LURE Centre Universitaire Paris-Sud 91405 Orsay, France. (+)Cavendish Laboratoty and DAMTP, Cambridge U.K. (x) C.N.A.M, CNRS URA 1103 75003 Paris, France.

We present a rigourous Bayesian formulation of the maximum entropy method (Maxent). Our previous "Historic" Maxent method maximised the entropy of a feasible reconstruction $\alpha(\tau)$ whilst forcing the data to fit a chi-squared constraint. The Bayesian "Classic" Maxentproduces instead the complete probability distribution (α given data), thus providing quantitative estimates of the reliability of the reconstruction. QMEM has been successfully applied to time-resolved fluorescence data from time-correlated photon-counting and phase-modulation techniques; a set of comparativeexperiments are analysed to show the distributions of lifetimes. We demonstrate that, in general, time-resolved fluorescence anisotropy (TRFA) data have not previously been correctly analysed. We introduce a 3-dimensional description of TRFA data (from both techniques) in terms of the distribution of lifetimes τ, rotational correlation times θ and initial anisotropies A_0, which are supported by extensive simulations and experiments. We present applications to protein dynamics study.

M-PM-D5

THE FLUORESCENCE DECAY KINETICS OF TRYPTOPHAN AND ITS DERIVATIVES IN SOLUTION: EVIDENCE FOR BOTH GROUND STATE AND EXCITED-STATE HETEROGENEITY. K. J. Willis, A. G. Szabo, and D. T. Krajcarski, Division of Biological Sciences, National Research Council, Ottawa, Ont. Canada, K1A OR6.

The decay kinetics of individual tryptophyl residues in proteins are often complex. The interpretation of these data are based on the current models which attempt to rationalize the emission properties of tryptophan and tryptophan containing peptides in solution. The biexponential decay kinetics observed for tryptophan and many of its derivatives are thought to arise from rotamers of the alanyl side chain which exist in the ground state. The data which we have obtained from measurements of a large number of tryptophan derivatives indicate that the biexponential decay kinetics are in certain cases, a consequence of an excited state reaction. We also find evidence for at least two spectrally distinct ground state species in all cases. These and other results on the photophysics of tryptophan and its derivatives will be presented and discussed.

M-PM-D6

Analysis of Non-Linear Stern-Volmer Fluorescence Quenching Data. *P.B. Contino & W.R. Laws,* Department of Biochemistry, Mount Sinai School of Medicine, New York, NY 10029

By comparing the dynamic quenching efficiency of various quenching agents under different conditions, the environment of a fluorescent chromophore, and thus a specific region of a biomolecule, can be characterized in terms of neighboring ionic groups and solvent accessability. Often, however, steady-state fluorescence quenching data do not follow the linear Stern-Volmer expression. This non-linearity suggests that other factors are involved, including static quenching and/or multiple fluorophores. Based on simulation studies, we have examined our ability to recover quenching parameters for a single fluorophore with static quenching, multiple fluorophores, and multiple fluorophores with static quenching. Static quenching was modeled as either a sphere of action (quenchers that might already be within the critical radius for quenching at excitation) or a ground-state complex (a weak fluorophore: quencher ground-state complex) mechanism. With the sphere of action model, the dynamic and static quenching parameters for a single fluorophore are ~~easily~~ recovered. With the ground-state complex model, however, the parameters describing the quenching of a single fluorophore are difficult to recover. For multiple fluorophores with only dynamic quenching, it is usually impossible to find a unique solution due to the number of independent variables. The dynamic quenching parameters may be recovered only if the fractional intensities are provided as constants to the fitting algorithm and if the dynamic quenching parameters are similar in magnitude. The addition of a static quenching mechanism to each chromophore results in even more parameters that have to be determined and the data can never be analyzed for a unique solution. If the dynamic quenching parameters and fractional intensities are known (i.e. obtained through time-resolved fluorescence quenching studies), then they can be used to help examine the steady-state data to evaluate the static quenching interaction(s). We have used this systematic approach to obtain more information about the local environment of tyrosine in model compounds and small peptides.

Supported by NIH Grants DK39548 and GM39750.

M-PM-D7

THERMAL UNFOLDING OF A STAPHYLOCOCCAL NUCLEASE MUTANT AS DETERMINED BY CHANGES IN DISTANCE DISTRIBUTION FROM FLUORESCENCE ENERGY TRANSFER MEASUREMENTS.

P.G. WU, E. JAMES AND L. BRAND, Department of Biology, The Johns Hopkins University, Baltimore, MD 21218, USA.

A mutant of single tryptophan-containing staphylococcal nuclease, K78C, where lysine 78 was replaced by cysteine, was labeled with a cysteine specific probe IAEDANS. Fluorescence decay studies of the Trp were used to estimate distance distributions between the Trp and IAEDANS. Measurements were done as a function of temperature from 4^0C (native) to 60^0C (denatured) both with and without Ca^{2+} and the inhibitor pdTp. Below 30^0C, the distance distribution of both the free nuclease and the enzyme with bound Ca^{2+} and pdTp can be adequately described by a single population. Above 40^0C, where the free but not the inhibitor-bound protein begins to unfold, two different populations are required to fit the data both with and without pdTp. One population has a compact structure and the other has an expanded and probably random structure. As the temperature rises, the population of the less-structured form increases. At the highest temperature used in this study (65^0C), the non-native compact structure is the major (60-70%) form of the denatured state. The finding of two denatured species by energy transfer measurements is consistent with the proposal by Shortle and Meeker(Biochemistry,29 936 (1989) that S. Nuclease can exist in two denatured states.(Supported by NIH grant #GM 11632.)

M-PM-D8

STUDIES ON THE ORIGIN OF FLUORESCENCE INTENSITY DECAY COMPONENTS IN RIBONUCLEASE-T1 BY SITE-SPECIFIC MUTAGENESIS

T.A. Feimlee, P.H. Axelsen, and F.G. Prendergast
Mayo Clinic and Foundation, Rochester, MN, 55905

The single TRP residue (TRP-59) in ribonuclease-T1 (RNAse-T1) exhibits a monoexponential fluorescence intensity decay at pH <6.0 but a biexponential decay at pH >7.0. This suggests that titration of a histidine residue in the vicinity of TRP-59 is responsible for this behavior. The role of specific residues in the origin of these decay components is being explored by means of site-specific mutations, computer graphics, and simulated molecular dynamics. HIS-27 is the nearest histidine residue to TRP-59 among the three histidines present in RNAse-T1. The mutation of HIS-27 to ARG yields an active enzyme with pH-dependent intensity decays that are similar to the wild type protein. However, the mutation of GLY-23 to ALA appears to eliminate pH-dependent changes. GLY-23 is adjacent to the TRP-59 side chain, and graphical analysis indicates that the C_β atom of ALA-23 in the mutated protein should be in direct contact with the TRP-59 side chain.

These results bear on the issue of whether fluorescence intensity decays are determined by residues in contact with fluorophore, or whether distant residues may be of overriding importance. Since the histidine residue which is most proximal to TRP-59 does not affect the decay characteristics of TRP-59, any effects due to the two remaining histidines (both of which are in the substrate binding site) should be mediated through the protein matrix. The absence of pH-dependent behavior in the ALA-23 mutant further supports the role of residues in immediate contact with the fluorophore in determining decay characteristics. Supported by GM 34847.

M-PM-D9

HAIR PHOTODAMAGE - A SPECTROSCOPIC STUDY

C. Pande. Clairol Research Labs. Stamford, CT. 06922.

Hair fibers belong to the keratin family of fibrous proteins, and contain small amounts of lipids and melanin pigment. Morphologically, hair structure has two distinct components. The outer 'shingle-like' cuticles, rich in cystine, enclose the inner corticular region. The latter consists of tightly packed elongated cortical cells which are oriented parallel to the fiber axis. These cells contain α-helical protein, arranged into crystalline fibrils, and embedded in cystine-rich amorphous matrix.

We have been interested in understanding the molecular basis of hair weathering. An essential element of this process is the exposure to solar radiation. Besides the apparent photobleaching of melanin, hair weathering results in a significant damage to hair keratin. Only wavelengths above 285 nm are important in this context, since shorter wavelengths are filtered out by the earth's atmosphere. The chromophores in hair keratin are the aromatic amino acids, particularly tryptophan, and the cystine disulfide bonds, which are weak absorbers in this wavelength region[1].

We have used fluorescence spectroscopy to probe the aromatic amino acid residues in hair. We find that hair weathering results in a significant loss of tryptophan. Using FTIR microspectrometry, we also find significant formation of cysteic acid resulting from cystine photoxidation. Preliminary data suggest that the loss of tryptophan is significantly faster than cysteic acid formation. It is, as yet, unclear whether the two processes are coupled.

We are currently evaluating various factors that influence the rate of tryptophan photodamage under controlled irradiation conditions. These studies will provide insight into the mechanism of tryptophan photodamage in hair, and in proteins in general.

[1] Creed, D. (1984) *Photochem. Photobiol.* 39, 4, 577-584.

M-PM-E1

INTERACTION OF DIFFERENT AGENTS THAT REMOVE THE INACTIVATION OF Na^+-CHANNELS WITH RAT BRAIN Na^+-CHANNELS IN PLANAR LIPID MEMBRANES. Samuel Cukierman, Division of Biomedical Sciences, University of California, Riverside, CA, 92521-0121.

Important technical and conceptual advances regarding the study of Na^+-channels have been accomplished by using substances that remove the channel's inactivation process. From the technical point of view, the use of these agents had permitted the biochemical reconstitution of Na^+-channels. On conceptual grounds, those different compounds provided insights into structure-function relationships in Na^+-channels as well as to contributing to a better understanding of how these ion channels work. An important unanswered question at the single channel level is: What happens when two different substances that affect the inactivation of the Na^+-channel are simultaneously presented to the channel? Using rat brain Na^+-channels reconstituted in a planar bilayer system, we have investigated the effects of the interaction of several of these substances on the gating and permeation properties of Na^+-channels. Batrachotoxin (BTX) (or veratridine (VT) or trypsin (TR)) was used to remove the inactivation of Na^+-channels and the following channel properties were investigated: the voltage dependence of the open probability (P_o) and, the opening and closing rate constants, the single channel conductance and, the relative permeability of the channel to Na^+ and K^+ ions. Once the channel was treated with one of the above agents, the addition of one or both of the other two substances, or the addition of aconitine, did not induce any alteration on the measured parameters. While the channel displays different gating and permeation properties with each of those substances, it was not possible to change a BTX-mode Na^+-channel into a VT (or TR)-mode. However TR, as well as Chloramine-T (CT) and N-bromosuccinimide (NBS) or N-bromoacetamide (NBA) have very profound effects on the gating of the BTX-treated channel while not affecting its permeation properties: they induced a shift in the P_o-V_m relationship to more hyperpolarized potentials. These effects are manifested only by the intracellular application of these substances. These voltage shifts are consistent with a mechanism by which the voltage-sensor of the channel is now measuring a different potential across the membrane since both the opening and closing rate constants are being shifted by the same voltage amount along the V_m-axis. Thus, in the absence of inactivation, these commonly used substances shift the gating curve of the channel to more hyperpolarized potentials. Since those chemicals have different mechanisms of actions on different aminoacid residues, an interesting possibility to explore is that the same region on the intracellular surface of the channel protein, containing those aminoacid residues, is being affected with a similar functional consequence.

M-PM-E2

DIFFERENCES BETWEEN THE SODIUM CHANNEL DISTRIBUTION ON RAT FAST AND SLOW TWITCH SKELETAL MUSCLE FIBERS

R.L. Ruff, Neurology Service Cleveland VAMC and Depts of Neurology and Neurosciences Case Western Reserve University School of Medicine, Cleveland OH 44106, USA.

In rat fast twitch and garter snake twitch muscle the Na current density is about ten-fold higher immediately adjacent to the endplate than at regions far from the end plate (Beam et al., 1985; Caldwell et al. 1986; Caldwell and Milton, 1988; Roberts, 1987). I examined whether the distribution of Na channels was similar on rat fast twitch omohyoid (OMO) and slow twitch adductor longus (AL) muscles using the loose-patch voltage clamp. Muscles were enzymatically treated to aid in dissection and in some cases to remove the nerve terminals. The maximum Na current density was measured at 3 or more sites in each of 3 different regions: 1) on the border of the endplate, 2) >200 μm from the endplate and 3) on the endplate OMO and AL fibers. The maximum Na current densities were largest for recordings from preparations in which the nerve terminals were enzymatically removed and currents were recorded from the exposed postsynaptic membrane (Table). The Na current density at the border of the endplate was higher than it was >200 μm from the endplate. For each of the 3 regions studied the Na current density on OMO fibers was higher. In addition, the increase in Na current at the border of the endplate compared to the extrajunctional membrane was greater for OMO fibers than AL fibers. These results suggest that the Na channel distribution are different on fast and slow twitch fibers.

Table: NA CURRENT DENSITY ON OMO AND AL FIBERS

	Na Current Density (mA/cm²)*	
Location	OMO	AL
Endplate	229±41 (n=11)	55.7±14.5 (n=9)
Endplate Boundary	110±15 (n=31)	28.9±2.0 (n=32)
Extrajunctional	12.7±2.1 (n=34)	7.25±0.5 (n=30)

* The Na current density of OMO fibers was greater than AL fibers at each of the three sites with $p<0.001$.

Supported by: Merit Reviewed Funding from the Dept. of Veterans Affairs and NIH Grant NS26661.

M-PM-E3

Rat IIA sodium channels retain their properties upon heterologous expression in mammalian cells

X.C. Yang[1], C. Labarca[1], J. Nargeot[3], O. Elroy-Stein[2], B. Moss[2], N. Davidson[1], and H.A. Lester[1], [1]Division of Biology 156-29, Caltech, Pasadena, CA 91125, [2]Laboratory of Viral Diseases, NIAID, NIH, Bethesda, MD 20892, [3]Centre de Biochimie Macromoleculaire, CNRS, LP 8402, B.P. 5051, 34033 Montpellier, France

We have expressed rat brain IIA Na^+ channels in chinese hamster ovary (CHO) cells and in cultured neonatal rat ventricular myocytes using vaccinia virus (VV). Infection of cells with a VV (vTF7-3) containing T7 RNA polymerase gene results in production of T7 polymerase, which in turn transcribes the IIA Na^+ channel cDNA controlled by a T7 promoter in a plasmid (pTM1-Na) that has been introduced into the cells by lipofection. More than 60 % of CHO cells 16-24 hours after co-infection/ lipofection expressed robust Na^+ currents: up to 1 nA recorded in 10 mM external Na^+. The expressed Na^+ channels showed all characteristics of mammalian brain Na^+ channels expressed from poly(A) RNA in oocytes: (1) threshold for activation of -30 mV, (2) maximal current at -10 mV in the peak I-V curve, (3) inactivation time constants ~ 2 ms, and (4) steady state inactivation with k=6.4 mV and $V_{1/2}$=46 mV. The Na^+ currents were reduced by 90% with 90 nM tetrodotoxin (TTX), suggesting a half-block concentration ~ 10 nM. The CHO cells after infection/ lipofection could be maintained for 5 days.

The endogenous Na^+ currents in neonatal rat ventricular myocytes had an activation threshold of -50 mV, a peak at -30 mV, inactivation time constants ~ 5 ms, and were reduced by 10% with 90 nM TTX, indicating a half-block concentration ~ 800 nM. In contrast, myocytes infected with vTF7-3 and lipofected with rat brain IIA Na^+ channel cDNA showed Na^+ currents with inactivation time constants ~ 2-3 ms, peaks at -20 mV, and greater sensitivity to TTX: 90 nM TTX reduced Na^+ currents by 40-80%. In the presence of 90 nM TTX, the remaining Na^+ currents behaved like the endogenous currents. These results indicate that ventricular myocytes lipofected with IIA Na^+ channel express two populations of Na^+ channels with different TTX sensitivity and gating kinetics. (Supported by NIH grants GM-10991 and NS-11756 and MDA fellowship to X.C.Y.)

M-PM-E4

Generation of Action Potentials in Previously Unexcitable cells

H.S. Hsu[1], X.C. Yang[1], C. Labarca[1], A. Karschin[1], O. Elroy-Stein[2], B. Moss[2], N. Davidson[1], H.A. Lester[1], [1]Division of Biology 156-29, Caltech, Pasadena, CA 91125, [2]Laboratory of Viral Diseases, NIAID, NIH, Bethesda, MD 20892

The minimum requirement for the generation of an action potential is the presence of Na^+ and K^+ channels at sufficient membrane densities. To express Na^+ channels, we use a transient expression system in which CHO cells are infected with a vaccinia virus carrying the bacteriophage T7 RNA polymerase and are also induced to take up a plasmid containing the cDNA for the rat brain type IIA Na^+ channel downstream from the T7 promoter and EMCV UTR. To express K^+ channels, we infect the same cells with a recombinant VV containing the Shaker H4 channel (Leonard et al PNAS 86, p7629,1989). In voltage-clamp experiments, non-infected CHO cells display little or no voltage-dependent currents. Cells exposed to either Na^+ or K^+ channel reagents display only Na^+ or K^+ currents, respectively. Cells exposed to both the Na^+ and K^+ channel reagents display both inward and outward voltage-dependent currents appropriate to both channel types. When stimulated with a current pulse, the coinfected cells fire all-or-none action potentials with a peak at positive potentials and an after-hyperpolarization.

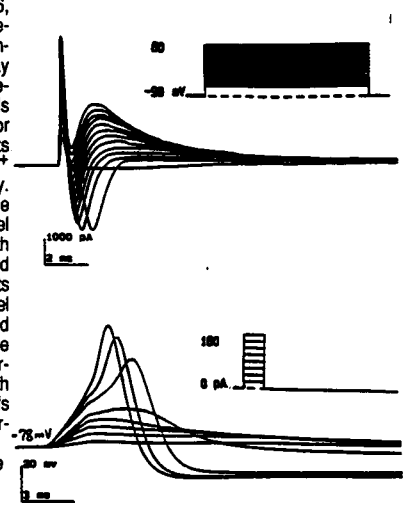

Support:NS-11756,Multiple Sclerosis Society.

M-PM-E5

MULTIPLE COMPONENTS OF INACTIVATION OF SODIUM CURRENT (I_{Na}) IN CULTURED RAT CHROMAFFIN CELLS.

A. Neely & C.J. Lingle. Dep. of Anesthesiology, Washington University. St Louis, Mo, 63110. (Sponsored by J.M. Sullivan).

I_{Na} recorded in primary cultures of rat chromaffin cells using the whole cell patch-clamp technique exhibits two components of inactivation. Here, we investigated the properties of slow and fast inactivation of I_{Na} in order to explore the role that slow inactivation may play in limiting the action potential firing rate.

1. Steady-state inactivation curves obtained with conditioning pulses lasting up to 200 msec were well-described by a double Boltzman function, consistent with the existence of at least 2 inactivated states. Following conditioning pulses of 2 seconds, steady-state inactivation was described by a single Boltzman distribution (50% inactivation from -56 mV to -48 mV).

2. The time courses of onset and recovery of inactivation to potentials near the normal cell resting potential were both described by double exponentials. However, the recovery time constants differed from the inactivation time constants, although the same equilibrium level of inactivation was reached in both cases. This indicates that the rate-determining states in the two processes differ.

3. The relative contribution of the different components of recovery from inactivation also depends on how inactivation was produced. When inactivation is produced by strong depolarizations resulting in maximum activation (+ 40 mV for 5 msec), recovery is rapid. Following inactivation produced by a long depolarization to intermediate potentials (-35 mV for 1 sec), the contribution of slow recovery is increased.

Taken together, these observations suggest that, in rat chromaffin cells, inactivation of I_{Na} involves at least two inactivated states selectively coupled to different closed or open states in the activation pathway.

M-PM-E6

FUNCTIONAL EXPRESSION OF THE RAT HEART I Na CHANNEL ISOFORM.

J. SATIN, L.L. CRIBBS, H.A. FOZZARD, and R.B. ROGART.
Dept. of Medicine, Section of Cardiology, University of Chicago, Chicago, IL 60637.

Functional Na channels are expressed by *Xenopus* oocytes injected with cRNA transcribed from the rat heart I cDNA clone (Rogart et al., P.N.A.S., 86:8170, 1990). The expressed rat heart I (RH-I) Na current has a relatively low affinity for tetrodotoxin (K_d = 1.52 μM) and saxitoxin (K_d = 44 nM) characteristic of native cardiac Na current. The current-voltage relationship and kinetics of RH-I I_{Na} are also similar to that of the native current. In contrast to the decay of expressed high TTX-affinity (K_d = 40 nM) and high STX-affinity (K_d = 0.35 nM) skeletal muscle clone (μI, Trimmer et al., Neuron, 3:33, 1989), RH-I I_{Na} decays rapidly without a prominent slow phase. The expressed RH-I current is typically 50 to 100 times smaller than that directed by μI in a given batch of oocytes. We conclude that the primary amino acid sequence of the rat heart I α-subunit is sufficient for expression of tetrodotoxin resistance, and the rat heart I clone is likely to account for tetrodotoxin-resistant phenotype of cardiac and denervated skeletal muscle.

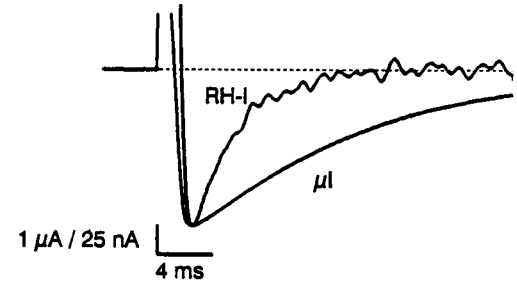

M-PM-F1

CALRETICULIN IS THE MAJOR Ca BINDING PROTEIN IN SMOOTH MUSCLE AND NON-MUSCLE SARCOPLASMIC/ENDOPLASMIC RETICULUM

R.E. Milner, S. Baksh, C. Shemanko, and M. Michalak.
Departments of Biochemistry and Pediatrics, University of Alberta, Edmonton, Alberta, Canada T6G 2S2

The major Ca binding protein in striated muscle SR membranes is calsequestrin, a protein which binds up to 50 moles of Ca per mole, with low affinity. Calreticulin, another Ca binding protein detected in these membranes, binds 25 moles of Ca per mole with low affinity and 1 mole of Ca per mole with high affinity.

We have investigated the distribution of these two Ca binding proteins in smooth muscle and non-muscle tissues. Liver ER and uterine smooth muscle SR membranes were tested for the presence of both cardiac and skeletal isoforms of calsequestrin, and for calreticulin, using Western blotting, Ca overlay and "Stains-all" techniques. Western blots probed with antibodies specific to both proteins revealed that only calreticulin is present in liver ER. In addition, we detected no evidence for any special calreticulin- or calsequestrin-enriched organelles in the liver cells. Uterine SR vesicles were also found to contain a protein band immunoreactive with anti-calreticulin antibodies, whilst showing no reaction with anti-cardiac or anti-skeletal muscle calsequestrin antibodies. This observation was confirmed by immunocytochemical studies of smooth muscle cells in culture. Finally, calreticulin, but not calsequestrin, mRNA was detected in uterine smooth muscle and in non-muscle tissues. Calsequestrin mRNA was only present in cardiac and skeletal muscle.

We conclude that calreticulin is the major Ca binding protein in both smooth muscle SR and non-muscle ER, whilst calsequestrin appears to be confined to cardiac and skeletal muscle. Calreticulin may, therefore, be a functional analogue of calsequestrin. (Supported by MRC, AHSF and AHFMR).

M-PM-F2

SULFHYDRYL OXIDATION INDUCES CALCIUM RELEASE FROM CANINE CARDIAC SARCOPLASMIC RETICULUM (SR) VESICLES

Sumanth D. Prabhu, Nikhat F. Zaidi, Meenakshi Nigam, Kuntala Shome and Guy Salama. Department of Physiology, University of Pittsburgh, Pittsburgh, PA 15261

As in skeletal sarcoplasmic reticulum (SR), sulfhydryl (SH) reagents interact with a critical SH on a Ca^{2+} channel protein inducing Ca^{2+} release from canine cardiac SR. SR vesicles were Ca^{2+} loaded either actively with an ATP regenerating system or passively by incubation with $CaCl_2$. Ca^{2+} transport was measured using antipyrylazo III at 720-790 nm. Heavy metal (HM) ions (Ag^+, Hg^{2+}), mercaptans (cysteine) plus Cu^{2+}, and "reactive" disulfides (RDSs) (compounds with a pyridyl ring adjacent to S-S bonds) all induce Ca^{2+} release at 10-100 μM. RDSs are absolutely specific to free SHs and oxidize low pKa SH sites via a thiol-disulfide exchange reaction, and thus open SR Ca^{2+} channels. Conversely, SH reducing agents (e.g. dithiothreitol) reverse RDS induced release and can result in active Ca^{2+} reuptake. Ca^{2+} pumps are not inhibited since RDSs stimulate Ca^{2+} dependent ATPase activity and also stimulate release from passively loaded SR (i.e. nonfunctional Ca^{2+} pumps). Furthermore, modulators of physiologic Ca^{2+} release (stimulation by adenine nucleotides and inhibition by ruthenium red, tetracaine, and Mg^{2+}) alter SH reagent induced Ca^{2+} release in a similar fashion. Thus, these agents appear to open a physiologic Ca^{2+} release channel via a specific interaction with SH sites on or adjacent to the channel. Covalent linkage of an easily identifiable label (e.g. biotin) to these SHs can then serve as a probe to isolate and identify these sites.

By analogy with skeletal muscle studies, a 106-kDa protein was isolated from canine cardiac SR, which shows immunoreactivity with monoclonal antibodies raised against rabbit skeletal 106-kDa Ca^{2+} release channel protein.

M-PM-F3

RYANODINE-AFFINITY COLUMNS PURIFY SULFHYDRYL-GATED 106-kDa Ca^{2+}-RELEASE CHANNELS BUT NOT "FEET" PROTEINS FROM SARCOPLASMIC RETICULUM VESICLES (SR).

M. Nigam, N.F. Zaidi, K. Shome, C. Lagenaur, and G. Salama. University of Pittsburgh, Department of Physiology, Pittsburgh, PA. 15261.

Ryanodine was coupled to epoxy-activated Shepharose 6B (Pharmacia) 100 mg ryanodine/3-ml of gel, pH 12, for 24 hrs, at 23°C. After coupling and washing, gels were stored in 1 M NaCl, 25 mM NaPipes, pH 7.1, at 4°C, until use. Measurements of [^{3}H]ryanodine indicated that 0.2-0.5 % of the ryanodine was linked to the beads (ie., columns contained 135-338 μM ryanodine). Heavy SR was solubilized (in 1 M NaCl, 1.6% CHAPS, 40 mM Tris-Maleate, 0.2 mM PMSF, 1 μg/ml leupeptin, pH 7.0-7.4, 1-5 mM ATP, and 100 μM free Ca^{2+}), incubated in the column for 2 h at 4°C, the run-through was collected, the columns washed 3-times with 10-ml of same buffer, then incubated and eluted 3-times with 3-ml of either: 10 mM NaCl, 40 mM Tris-Maleate or: 1 M NaCl, 40 mM Tris-Maleate, and 5 mM Mg^{2+}; plus protease inhibitors for 30 minutes at 4°C, to dissociate proteins immobilized on the columns. Fractions were analyzed for protein content by SDS-PAGE followed by silver staining, Western, and/or immuno-dot blots. Run-throughs contained 90% of the SR proteins, including 565-kDa feet proteins; washes 1-3 contained primarily ATPase, and elutions sulfhydryl-gated 106-kDa Ca^{2+}-release channels. Controls showed that a) sham columns (ryanodine substituted by glucose) did not selectively retain 106-kDa or other SR proteins, b) addition of 100 nM or 10 μM ryanodine to solubilized SR prior to ryanodine-affinity purification, blocked the binding of 106-kDa channels to the columns, and c) incorporation of 106-kDa eluted from the ryanodine column in planar bilayers resulted in Ca^{2+}-channel fluctuations, activated by mM ATP, Ca^{2+}, SH-oxidizing agents, inhibited by SH-reducing agents, Mg^{2+}, and blocked by ryanodine. Thus, the SH-gated 106-kDa Ca^{2+}-release channel is the receptor site for ryanodine.

M-PM-F4

UNIQUE PHOSPHORYLATION SITE ON THE CARDIAC RYANODINE RECEPTOR REGULATES CA^{2+} CHANNEL ACTIVITY.

D.R. Witcher, R.J. Kovacs, H. Schulman*, and L.R. Jones. Krannert Inst. of Cardiology, Depts. of Medicine and Pharmacology, I.U. Sch. of Med., Indpls., IN 46202, *Stanford Univ. Sch. of Med., Stanford, CA 94305.

The purpose of this study was to examine the role of multifunctional Ca^{2+}/calmodulin-dependent protein kinase (CaM K) in phosphorylating the cardiac ryanodine receptor (RR). We observed that the RR in cardiac junctional SR vesicles was an excellent substrate of CaM K, but that the RR of fast and slow skeletal SR vesicles was barely phosphorylated. In order to understand the significance of the preferential phosphorylation of the cardiac RR, we isolated and sequenced the cardiac phosphorylation site. A single phosphopeptide (RISQTSQVSVDAAHGYSP) was obtained, the sequence of which matched identically with residues 2807-2824 reported for the cardiac RR from cDNA analysis (Otsu *et al., J. Biol. Chem.* 265:13472, 1990). When compared with the corresponding region of the skeletal muscle RR, there were 9 mismatches, apparently accounting for the poor skeletal RR phosphorylation. Consistent with this, an antibody generated to this unique cardiac phosphorylation site reacted only with the cardiac ryanodine receptor on Western blots, and selectively immunoprecipitated only cardiac [^{3}H]ryanodine binding sites. Phosphorylation of the cardiac RR by CaM K activated the Ca^{2+} channel. Using the planar bilayer method, we observed that 3 μM CaM reduced p(open) 42%, whereas subsequent addition of CaM K increased p(open) 58%. We conclude that phosphorylation of serine 2809 provides a unique mechanism for preferential regulation of the cardiac isoform of the RR. Phosphorylation of the cardiac RR during β-adrenergic stimulation may increase Ca^{2+} efflux from the SR and contribute to the positive inotropic response.

M-PM-F5

INVOLVEMENT OF THE ~28-KILODALTON PROTEIN OF THE TRANSVERSE TUBULAR MEMBRANE IN EXCITATION-CONTRACTION COUPLING

T. Ohkusa[a], J.J. Kang[a], B. Antoniu[a], M.S. Rosemblatt[a], S.D. Jay[b], K.P. Campbell[b], and N. Ikemoto[a,c] (a. Dept. Muscle Res., Boston Biomed. Res. Inst., Boston, MA 02114; b. HHMI and Dept. Physiol. Biophys., Univ. of Iowa, Iowa City, IA 52242; c. Dept. Neurol., Harvard Med. Sch., Boston, MA 02115)

As shown recently (ref.1), the DHP receptor-specific agents (e.g. nifedipine and a monoclonal antibody directed to the α1 subunit) inhibit the slow phase of depolarization-induced Ca^{2+} release from SR in vitro with little effect on the fast phase. This suggests that the slow phase is mediated by the DHP receptor, while the fast phase by other protein(s). The following results suggest that the ~28 kDa protein, which is characteristic of the T-tubule membrane and is not a part of the DHP receptor (ref.2), is responsible for the mediation of the fast phase. Two monoclonal antibodies, mAb IXE112 (IgG→28 kDa protein or TS28, ref.2) and mAb TT2 (IgM→27.5 kDa protein, ref.3), were found to react with a common antigen. Effects of these antibodies on various kinetic parameters of the fast (f) and slow (s) phases of depolarization-induced Ca^{2+} release - the amounts of Ca^{2+} released (A_f and A_s) and the rate constants of Ca^{2+} release (k_f and k_s) - were investigated. Both antibodies (e.g. at 1:50 mAb:protein w/w) produced preferential inhibition of the fast phase leading to a significant reduction of k_f. The fact that the fast phase is inhibited preferentially by the antibodies directed to the ~28 kDa protein, while the slow phase by the DHP-specific agents, suggests that the ~28 kDa T-tubule protein and the DHP receptor are involved in two distinguishable signal transmission pathways, respectively.

(Supported by Grants from NIH and MDA).

Refs.: 1. Ohkusa, Smilowitz, and Ikemoto, Biophys. J. 57, 498a, 1990; 2. Jorgensen, Arnold, Shen, Yuan, Gaver, and Campbell, J. Cell Biol. 110, 1173, 1990; 3. Rosemblatt, Pirez, Antoniu, Reilley, and Ikemoto, Transduction in Biological Systems (Eds. Hidalgo et al.) Plenum, 371, 1990.

M-PM-F6

CLONING AND SEQUENCING OF HUMAN CARDIAC CALSEQUESTRIN.

Jing-Lun Wu and Terrence L. Scott, Dept. of Muscle Research, Boston Biomedical Research Institute, 20 Staniford St., Boston, MA 02114

Clones of calsequestrin have been isolated from a human cardiac cDNA library. The complete sequence of a 2737 bp calsequestrin cDNA clone has been determined. Northern blots probed with calsequestrin oligonucleotides indicate that this represents a full-length transcript.

The cDNA encodes a sequence of 399 amino acid residues, with a presumed signal sequence of 18 residues, in analogy with canine cardiac calsequestrin (Scott, B.T., et al., 1988). Similarly, the human transcript has a second open reading frame and contains two potential glycosylation sites. The mature cardiac protein is 21 residues longer than the human skeletal form and shows significant differences in amino acid homology from it (Scott and Ali, 1989). The human and canine cardiac proteins differ in length and have significant amino acid differences primarily at the COOH terminus.

The human cardiac calsequestrin has been overproduced in a bacterial expression system. The expressed protein is presently being purified and its properties determined. Supported by NIH GM32247 and an Established Investigatorship of the AHA to TLS.

M-PM-F7

COMPLETE SEQUENCE DETERMINATION OF THE CARDIAC SARCOLEMMAL (SL) 15-KILODALTON PROTEIN.

Cathy J. Palmer, Bruce T. Scott, and Larry R. Jones, Krannert Inst. of Cardiology, Dept. of Med., Ind. Univ. Sch. of Med., Indpls., IN 46202.

The 15-kilodalton protein (15K), a potential regulator of ion flux, is the major SL substrate for cAMP-dependent protein kinase (PK-A) and protein kinase C (PK-C) in myocardium. In the work described here, 15K was purified, sequenced, and cloned. 15K phosphorylated by PK-C was isolated from cardiac SL vesicles and analyzed by gas-phase amino acid (aa) sequencing. The N-terminus was not blocked and yielded aa residues 1-50. Overlapping proteolytic phosphopeptides yielded 22 additional residues at the C-terminus. A cDNA clone encoding 15K was identified using oligonucleotide probes and isolated from a canine cardiac λgt10 library. The clone was 654 bp long, containing a coding region of 279 bp flanked by 102 bp of 5' and 273 bp of 3' untranslated sequence. Both a polyadenylation signal and a poly(A) tail were present, suggesting the clone was a full-length copy of the mRNA. The deduced aa sequence verified that 15K contains 72 aa residues plus an N-terminal signal sequence of 20 residues. The mature protein has a Mr=8409. Analysis of the primary structure of the processed protein by hydropathic profiling identified a single hydrophobic domain of 20 uncharged residues sufficient to traverse the SL membrane. A stop-transfer signal containing three Arg residues and a Lys flanks the transmembrane segment on the C-terminal side, suggesting 15K is oriented in the membrane with its 35 C-terminal residues facing the cytoplasm. This C-terminal domain contains >90% of ^{32}P incorporated into 15K with several predicted posphorylation sites for PK-C, as well as sites for PK-A and Ca^{2+}/calmodulin-dependent protein kinase. Dephosphorylated 15K is remarkably basic, with a calculated pI of 10.3, in contrast to the phosphorylated forms of 15K, which have neutral or acidic pIs. The change in overall protein charge upon phosphorylation may reflect the mechanism of action of 15K, as suggested for the cardiac regulatory protein phospholamban.

M-PM-F8

AFFINITY & ACCESSIBILITY OF OCCLUDED Ca SITES ON SR ATPase.

Jose Amaral* and Carol Coan+, *Dept. of Biochemistry, Institute of Biomedical Science, Federal University of Rio de Janeiro, 21910 Brazil, and +Dept. of Physiology, University of the Pacific, San Francisco, CA 94115.

γ,β bidentate CrATP will form an exchange inert coordinate bond with a ligand at the catalytic site of the SR ATPase to produce a complex in which the Cr^{3+} links the enzyme to the phosphate moieties of ATP, trapping Ca^{2+} in an intermediate stage of transport where it remains occluded. We have titrated this complex with EGTA to obtain binding constants for the two occluded Ca^{2+} sites, and to characterize the degree of occlusion in terms of the release rate of the Ca^{2+}. We find the Ca^{2+} to be released from the two sites independently while they are retained in the high affinity state. The site with the higher affinity (Kd = .04 μM) is highly occluded ($t_{1/2off}$ = 120 min), while the site with the lower affinity (Kd = 6 μM) is much less occluded ($t_{1/2off}$ = 4 min) (all data at pH 6.8, 37 °C).

We have also been able to titrate the occluded sites directly, by first forming the CrATP-ATPase complex in the presence of EGTA. The high stability of the Cr^{3+} coordinate bonds allow this complex to be formed slowly, although it has the functional properties of the E-P formed with MgATP and Ca^{2+}. We then find the sites to bind Ca^{2+} independently (vs the cooperative binding observed before occlusion), with the highest affinity site binding Ca^{2+} without saturation of the second site.

This data gives some of the first evidence that the site with higher affinity exists independently of the site with lower affinity, although it remains highly occluded. It also gives one of the first independent measurements of the Kd's of the two sites (otherwise obtained from a best fit to the cooperative binding curve). Taken together our data suggest that the cooperativity normally observed in the cycle is due to the high degree of occlusion of the highest affinity site, which is reached in the initial state only after Ca^{2+} binds to the more exposed site of somewhat lower affinity.

M-Pos1

A DURABLE & PRECISE HYDRAULIC MICROMANIPULATOR BASED ON A COMPACT, STAGE - MOUNTABLE HUXLEY-STYLE SUSPENSION. John W Krueger, Albert Einstein College of Medicine, Bronx, N.Y. 10461

I describe a stable remote controlled micromanipulator that is easy to construct and has good dynamic capabilities. Small metallic bellows are used for hydraulic control, where all fluid connections are made by standard metal 1/16" HPLC fittings. The device is an inverted cradle suspension of folded lever arms, inspired by the principles utilized in the Huxley-style micromanipulator (J Physiol 157:5P, 1961). In my design, vertical motions have minimal cross-coupled horizontal error. Vertical error that arises at the extremes of displacement in the two horizontal axes due to the parallelogram suspension can be hydraulically corrected by the remote controller. Thus, in creating displacements that are mutually perpendicular, the position of the microtool more faithfully corresponds to the micrometer settings. Being compact, the device can be mounted on -or suspended over- a microscope stage. All planes of manipulation are brought near to the specimen, and the cantilevering of the microtool that i) is a source of vibration and ii) limits the load bearing in larger devices that can only be placed alongside the microscope is reduced. One device suits both right or left handed use. Working range is 1.6mm; with water, any error due to thermal expansion is ~1μm/°C. Performance was tested by the electronic detection of the position of a microtool (J. Gen. Physiol. 84: 475, 1986). Manual repositioning by micrometer action is better than <0.2μm: Overshoot is <0.2μm with rapid advancement of a 1# load, cantilevered at 6cm. The inelastic bellows and low mass of fluids permit good acceleration. Dynamic response was tested by backing a piezo-electric pusher against the end of one bellows opposite to its micrometer in the remote controller. With GE-SF96 silicone fluid (5cstk), the all brass device advanced a microtool ~1mm/s with 1μm overshoot in response to a 10μm step input by piezoelectric control. An aluminum device filled with water should be 2-3 times faster.

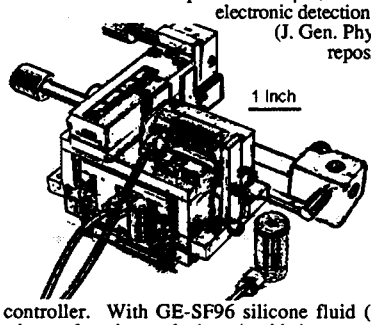

M-Pos2

CALCULATING APPARENT VALENCE OF MUSCLE PROTEINS USING A DONNAN SYSTEM: A CAN OF WORMS. **D. Maughan, R. Godt, J. Thomas, J. Hurley (Intro. by G. Webb) Dept. Physiology & Biophysics, U. Vermont, Burlington, VT 05405 and Dept. Physiology & Endocrinology, Med. College of Georgia, Augusta GA 30912.**

The electric field due to fixed proteins probably influences the cellular location of most mobile proteins, including glycolytic enzymes. This influence will of course vary with the enzyme's apparent valence, z, which is unknown. Here we estimate z using a defined Donnan system of polysaccaride "worms" (SeaKem HEEO agarose) bathed in salt solutions to which purified muscle proteins were added (10 proteins, 0.036 ug/ul). Potentials, U, between worm and bathing solution depended on ionic strength (IS) according to Donnan theory: U varied between -3.8 mV and -0 mV over the range 50-500 mM IS. The relative amount of each protein in the worm was measured by SDS-PAGE; steric exclusion was factored out by dividing the amount of each protein in the worm bathed in 50 mM IS solution by the amount in 500 mM IS (ratio denoted r). From Donnan theory, z = -(RT/F U) ln r. Of 11 glycolytic enzymes examined at pH = 7, T = 20°, about half distributed in accordance with Donnan theory and published isoelectric points (pI) (e.g., glyceraldehyde 3-P dehydrogenase, pI = 8.5, z = +3.1±1.2; pyruvate kinase, pI = 6.5, z = -0.9±1.7), whereas others did not (e.g., phosphoglucose isomerase, pI = 9.2, z = -1.8±1.0; lactate dehydrogenase, pI = 8.6, z = -4.7±2.5). The reasons for the discrepancies between observed and predicted sign of the valence in some cases remain obscure. **[Supported by NIH R01 AR38980 and NIH AR31636]**

M-Pos3

EFFECTS OF TRIMETHYLAMINE N-OXIDE (TMAO) ON CROSS-BRIDGE PROPERTIES OF SKINNED SKELETAL MUSCLE FIBERS.

M.A. Andrews, D.A. Martyn*, R.T.H. Fogaça, and R.E. Godt; Depts. of Physiol. & Endo., Medical Coll. GA, Augusta GA 30912, and *Physiol. & Biophys., Univ. of Wash., Seattle WA 98195.

Recently we (Fogaça *et al.*, *Biophys. J.* 57:546a, 1990) reported that TMAO protects skinned muscle fibers from the inhibitory effects of elevated ionic strength on maximal Ca^{2+}-activated force (Fmax). We suggested this might be due to stabilization of the actomyosin-ATPase by TMAO, as has been observed with other proteins (e.g., Arakawa & Timasheff, *Biophys. J.* 47:411-414, 1985). We investigated these effects further using detergent skinned fibers from rabbit psoas, measuring Fmax, stiffness (using 1 kHz oscillation), and the maximal velocity of shortening (Vmax, with slack test) at 10-15°C. Increasing ionic strength over the range 90-390 mM with K methanesulfonate progressively decreased both Fmax and stiffness. At any ionic strength TMAO (300 mM) increased both Fmax and stiffness proportionally. Vmax was similar at 165 and 240 mM, and was unaffected by TMAO. Rigor force from fibers initially put into rigor in a 0 MgATP solution (pCa 4) with 165 mM ionic strength was unaffected by subsequent changes of ionic strength over the range 90-390 mM, whereas rigor stiffness decreased monotonically with elevation of ionic strength. At all ionic strengths tested, addition of TMAO increased rigor stiffness without altering rigor force. Thus elevated ionic strength appears to inhibit cross-bridge attachment (in ATP-containing solutions) and to decrease the stiffness of attached cross-bridges. Both these effects of increased ionic strength are ameliorated by TMAO. (Support: NIH AR 31636 and HL 31962).

M-Pos4

FORCE-CALCIUM RELATION OF FREEZE-DRIED HUMAN FIBRES OF THE RECTUS ABDOMINIS MUSCLE AT DIFFERENT SARCOMERE LENGTHS. T. Blangé, F.A.M. van Kaam*, B.W. Treytel, C.R. van den Hoogenband# & J. de Vries$. Dept. Physiol, Univ. of Amsterdam, *Dept. Med. Phys. & Bioph., Univ. of Nijmegen, #St Anna Hospital,Geldrop & $Maasland Hospital,Geleen. The Netherlands.

Human skeletal muscle preparations of 20 mm in length and maximally 5 mm in diameter were dissected from the Rectus abdominis (RA) muscle of six patients undergoing current surgery. The muscle preparations were depolarized, frozen in liquid nitrogen and dried above silicagel at -25 °C during three weeks. Single fibres of 4-7 mm in length could easily be dissected from the dried preparations. Prior to activation the fibres were immersed in relaxing solution, first at 4 °C (pH=7.0) to prevent inclusion of air bubbles and subsequently during at least 5 minutes at room temperature (22 °C; pH=7.0). Single fibres were then incubated cyclically in high EGTA relaxing solution (20mM), low EGTA solution (0.2mM) and activation solution of a particular $[Ca^{2+}]$. At maximal activation fibres developed a tension of up to 250 kPa (2.5 kg/cm^2). Forces measured 1 minute after start of activation were used to determine the force-$[Ca^{2+}]$ relation. Hill-curves, in which T_{rel}, force relative to maximal force (at pCa 4.0), is taken to be $T_{rel} = [Ca^{2+}]^n/(K^n+[Ca^{2+}]^n)$, have been fitted as to K and n by means of a least mean square method. The resulting pCa_{50} (=-logK) and n values appeared not to depend on sarcomere-length in the range above 1.8 μm. The values derived so far for 9 fibres amounted to pCa_{50} (mean ± sd) = 5.9 ± 0.2 and n = 2.2 ± 0.4.

M-Pos5

FAST-TO-SLOW TRANSFORMATION OF MAMMALIAN SKELETAL MUSCLE: ANALYSIS AT THE SINGLE FIBER LEVEL. Peter J. Reiser, Jamil Jacobs-El, Brenda R. Eisenberg. Dept. of Physiology and Biophysics, Univ. of Illinois, Chicago, 60680.

Mammalian skeletal muscle undergoes transformation with respect to contractile protein isoform expression and contractile properties following changes in motor activity patterns. Only a few studies have examined the relationships between specific changes in activity, isoform expression and contractile properties. The objectives of the present study were to impose an alteration in activity which causes fast-to-slow transformation on the normally fast-twitch adult rabbit tibialis anterior (TA) muscle and to examine the adaptive responses at the single fiber level. The right TA muscle was continuously stimulated in situ for 21 days with electrical pulses via the peroneal nerve. The contralateral TA and slow soleus muscles served as controls. A total of 30 skinned fibers were studied. The maximal shortening velocity (V_{max}) and tension-generating ability (i.e., peak isometric tension/fiber cross-sectional area, P_o/CSA) were measured ($\bar{x} \pm SD$):

	Control TA	Stimulated TA	Soleus
No. of fibers:	12	12	6
V_{max} (fl/s):	377 ± 0.34	1.53 ± 0.77	0.94 ± 0.10
P_o/CSA (kN/m^2):	168 ± 0.32	140 ± 30	199 ± 32
CSA ($10^3 \mu m^2$):	2.83 ± 1.31	2.38 ± 0.76	2.89 ± 0.52

The largest fibers in control TA had a slightly greater V_{max} (3.95 fl/s) than the remaining fibers (3.58 fl/s). The large fibers in stimulated TA had a much lower V_{max} (1.07 fl/s) than the small fibers (2.45 fl/s). Immunochemistry with a slow myosin antibody showed two sets of fibers in stimulated TA: small- to intermediate-sized fibers with variable stain intensity indicating slow and mixed myosin composition and another set of large slow fibers. SDS-PAGE of multifiber samples of stimulated TA revealed shifts in myosin heavy and light chains and in troponin (Tn) subunits. The shift toward slow TnT appeared to be more complete than that in TnI. Single fiber analysis has identified two sets of fibers in transforming TA muscle with distinct contractile properties and isoform expression. Supported by NIH and MDA.

M-Pos6

WING BEAT ANALYSIS OF DROSOPHILA MELANOGASTER. M. Yamakawa & D. Maughan, Dept. of Physiology & Biophysics, U. of Vermont, Burlington, VT 05405.

Genetic mutants with altered expression or modification of contractile and regulatory proteins in asynchronous indirect flight muscles (IFM) exhibit a range of flight impairment. Wing beat analysis of flight impaired mutants can provide a link between flight ability and the underlying changes in molecular structure. Wing beat depends on both the energy supply of the contractile elements and the resonant (viscoelastic) properties of the flight muscle, cuticle, and the load on the wings. To characterize the resonant properties of the system, we measured the primary peak frequency, f, and a unitless index of the sharpness of the peak, q, in the frequency spectral profile of the wing beat. Wing beat was recorded by an optical tachometer (Unwin & Ellington, 1979, J. Exp. Biol. 82: 377) and the frequency components extracted by a spectrum analyzer after signal conditioning. We calculated q by dividing f by its half-power frequency band width. Low q reflects a highly damped (i.e., less efficient) system. For typical wild type Canton S, f;q = 210 Hz;80 and 165 Hz;60 at 22^o and 13^{o}C. For E38, a IFM specific flight-impaired mutant (Warmke et al., 1989, Genetics 122: 139), f;q= 140 Hz;30 and 155;30 at 22^o and 29^{o}C. CS still flies at 13^{o}C and E38 is still flight impaired at 29^{o}C, although at these temperatures they have comparable wing beat frequencies; q values, however, differ by a factor of two, suggesting that q may be a good index of flight impairment. These results suggest that f and q can, as a first approximation, provide both an index of IFM-related flight function and a quantitative link to the underlying changes in molecular structure. [Supported by NIH RO1 AR40234]

M-Pos7

IDENTIFICATION OF A SOURCE OF OSCILLATIONS IN STRIATION SPACING ESTIMATED BY LASER DIFFRACTION DURING RAMP SHORTENING IN MUSCLE. K. Burton* and A.F. Huxley†
*MRC Muscle and Cell Motility Unit, King's College London and †Physiological Laboratory, Cambridge University, U.K.

A source of oscillations superposed on an otherwise linear sarcomere length change estimated by laser diffraction has been characterised. The diffraction patterns were obtained from resting and active skinned single rabbit psoas fibers at 5^{o}C. Several features of the oscillations confirm those of Altringham, Bottinelli, & Lacktis (1984, Nature 307:653): 1) The amplitude and number of oscillations for a given length change are independent of velocity, 2) these are accompanied by oscillations in intensity at the same frequency, and 3) the period of each oscillation is about the time required for one striation to pass the center of the beam. The amplitude of these oscillations was a strong function of the amount of light scattered from a surface 0.1-1 mm below the fiber. The amplitude of oscillation was 3-5 nm for a scattered intensity below 0.5% the diffracted intensity, and was reduced either by reducing the scattered intensity or by increasing the separation between the scatterer and fiber. Oscillations of this kind are expected to result from interference of scattered light with light diffracted by the fiber, causing variation of intensity within the diffracted beam so that its centroid is displaced. The displacement of the centroid will vary with the relative phase of the scattered and diffracted light and, at the first diffraction order, this shifts by one cycle per sarcomere length movement of the fiber. Theory for the case of a point scatterer gave the correct order of magnitude for the effect. As a further test, a grating was translated through the beam. The apparent grating spacing also exhibited oscillations with characteristics similar to those obtained from fibers, but with a lower amplitude. Oscillations of larger amplitude were observed if the pattern between orders was monitored, indicating that diffuse scatter from the grating also contributes. Our observations may account for regular series of oscillations observed by Granzier & Pollack (1985, J. Physiol. 362:173) using laser diffraction and those observed and eliminated by Goldman (1987, Biophys. J. 52:57).

M-Pos8

SHORTENING VELOCITY AND POWER OUTPUT OF SKINNED MUSCLE FIBERS FROM MAMMALS HAVING A 25000-FOLD RANGE OF BODY MASS
C. Y. Seow and L. E. Ford, Department of Medicine, The University of Chicago, Chicago, IL 60637

The shortening velocity of single skinned fast and slow skeletal muscle fibers were measured at 5-6 °C in five animal species having a 25,000-fold range of body size (mouse 20g, rat 200g, rabbit 2kg, sheep 55kg, cow 160 & 500kg). While fiber diameter and isometric force showed no dependence on animal body size, maximum shortening velocity in both fast and slow fibers and maximum power output in fast fibers were found to vary with the -1/8 power of body size. Maximum velocities of fast fibers ranged from 0.79 $\mu m \cdot s^{-1} \cdot$ half-sarcomere^{-1} in the large cow to 2.85 in the mouse. With slow fibers the values for large cow and mouse were 0.38 and 1.61, respectively. Maximum power output in slow fibers showed a slightly greater (-1/5 power) dependence on body size. The isometric force produced by the fibers was correlated (r=0.74) inversely with fiber diameter. For all sizes of animal the average maximum velocity was 1.7 times faster in fast fibers than in slow fibers. The large difference in mechanical properties found between fibers from large and small animals suggests that properties of the contractile proteins vary in a systematic manner with the body size. These size dependent changes can be used to study the correlations of structure and function of these proteins. Experimental results also suggest that the different metabolic rates observed in different sizes of animals could be accounted for, at least in part, by the difference in the properties of the contractile proteins.
(Supported by USPHS Grant HL44398 and a MRC of Canada Fellowship).

M-Pos9

FORCE-VELOCITY MEASUREMENTS IN WHOLE FROG SARTORIUS MUSCLE AT SHORTENING SPEEDS UP TO 8 Vmax

John S. Seo, Peter C. Krause, Thomas A. McMahon. Division of Applied Sciences, Harvard University, Cambridge, MA, 02138.

We performed isovelocity shortening experiments on whole frog sartorius muscle at lengths well above rest length and over a range of velocities corresponding to 0.2 to 12 muscle-lengths/sec. The tension measured in the muscle remained positive throughout each shortening experiment. Data was collected at two temperatures, 2 ± 1 and 12 ± 1 °C. By subtracting the tension record of an unstimulated run from the tension record in a fully-stimulated run, the apparent developed tension of a muscle throughout the ramp shortening was measured at a given velocity. Under the assumption that the passive tension is not significantly affected by stimulation, the apparent developed tension was interpreted to be due solely to activated crossbridges. This assumption is a point of controversy [Morgan, Claflin, Julian, Biophys. J., 57,1001-1007 (1990)]. Analysis of the apparent developed tension yielded a force-velocity curve which extends to velocities 8 times higher than Vmax, the velocity at which the muscle's apparent developed tension was zero. This force-velocity curve does exhibit apparent negative tension above Vmax, but not as predicted by the Hill 1938 Curve: $T'=(1-v')/(1+v'/k)$, where k is the Hill constant, and T' and v' are normalized tension and velocity. The data is well-fitted within the entire velocity range by a modified Hill constant $k=1/(p+qv')$, where p and q are constants with approximate values of 3 and 4.

M-Pos10

DESIGN OF MUSCULAR SYSTEMS. Lawrence C. Rome and Andrzej A. Sosnicki. Biology Dept, Univ of Penn, Philadelphia, PA 19104

The basic components of muscle contraction are understood. The ones that can be varied (e.g., actin filament length, maximum velocity of shortening [V_{max}], and fiber orientation) can be considered design parameters. What are the rules (design constraints) that govern how these design parameters vary? A first constraint is the extent of myofilament overlap. We know from isolated muscle experiments that force generation is a function of myofilament overlap. We found that the myofilament lengths of carp red and white muscle are the same as in frog. During slow swimming, carp red fibers are used at sarcomere lengths of 1.91-2.22 μm, where no less than 96% maximal tension is generated. If the red fibers powered the extreme "escape response", they would have to shorten to 1.45 μm. Instead, the white fibers are recruited and due to their helical orientation and 4-fold higher gear ratio, they can power the response while shortening to only 1.75μm (where they generate no less than 85% maximal tension. Hence, the white fibers can power the "escape response" and the red ones power slow swimming, while each works at near optimal overlap and force generation. A second important design constraint is V/V_{max} (where V is the shortening velocity of fibers). We know from isolated muscle experiments that maximum power generation and maximum efficiency are achieved over a narrow range of V/V_{max} values (0.2 to 0.4). Carp power their slow swimming with red muscle (low V_{max}) and their fast movements with white muscle (high V_{max}) while each works within this optimal range of V/V_{max}. Further, if temperature is dropped by 10°C, the 1.6-fold drop in V_{max} of red muscle is matched by a 1.6-fold drop in maximum V (and swim speed), so that the muscle operates over the same V/V_{max} at each temperature. In addition, our experiments on fast swimming scup show that they use their red muscle over precisely the same V/V_{max} as the slow swimming carp. Finally, in mammals, the scaling of V with body size ($M_b^{.16}$) is matched by a similar scaling for V_{max} ($M_b^{0.18}$). Thus muscles operate at the same V/V_{max} values in small and large mammals. Hence, in all 4 cases examined, V/V_{max} is maintained constant and thus is a constraint. NIH AR38404.

M-Pos11

MECHANICAL ACTIVITY OF CRUSTACEAN MUSCLE: SOME PHYSIOLOGICAL ASPECTS. M.C. García and C. Zuazaga. Inst. of Neurobiology. U. of Puerto Rico Med. Sci. Campus, San Juan, P.R. 00901. U.S.A.

There is relatively little information about the muscle physiology in crustacea as compared with vertebrate muscle. We examined some characteristics of the striated muscle of freshwater crustacean Atya lanipes. Isometric tension developed by bundles of 15-20 fibers at 20-22°C was recorded by a Cambridge Tech. transducer whose output was stored in a VCR; electrical estimulation was produced via two parallel platinum electrodes. Van Harreveld's solution was used. Mechanical responses to single or tetanic stimuli were completely abolished in calcium free solution. Caffeine (3 - 4 mM) produced oscillatory mechanical responses that were evident during the plateau phase of the caffeine contracture. Caffeine contracture stronglydepended on external calcium: peak tension of these contractures decreased to ca. 20-30% (n = 3) in Ca^{2+}-free solutions. Potassium contractures were produced by isotonic replacement of NaCl with KCl. The relation between tension and log $[K^+]_o$ rose along an S-shaped curve when K^+ was raised. The contracture threshold was about 20 mM, half maximum tension was reached at ca. 80 mM (n = 7-9). The time course of contractures was typical of tonic muscles of vertebrates. Decreasing external Na^+ to 34% (replaced with n-methyl-glucamine) induced contractures and potentiation of tetanic (20 Hz) response, these contractures increased when external Na^+ was completely eliminated. Finally, the relation between tetanic tension and sarcomere length was studied: maximum tension was obtained at S.L. ca. 10.6 μm (n = 3). These results suggest that tension development in this muscle: a) depends strongly on both extracellular Ca^{2+} and Na^+; 2) responds to $[K^+]_o$ in a concentration dependent manner; 3) responds to caffeine, which probably triggers a Ca induced-Ca release mechanism; 4) tension depends on sarcomere length in agreement with the sliding filament theory.

Supported by NIH grant No. NS07464.

M-Pos12

VARIATION OF CALCIUM SENSITIVITY OF SKINNED RABBIT PSOAS FIBERS AT LONG SARCOMERE LENGTHS IS NOT RELATED TO THE CHANGE IN LATTICE SPACING. B.H. Bressler and L. Morishita, Department of Anatomy, University of British Columbia, Vancouver, B.C.

In a previous report from our laboratory (Biophys. J., 57, pg. 539a) we demonstrated that the calcium sensitivity of skinned skeletal muscle fibers was altered at different sarcomere lengths. For stretched fibers (>2.2μm) we proposed that the altered sensitvity was related to sarcomere length but not necessarily the compression of the lattice spacing. The current experiments were designed to further investigate this assumption. Force-pCa curves were obtained from skinned rabbit psoas fibers at sarcomere lengths of 2.2μm and 2.6μm in solutions containing 1%, 3%, or 5% Dextran or 3% PVP. Compression of the filament lattice spacing with Dextran or PVP did not result in a shift of the force-pCa curve. The exception to this was a moderate shift of the curve, indicating increased calcium sensitivity, in fibers held at 2.6μm and activated in a solution containing 3% PVP. There was no effect of 3% PVP seen on the force-pCa relation in fibers at 2.2μm. Contrary to the report of Martyn & Gordon (JMRCM, 9:428-445, 1988) these results would support our previous findings that the change in calcium sensitivity of skeletal muscle fibers at long sarcomere lengths cannot be accounted for by a change in the lattice spacing. (Supported by the MRC)

M-Pos13

LENGTH-TENSION RELATIONSHIPS DURING SHORTENING OF TIBIALIS ANTERIOR AND SEMITENDINOSUS MUSCLE FIBERS OF THE FROG.

DR Claflin, DL Morgan* and FJ Julian, Department of Anesthesia Research Labs., Brigham & Women's Hospital, Boston, MA 02115; *Monash University, Clayton, Victoria, Australia.

Bagni et al. (*J. Physiol.* 401:581-595, 1988) reported that the plateau of the length-tension (l-t) relationship of fibers from the tibialis anterior (TA) muscle occurs over a range of sarcomere lengths approximately 0.10μm shorter than for fibers from the semitendinosus (ST) muscle. They pointed out that this difference would be expected if the thin filaments of the TA fibers are approximately 0.10μm shorter than those of the ST fibers. In this case, the descending limb of the l-t relationship should be similarly displaced. We recently reported a novel technique for determining the l-t relationship by making tension measurements during shortening at constant velocity (Claflin, Morgan & Julian, *Biophys. J.* 57:548a). By measuring tension during shortening, the complications due to sarcomere non-uniformities are circumvented, without complex length-clamping procedures, by simply avoiding the large change in slope in the force-velocity relationship about zero velocity. Constant velocity (ramp) shortening movements were applied 500ms after the onset of a fixed-end tetanic contraction using fibers isolated from the dorsal head of ST muscles and the ventral head of TA muscles from the frog (*R. temporaria*). Ramp rates were 10, 20, 30 & 50% of unloaded shortening velocity as measured at the plateau of the l-t relationship. Ramps at each velocity were applied from a series of sarcomere lengths ranging from 2.3μm to 3.0μm. The tension was plotted against sarcomere length with the four values of velocity as a parameter. For each velocity and both types of fiber, the tension measured during shortening was a linear function of sarcomere length over this range. For each fiber, four straight lines with a common sarcomere length intercept were fitted, each slope being chosen to minimize the sum of squared deviations of that line from the points for that velocity, and the intercept chosen to minimize the total sum of the squared residuals over all the points. The averages of the best-fit intercepts were 3.65±0.02 for the ST fibers and 3.53±0.01μm for the TA fibers (means±SEM, n=6). We conclude that the difference that has been reported between the plateaus of the l-t relationships of fibers from these two muscles also exists for the descending limb and the maximum length for tension generation, consistent with a difference in thin filament lengths within the same animal. Support: NIH grants AR07972 (DRC) and HL35032 (FJJ).

M-Pos14

SMALL SHORTENING HAS SIMILAR FORCE-AUGMENTATION EFFECT IN FIBER-ISOMETRIC AND IN SARCOMERE-ISOMETRIC TETANI. Arie Horowitz, Manfred H. P. Wussling and Gerald H. Pollack, Center for Bioengineering WD-12, University of Washington, Seattle WA 98195.

At the same initial length, isometrically contracting fibers produce significantly higher forces than sarcomere-length clamped fibers. The common explanation for the higher fiber-isometric force is inhomogeneity: sarcomeres at the fiber ends undergo large shortening and climb up the descending limb of the force-length relation. However, we and others (Burton *et al.*, 1989) have observed that, except for minute initial shortening, sarcomeres located in an intermediate zone between the center and the ends of the fiber remain isometric during most of the tetanus. These "intermediate" sarcomeres undergo only small shortening of less than 3% at the beginning of the tetanus, at a speed of 0.2 to 2.0 μm/s-sarc. The magnitude and speed of shortening are similar to the releases we previously imposed on length-clamped sarcomeres (Horowitz and Pollack, 1990). Such releases induced a significant augmentation of the subsequent steady tetanic force level. The force-length relation we constructed for the "intermediate" sarcomeres resembles the force-length relation reported by other investigators for fiber-isometric tetani: at sarcomere-length of 3.2 μm, for example, the fiber-isometric tetanus produced 140% more force than the sarcomere-isometric tetanus. It appears that slight pre-shortening can account for the high force production both in fiber-isometric tetani and in sarcomere-isometric tetani in which the isometric phase is preceded by release.

M-Pos15

FORCE INHIBITING EFFECT OF A SYNTHETIC TnI-PEPTIDE, AND MASTOPARAN IN MUSCLE: *MECHANISM OF THIN-FILAMENT COOPERATIVITY*

ÁRVIND BABU AND JAGDISH GULATI, *Albert Einstein College of Medicine, Bronx, NY*

To study the mechanism of the interaction between adjacent TnC molecules on thin-filament cooperativity, we have compared the effects of three force-inhibiting agents acting via TnC: (1) mastoparan, a natural peptide (INLKALAALAKKIL), binds an unspecified TnI-interacting region of TnC, (2) a synthetic TnI-peptide (GKFKRPPLRRVR; gift of J Van Eyke & R Hodges) binds the Ca-dependent residues 90-100 on TnC, and (3) trifluoperazine (TFP), acts by binding hydrophobic patches of TnC. pCa-force relations of skinned rabbit psoas fibers were measured. Concentrations of the inhibitors were selected to give 30% force. The activation curves with mastoparan and TnI-peptide were found to be shifted towards higher free Ca (by 0.3 pCa units), similar to TnC extracted fibers. With trifluoperazine, on the other hand, there was no rightward shift. Similarly, the Hill coefficient (index of cooperativity) was one half with the peptides, as with partial TnC, but in contrast we found no decrease in cooperativity with trifluoperazine. The results indicate that cooperative interaction between the TnC-TFP molecules on the thin-filament strand was normal despite the inability to switch-on force-producing cross-bridges. In contrast, the peptide-inhibitors completely inactivated TnC. The results suggest that the interaction between TnC molecules requires fully active Ca-binding species to mediate cooperativity in skeletal and cardiac muscles, and further support the earlier results with the inactive mutant CBM2A (Gulati: *J.Physiol.* 420,139P,1990). [Supported by NIH & NYH]

M-Pos16

ATP DEPLETION DECREASES PCR USE AND ACID FORMATION IN SKELETAL MUSCLE CONTRACTING IN SITU. J. M. Foley, S. J. Harkema, and R. A. Meyer.

ATP was reduced by half in rat gastrocnemius muscle by repetitive tetanic stimulation (1 Hz @ 100 Hz, 100 ms for 3 min, 2 bouts separated by 5 min). ATP recovery from IMP was blocked by administration of the adenylosuccinate synthetase inhibitor hadacidin (N-formyl-N-hydroxyaminoacetate, total dose 300 mg/kg, ip). In vivo NMR spectra and chemical analysis confirmed that ATP was depleted by over 30% in hadacidin-treated muscles 75 min post-stimulation compared both to nonstimulated muscles and to identically-stimulated and recovered muscles in saline-injected controls. Post-recovery PCr content and peak isometric twitch tension were not different between groups ($p > .05$). During a subsequent 8 min of 0.75 Hz twitch stimulation, decreases in PCr and increases in calculated cytoplasmic ADP were smaller in ATP-depleted compared to control muscles, although peak twitch force was unchanged. Time constants for PCr hydrolysis and resynthesis were 30-60 s longer in ATP-depleted muscle.

In muscles subjected to a final tetanic bout, ATP declined 50% in controls, but was reduced no further in muscles already ATP depleted. PCr hydrolysis was again greater in controls, and acidification was much more extensive in controls ($\Delta pH = -0.55 \pm 0.08$ (mean ± SE, n=5) vs. -0.17 ± 0.02 in depleted muscles). Total force production over the 3 min was not different between groups, although the ATP-depleted muscles exhibited an initial 10-20 s staircase of tetanic force. This phenomenon had also been observed in both control and hadacidin groups in the second of the two initial tetanic bouts, but was not seen in the final tetanic stimulation in recovered controls.

These results indicate that depletion of about half the ATP content of fast-twitch muscle may be associated with increased efficiency of isometric force development.

M-Pos17

A COMPARISON OF FATIGUE IN THE SOLEUS MUSCLE FROM ADULT AND AGED FEMALE MICE.

S.M.Ronaldson, S.I.Head and D.G.Stephenson;
La Trobe University, Melbourne, Australia, 3083.

The skeletal muscle fibre population in mammals is known to change with age. In the muscles of aged mammals there is an increased proportion of slow oxidative fibres. The aim of the study was to characterize the profile of fatigue and recovery from fatigue in the soleus muscle from adult (3-4 months; C57BL10) and aged (26 months; C576J) female mice.

The soleus muscles have been tetanically stimulated, at 100 Hz for 1 s with supramaximal pulses (1 ms width), in Krebs physiological saline at 19 - 22 C. No significant change ($P > 0.05$, t-test) has been observed in the tetanic tension of the soleus muscles from adult (mean ± s.d: 28.6 ± 9.0 N/cm^2) and aged (32.3 ± 7.5 N/cm^2) mice. Cross-sectional area has been calculated by dividing the muscle mass by muscle density and muscle length.

Fatigue was induced by tetanically stimulating the muscle every 2 s until the tetanic force decreased to 50% of the initial value. There was a linear decrease in tetanic force during fatigue of the soleus muscle. More tetani were required in the soleus from the aged animal (41 ± 5) to reach 50% of the initial force than in the soleus from the adult animal (35 ± 7) to induce this level of fatigue, however the difference was not statistically significant ($P > 0.05$). The muscles generally fully recovered (106 ± 10 %) from fatigue and recovery was measured as the time to 50% (half-time) of the final recovery force. The half time recovery was 1.67 ± 0.55 mins and 1.60 ± 0.55 mins for the soleus muscle from the adult and aged mice respectively. This recovery result was not statistically significant ($P > 0.05$).

M-Pos18

ALTERATION OF THE CREATINE KINASE ISOZYME DISTRIBUTION BY OVEREXPRESSION OF THE B SUBUNIT IN TRANSGENIC MOUSE MUSCLE.

J. Brosnan, S. Pattabhiraman, T. Van Dyke* and A. Koretsky.
Dept. Biol. Sci., Carnegie Mellon Univ. and *Dept. Biol. Sci., Univ. of Pittsburgh, Pittsburgh, PA 15213.

Expression of the different genes (M, B and mitochondrial) of creatine kinase is regulated in a developmental and tissue specific manner. The protein products of the M and B genes dimerize to form the active enzyme (MM, MB and BB) whereas the mitochondrial form is believed to function as an octomer. The existence and localization of the various isozymes within muscle has resulted in the proposal of a creatine kinase shuttle. This shuttle is believed to couple the efficient formation and utilization of ATP within the working muscle. The subcellular localization of creatine kinase isozymes are postulated to be essential to the shuttle. The CK_{mito} form is located between the mitochondrial membranes and the dimeric CK_{mm} is at the M-line of the myofibril. In vitro studies on stripped myofibrils indicate that neither CK_{BB} nor CK_{MB} can bind at the M-line in mammalian systems. In order to investigate the role and validity of the creatine kinase shuttle we have produced transgenic mice which overexpress the B isozyme under the control of the rat skeletal -actin promoter. Positive mice were identified using the polymerase chain reaction and the integrity of the transgene determined by Southern blot analysis. Isozyme analysis revealed that there were elevated levels of MB and BB within the skeletal muscle of the transgenic animals. The level of MM was reduced. These results show that the rat -actin promoter is sufficient to direct expression of high levels of the B subunit to mouse skeletal muscle. In addition, the B subunit is stably incorporated into active creatine kinase leading to a switch in isozyme distribution in muscle. These mice are currently being investigated to determine the effects of this isozyme shift on the physiology and biochemistry of the transgenic muscle.

M-Pos19

CALCIUM REQUIREMENT FOR ALUMINOFLUORIDE INHIBITION OF SKINNED MUSCLE FIBER FORCE.

P.B. Chase and M.J. Kushmerick, Depts. of Radiology and Physiology & Biophysics, Univ. of Washington, Seattle, WA 98195

Metallofluoride complexes, such as aluminofluoride (AlF_x), form stable complexes with G-proteins and GDP and are thought to be high-affinity analogs of inorganic phosphate (Pi) (Chabre, 1990, *TIBS* **15**:6). AlF_x is also a potent inhibitor of skinned muscle fiber force. Adding 10 mM NaF and 0.01 - 3 mM $Al(NO_3)_3$ to activating solution (pCa 4 - 4.5, pH 7.1, 12°C) reversibly inhibited steady-state force; recovery from inhibition occurred slowly ($t_{0.5}$ ~ 4 min). The extent of inhibition was a function of the amount of Al added, with maximum inhibition >96%. Unloaded shortening velocity, determined by the slack test, was also inhibited by AlF_x but to a lesser extent than force. The onset of and recovery from inhibition were slower in relaxing conditions (pCa >8) than at full activation; the kinetics of AlF_x binding to and dissociation from its inhibitory site were enhanced during crossbridge cycling, as with orthovanadate (Vi) (Dantzig & Goldman, 1985, *J. Gen Physiol.* **86**:305). Long-lived inhibition in relaxing conditions is similar to S1, with trapped Vi, in the absence of interaction with actin (Goodno, 1979, *PNAS* **76**:2620; Goodno & Taylor, 1982, *PNAS* **79**:21). Enhancement of the recovery rate from inhibition by active crossbridge cycling is similar to the increased rate of Vi release from S1 in the presence of actin (Goodno & Taylor, 1982; Dantzig & Goldman, 1985). The results are consistent with AlF_x being a Vi-like analog of Pi which inhibits the force-generating interaction of actomyosin in skinned fibers.

Supported by NIH grant HL31962.

M-Pos20

NON-UNIFORM VOLUME CHANGES IN ISOLATED FROG SKELETAL MUSCLE FIBERS DURING ISOMETRIC TETANI: DETECTION BY HIGH-SPEED, IMAGE-INTENSIFIED DIGITAL MICROSCOPY.

V. Arlene Morris, Laura A. Quesenberry, Ian R. Neering* and Stuart R. Taylor*, Department of Pharmacology, Mayo Foundation, Rochester, MN 55905.

We used isolated, intact, frog skeletal muscle fibers and a high-speed, intensified, digital imaging system to measure cross-sectional area along 1 mm lengths of a fiber while simultaneously recording tendon-to-tendon tetanic force. Rapid volume changes and active force developed immediately upon excitation. Cross-sections along the axis of resting cells were compared with the same sections during the plateau of contraction. Imaging was confined to the central third of the cells (4-7 mm long) where axial force was maximum, constant, and isometric as opposed to the ends which were conical, covered by tendons, and shorten even when the central portion is isometric. Fibers selected for detailed analysis were (1) isolated and stimulated at least 18 hours before a complete experiment, (2) showed small (<3%), reproducible axial translations during the tetanic plateau, and (3) maintained constant tension (< 3% change) during the plateau. Two-dimensional images were made every 25 um along 25-50% of a cell's length and 17 of the 19 tetani selected for this report showed that volume increased between about 5 and 40% (average 20%) during an isometric tetanus. Patterns of non-uniform changes were closely reproduced in each contraction with no relation to the duration of a brief tetanus (<20 sec), were unique and reproducible along the cell, and not predicted by the cell's resting area or shape (circularity). As previously proposed from EM analysis, the Z disc expands when cross-bridges are bound and there must be a perpendicular component to tension (Goldstein et al., 1988. J. Gen. Physiol.92:113). Our data on live, intact cells imaged at high speed support this idea.

Supported by the Australian NH & MRC (IRN), the NIH NS 22369, NSF DMB-85034964 and Pittsburgh Supercomputer Center DCB-890009P (SRT).

M-Pos21

OPTICAL ELLIPSOMETRY STUDIES OF THE CROSS-BRIDGE ORIENTATION IN INSECT FLIGHT MUSCLE AT LOW IONIC STRENGTH. S. Shen, R.J. Baskin, and Y. Yeh, Departments of Applied and Zoology, University of California, Davis, CA 95616

Characterization of the orientation and distribution of myosin cross-bridge at low ionic strength is of interest since the equilibrium state with weakly attached cross-bridges at low ionic strength has been proposed to be a normal transient step in the cyclical interaction of myosin heads with actin and ATP during contraction. Measurements sensitive to the cross-bridge orientation in chemically skinned single fibers of the dorsal, longitudinal muscle of the insect *Lethocerus colessicus* (full overlap SL = 2.95 μm) have been performed under low ionic strength conditions using laser diffraction ellipsometry. Determination of both the total birefringence, Δn, and the differential field ratio, DFR, is necessary for complete characterization of the optical polarization state. Changes in the elliptical polarization state of the diffracted light from resting fibers were recorded when the ionic strength was lowered from μ = 113 mM (normal resting state) to μ = 36 mM. Changes were also recorded on the same fibers for the transition from normal μ resting state to normal μ rigor state. For the transition from the resting to the rigor state at normal ionic strength, a decrease of 3.8 ± 0.7% (mean ± s.d., n = 20) in birefringence and a decrease of 0.025 ±.004 in DFR value were recorded. For the transition from normal μ resting state to low μ resting state, the decrease in birefringence was 2.7 ± 0.8% and a decrease in DFR of 0.013 ± .003 were measured. A significance level of $p < 0.05$ was achieved. On applying our theoretical model to the above data, we found the average cross-bridge orientation at low ionic strength was intermediate between rigor (considering both lead and rear cross-bridges) and the averaged angle of cross-bridges in the resting state. If we assume the average angle for these weakly attached cross-bridges to be 90°, the number of weakly bound myosin heads should be less than 50% with the remaining heads in a relaxed state. Correlation between stiffness measurements and optical data will be further discussed.

M-Pos22

DIFFRACTION ELLIPSOMETRY STUDIES OF SKELETAL MUSCLE TRANSIENTS. W. L. Kerr, R. J. Baskin, and Y. Yeh, Graduate Group in Biophysics, Depts. of Zoology and Applied Science, University of California, Davis, California 95616

We used the technique of diffraction ellipsometry to study cross-bridge orientation in actively contracting, single skeletal muscle fibers. The polarization state of light scattered into the first diffraction order is described by two parameters: the differential field ratio (r), which describes the difference in amplitudes between orthogonally propagating field vectors, and the relative phase or birefringence (Δ n) between those fields. In this study, we report on changes in the differential field ratio. These changes can be related to structural features of the muscle by modelling the intrinsic and form contributions they present to the optical anisotropy.

Decreases in r were observed for fibers upon tetanic stimulation, with a time constant that leads tension development . The size of the change diminishes with increasing sarcomere length. We have also observed transient decreases and subsequent recovery in r upon quick stretch or release of contracting muscle. For releases of 60Å per half sarcomere, r decreased an average of 10% simultaneous with the length step. Rapid and slow recovery phases of r were seen for releases, but only slow recovery was seen in stretches. These results will be discussed in terms of current models, particularly focussing on orientations of S-1 and S-2.

M-Pos23

THE EFFECT OF THIN FILAMENT REMOVAL BY GELSOLIN ON ELASTIC PROPERTIES OF INSECT MUSCLE. Henk Granzier & Kuan Wang, Chem. Dept., Clayton Fndt. Biochem. Inst., University of Texas, Austin, TX 78712.

We have recently reported the protein composition and static and dynamic stiffness of several insect muscles (Biophys, J., 57, 554a) with the aim to elucidate the mechanical function of giant cytoskeletal proteins. In this work we investigated the potential contribution of thin filaments to the mechanical properties of passive insect muscle by studying fibers that have been treated with gelsolin to selectively remove thin filaments (Funatsu et al. 1990. J. Cell Biology, 110, 53-62).

Single fibers from flight and leg muscles of giant waterbug (*Lethocerus griseus)* and honey bee (*Apis mellifera*) were mechanically skinned and force, fiber length, and sarcomere length were measured under relaxing, rigor and activating conditions (Granzier et al., 1987, J.Muscle Res. Cell Mot., 8, 242). Static stiffness was determined after a ramp-like slow stretch and a 3 min period of stress-relaxation. Dynamic stiffness was measured continuously by stretching the fiber sinusoidally at 2 KHz (amplitude 0.1% of the slack length) and by varying the frequency at set periods over a range from 10^{-5} to 3 KHz, while recording changes in force (dynamic stiffness) and its phase shift (viscous modulus). These parameters were monitored before, during, and after the gelsolin treatment (purified from human plasma and used at 0.3 mg/ml). To assay the removal of actin by gelsolin, the fiber that had been used for the mechanical experiment was cut into two segments: one was stained with rhodamine-phalloidin and the other was analyzed by SDS-PAGE.

The static stiffness measurements in relaxing solution indicated that the flight muscles of the waterbug and the bee are both very stiff. In contrast, the leg muscle of waterbug is about 100 times more compliant. SDS gel patterns of all muscles, including the leg muscle, indicate the presence of several giant proteins larger than myosin heavy chain. Thus, a simple correlation between static stiffness and the presence of these giant proteins does not exist.

The viscous moduli exhibited a minimum and approached zero at about 10 Hz for waterbug flight and leg muscles and at about 200 Hz for bee flight muscle. Thus, at such frequencies these fibers are pure elastic and dissipate little strain energy. Outside this frequency range the fibers are viscoelastic.

Thin filament removal by gelsolin in a calcium containing rigor solution caused rigor force to decrease rapidly to about 10% of its initial value. However, dynamic stiffness decreased by only about 50%. When the fiber was then transferred into activating solution, dynamic stiffness was again less depressed than active force. In relaxing solution static stiffness was not affected by gelsolin. However, the dynamic stiffness and the phase shift of passive force were both reduced, especially at frequencies higher than about 200 Hz.

It appears that part of the stiffness that is generated upon activation is gelsolin insensitive, and currently we are investigating whether this stiffness is cytoskeletal based. Our finding that thin filament removal results in a reduction of both dynamic stiffness and the phase shift of force under relaxing solutions opens the intriguing possibility that thin filaments and elastic cytoskeletal proteins are mechanically linked and interact in a viscoelastic manner manner.

M-Pos24

EVIDENCE FOR THE CROSSLINKING OF AN ELASTIC ELEMENT OF SKELETAL MUSCLE FIBERS

Vincent A. Barnett and Mark Schoenberg
Laboratory of Physical Biology, NIAMS, NIH. Bethesda, Maryland

We have been able to create weakly-binding myosin crossbridges using two different maleimide reagents. Treatment of relaxed chemically-skinned psoas fibers with either the monofunctional reagent N-phenylmaleimide (NPM) or the bifunctional crosslinker p-phenylenedimaleimide (pPDM) results in crossbridges whose stiffness in the presence and absence of ATP is like that of relaxed muscle.

We have discovered some subtle differences in the mechanical responses of muscle fibers modified by pPDM when compared to fibers modified by NPM. We are trying to exploit these differences to learn more about muscle function.

What we have found is that the chord stiffness of pPDM-treated fibers was consistently elevated by a small increment above that of relaxed control fibers or NPM-treated fibers. The chord stiffness was measured using a 2.0 nm per half-sarcomere ramp stretch. This small increase in resting stiffness was accompanied by a large (approximately 2-fold) change in resting tension. The resting tension was determined by applying a 0.25 μm per half sarcomere stretch in the presence of ATP and measuring the resultant force.

We have also found a marked difference in the SDS-PAGE pattern of muscle proteins after pPDM treatment of muscle fibers when compared to control and NPM-treated fibers. In addition to the crosslinking of SH1 to SH2, pPDM forms links between myosin heavy chains creating myosin dimers and higher oligomers. We also observed that the migration of the elastic protein titin as well as that of nebulin were affected. pPDM-treatment of muscle fibers decreased the amount of titin and nebulin migrating at their customary positions on a 2-12% gradient gel, this was accompanied by the appearance of a new non-myosin band at the top of the gel matrix. All other muscle proteins were unaffected.

The small elevation of the resting stiffness, the large increase in resting tension and the change in protein mobility on gradient gels after pPDM treatment leads us to a simple model. We hypothesize that the creation of weakly-binding crossbridges is due to the reaction of pPDM or NPM with the crossbridge head and that the effect of pPDM on the resting tension and stiffness is due to its reacting with and possibly crosslinking titin (connectin) and/or nebulin.

M-Pos25

MECHANICAL DETECTION OF WEAKLY-BINDING M·ATP CROSSBRIDGES
Mark Schoenberg, NIAMS, NIH, Bethesda, MD 20892.

Weakly-binding myosin·ATP crossbridges, because of their extremely rapid detachment rate constants, are not readily detected with the kinds of stiffness measurement techniques popular in the 1960's. They are, however, readily detectable with many of the higher frequency response techniques available today. In interpreting the results of stiffness experiments, it is important to know to what extent crossbridges in the weakly-binding M·ATP state are detected. This is determined as follows: Consider a fiber having a population of rapid equilibrium crossbridges with detachment rate constant, k_b. If the fiber is instantaneously stretched at time 0 by an amount Δl, the force response to the stretch will be $nK\Delta l u_{-1}(t)\exp(-k_b t)$ where nK is the full stiffness of the attached crossbridges and u_{-1} is the Heaviside step function. Given the approximately linear response of a resting fiber to small mechanical stretches (Schoenberg, 1988, Biophys. J., 54:1105), it is possible to use the above and linear superposition theory to calculate the response of equilibrium crossbridges to any length change. Calculating the response to a ramp stretch or a sinusoid, we can determine the fraction of the true full stiffness that will be detected by a given duration ramp or a given frequency sinusoid. This information is summarized below for crossbridges having a detachment rate constant of 10^4 s^{-1} like the M·ATP crossbridge.

Type	dur. or freq.	fraction detected
ramp	1 ms	0.10
ramp	0.2 ms	0.43
ramp	0.1 ms	0.83
sinusoid	500 Hz	0.30
sinusoid	1000 Hz	0.53
sinusoid	2000 Hz	0.88

M-Pos26

MYOSIN HEADS FUNCTION INDEPENDENTLY DURING FORCE GENERATION.
Greg Wilson, Sarah Shull & Roger Cooke. Dept. Biochem./Biophys., Box 0524, UC San Francisco, Ca., 94143.

To investigate the interactions between the two heads of myosin, we used vanadate (Vi), an analog of inorganic phosphate, to trap spin-labeled (SL) ATP analogs on the myosin heads of skinned rabbit skeletal muscle fibers. Similarly to MgADP, MgSLADP forms complexes with the myosin heads which are stable for long periods of time in the relaxed state. We found that force generation declined in proportion to the $\log_{10}$[Vi] in Ca^{2+}-activated fast-twitch and slow-twitch fibers. This is consistent with models in which trapping of one myosin head does not influence trapping of the other head of the same molecule. Electron paramagnetic resonance spectroscopy of the trapped myosin-MgSLADP-Vi complexes in thin slow-twitch fiber bundles also showed that force declined in proportion to the increase in the number of trapped heads. These results show that the two heads function independently. The [Vi] for reducing force to half in fast-twitch fibers was 70uM, similarly to Dantzig & Goldman (J. gen Physiol. 86, 305 (1985)) but was greater for slow-twitch fibers (110uM). Force was almost abolished when the [Vi] was ~1.3mM for fast-twitch fibers and ~6.1mM for slow-twitch fibers. When MgSLADP was trapped in bundles of slow-twitch fibers force generation was reduced by half when the [Vi] was ~850uM and was almost abolished when [Vi] was around 15mM. This reflects different properties of the SLATP. Force and fiber stiffness declined in proportion in both fast-twitch and slow-twitch fibers when they were activated in the presence of MgATP with increasing [Vi]. This supports the view that fibers become relaxed after trapping with Vi due to dissociation of cross-bridges. This is also consistent with the finding that trapped heads do not affect shortening velocity by dragging on the thin filaments.

Therefore, when one head of a myosin molecule is trapped, the other head generates the same amount of force, and contributes equally to fiber shortening and stiffness, as it would with an untrapped partner.
Supported by USPHS AM30868 and by an MDA Fellowship to GW.

M-Pos27

AN APPARATUS TO MEASURE IN VIVO BIOMECHANICAL BEHAVIOR OF DORSI- AND PLANTARFLEXORS OF THE MOUSE ANKLE.
J.A. Ashton-Miller, Y. He, V.A. Kadhiresan, D.A. McCubbrey and J.A. Faulkner, Dept. of Mech. Eng.& Appl. Mech., University of Michigan, Ann Arbor, MI 48109.

An apparatus was developed to quantify the biomechanical behavior of the dorsi- and plantarflexor muscles of the mouse ankle, non-invasively. When either the dorsi- or plantarflexor muscle group is activated by electrical stimulation of either the peroneal or tibial nerve, the apparatus measures the moment developed about the ankle. The moment developed may be measured during isometric and isovelocity shortening or lengthening contractions. Displacements may be performed over the full 110° range of ankle motion with an angular resolution of 0.09°. When the foot is positioned at 90° to the lower leg, bidirectional isovelocity ramps up to 1100°/s are possible. These velocities are equivalent to velocities in fiber lengths/s (L_f/s) of 2.34 for fibers in tibialis anterior muscle and 11.9 for those in gastrocnemius muscle. Measurements provided by the apparatus at 37°C with a stimulation frequency of 150 Hz were validated in situ with a Cambridge servomotor. During single contractions of dorsi- and plantarflexor muscle groups, maximum isometric tetanic force was 1.4 N and 3.7 N, power output at 2.2 L_f/s was 3.1 mW and 5.8 mW, and power absorption at 0.5 L_f/s was 4.9 mW, and 9.0 mW, respectively. These values are in reasonable agreement with data from the same muscle groups tested in situ. We conclude that the apparatus provides valid measurements of force and power of the dorsi- and plantarflexor muscle groups.
(Supported by AG-06157 and NS-24058).

M-Pos28

REPEATED EXPOSURES TO A LENGTHENING CONTRACTION PROTOCOL PREVENTS SUBSEQUENT INJURY.
John A. Faulkner, Julie A. Opiteck, and Susan V. Brooks, Department of Physiology, University of Michigan, Ann Arbor, MI 48109-0622, U.S.A.

A protocol of repeated lengthening contractions injured extensor digitorum longus (EDL) muscles in young mice in situ such that maximum force (P_o) was 30% at 3 days, 55% at 7 days and returned to control values by 30 days (Brooks & Faulkner, Am. J. Physiol. 258:C436, 1990). We tested the hypothesis that if a lengthening contraction protocol was repeated every 7 days the P_o at 7 days would eventually return to the control value and, under these circumstances, the muscle fibers would not be injured by a lengthening contraction protocol that previously produced severe injury. A non-invasive lengthening contraction protocol of the dorsiflexor muscle group initially reduced P_o at 7 days to 90% of the control value. After six repetitions of the protocol the mean P_o was not different from the initial control value. The EDL muscle was then exposed to an in situ lengthening contraction protocol. At 3 days, when signs of injury are most severe, P_o was not different from the control value and histological sections showed no evidence of loss of fibers, or injury to fibers. In spite of the absence of injury, compared to control values muscle mass was 20% greater and specific P_o was 20% less. We conclude that repeated exposures to a protocol of lengthening contractions that initially induced injury to fibers result in structural adaptations in fibers that prevent subsequent injury. (Supported by AG 06157).

M-Pos29

NMR-STUDIES OF THE STRUCTURE OF ACTIN 1-28 IN SOLUTION AND BOUND TO TROPONIN OR MYOSIN-S1.

F. D. Sönnichsen, J. Van Eyk, R. S. Hodges, B. D. Sykes, Department of Biochemistry and MRC Group of Protein Structure and Function, University of Alberta, Edmonton, T6G 2H7, Canada.

In striated muscle the two major interactions of actin are the binding to myosin which modulates the ATPase activity, and the Ca^{2+} dependent binding to the troponin-complex which regulates the contraction-relaxation cycle of the muscle cell. Both interactions have been shown to involve the amino-terminal residues of Actin (1,2). Being interested in the structure of this region of actin, we synthesized the synthetic peptide analogue actin 1-28 amide and used 2D-NMR spectroscopy (NOESY and transferred NOESY) to determine the structure of this peptide in solution and bound to either the troponin-complex or to myosin S-1 fragment. The results show that actin 1-28 amide in solution is mostly extended. A loop was detected between G^{13}- L^{16} and there is additional evidence for a structured area between G^{23} - A^{26}. Upon binding the peptide undergoes a conformational change in three areas. The major binding sites are located at the first and last 8 residues of the peptide. The N-terminal site exhibits an identical conformation when bound to troponin or myosin, while the C-terminal site of the peptide clearly shows differences, which may be responsible for the observed differences in peptide-protein affinity. The third area lies almost in the middle of the peptide (D^{11} - N^{12}) and could serve as a hinge region between the two binding sites. The derived structural information is compared with the X-ray crystal structure (3).

(1) see E. Reisler et al. (1990), Biochemistry 29, 8503 - 8508.

(2) J. Van Eyk, R.S. Hodges, unpublished.

(3) K.C. Holmes et al. (1990), Nature 347, 37 - 44.

M-Pos30

CROSSLINKING OF ACTIN WITH N-(4-AZIDOBENZOYL)-PUTRESCINE: A TEST OF THE F-ACTIN MODEL Marshall Elzinga and György Hegyi, NYS Institute for Basic Research in Developmental Disabilities, Staten Island NY 10314

We have synthesized a new photoactivatable crosslinker for proteins, N-(4-azidobenzoyl)-putrescine, and have used it to measure the proximity of two sidechains in adjacent actin monomers in F-actin. The reagent was incorporated into rabbit skeletal muscle G-actin, by transglutaminase, at residue Gln-41. The modified actin was polymerized, and crosslinking was induced by photogeneration of an active nitrene. Oligomers were separated from uncrosslinked monomers by S-200 gel filtration, and a crosslinked peptide complex was isolated from an Arg digest of the actin. The crosslinked peptides included residues 40-62 (which contained Gln-41) and residues 96-116. Sequence analysis showed that the actual crosslink was between Gln-41 and Lys-113. These results indicate that the carbonyl group of the sidechain of Gln-41 of one monomer is 12-14 Å from part (probably the ε-amino group) of the sidechain of Lys-113 of an adjacent monomer within F-actin.

This crosslink and the phenylene-dimaleimide crosslink between Cys-374 and Lys-191 (Elzinga and Phelan, PNAS 81, 6599) provide crucial tests for the recently published model of F-actin (Holmes et al, Nature 347, 44). Although atomic coordinates of the side-chains are required for a definitive analysis, the model seems to accomodate the crosslink distances. The Cys-374 : Lys-191 crosslink would involve monomers in opposite strands, while the Gln-41 : Lys-113 crosslink would involve sidechains from adjacent monomers in a given strand. Thus the chemical crosslinking seems to corroborate the published F-actin model. (Supported by the NY State Office of Mental Retardation and Developmental Disabilities, and by NIH grant HL-21471.)

M-Pos31

PHALLOTOXIN BINDING TO BOTH OLIGOMERIZED AND POLYMERIZED (FILAMENTOUS) ACTIN INVESTIGATED BY THE FLUORESCENCE ENHANCEMENT OF RHODAMINE-PHALLOIDIN UPON ITS INTERACTION WITH ACTIN. Zhijian Huang, Rosaria Haugland and Richard P. Haugland, Molecular Probes, Inc., 4849 Pitchford Avenue, Eugene, OR 97402

Fluorescent-labeled phallotoxins are well known for their actin binding and visualizing properties in various biological systems. We demonstrated that the fluorescence of phallotoxins conjugated to 5 different fluorophores (rhodamine, fluorescein, NBD, Bodipy™ and coumarin) significantly and specifically increase upon their binding to actin. Rhodamine-phalloidin has the greatest fluorescence enhancement of 10-fold. The fluorescence enhancement of rhodamine-phalloidin was successfully used to determine its binding to actin, binding constant and binding stoichiometry. Based on an accurate mathematic analysis and experimentation, the binding constant of any other phallotoxin, including unlabeled phalloidin and biotinoylphallacidin, can also be conveniently and quantitatively determined by means of their competition with rhodamine-phalloidin. The fluorescence enhancement and competition measurements eliminate the need for hazardous and elaborate radioactive labeling and equilibrium dialysis for the binding determination, as well as the potential error in binding determination due to the separation of bound phallotoxin from free phallotoxin which would result in a change in binding conditions. The binding constants that were obtained, in the form of the ratio over phalloidin binding constant ($1.14 \cdot 10^8 M^{-1}$) are: phalloidin 1.0, rhodamine phalloidin 0.16, fluorescein phalloidin 0.33, NBD-phallacidin 0.35, Bodipy™-phallacidin 0.19, coumarin-phallacidin 0.11, biotinoylphallacidin 0.64. The fluorescence enhancement of rhodamine-phalloidin also provides a direct and simultaneous measurement of actin nucleation or polymerization in the presence of the phallotoxin. The fluorescence measurement shows that there is about 15% rhodamine phalloidin binding to the equimolar and fully depolymerized actin compared to the 80% binding to the same equimolar but polymerized actin, indicating that even depolymerized actin can form the transient oligomers which are then bound and stabilized by phallotoxin. The fluorescence development of rhodamine phalloidin upon actin polymerization can also be observed with 0.1 μM actin, a concentration much lower than the critical concentration without phalloidin, suggesting phalloidin dramatically lowers the actin critical concentration of polymerization. Supported by N.I.H. grant GM 37347.

M-Pos32

FLUORESCENCE QUENCHING OF ETHENO-NUCLEOTIDES IN g- AND f-ACTIN

D. D. Root and E. Reisler, Dept. of Chem. and Biochem. and the Mol. Biol. Inst., UCLA, Los Angeles, CA 90024

Recent publication of the atomic structure of g-actin (Kabsch, *et al.*, Nature 347:37, 1990) raises questions about how the conformation of actin changes upon its polymerization. We examined the effects of various quenchers of etheno-nucleotides bound to g- and f-actin to assess polymerization-related changes in the nucleotide site. An antibody (IgG) to the etheno-group quenched the fluorescence of etheno-nucleotides bound to g- and f-actin, indicating that even a large molecule can access the bound nucleotides. The Mg^{2+}-induced polymerization of actin quenched the fluorescence of the etheno-nucleotide by approximately 20% simultaneously with the increase in light scattering by actin. Further indication of a conformational change at the nucleotide binding site was that positively, negatively, and neutrally charged collisional quenchers showed greater accessibility to f-actin than to g-actin. The difference in accessibility of the nucleotide between g- and f-actin was greatest for I^- indicating that the environment around the etheno-group is more positively charged in the polymerized form of actin. Since ε-ADP, ε-ADP-g-actin, and f-actin derived from ε-ADP-g-actin showed the same accessibilities to I^- as their ε-ATP forms, different accessibilities of the nucleotides in g- and f-actin can not be attributed to differences between ε-ADP and ε-ATP.

M-Pos33

CATION BINDING TO THE HIGH AFFINITY SITE REGULATES NUCLEOTIDE BINDING TO ACTIN. L.C. Gershman, L.A. Selden, J.E. Estes. Research and Medical Services, VA Medical Center, Albany, and Depts, of Physiology & Cell Biology and Medicine, Albany Medical College, Albany, NY 12208.

We propose that the mechanism of dissociation of actin-bound nucleotide is highly dependent on whether or not the high affinity divalent cation site on actin is occupied. At high free [metal] when the high affinity site is fully occupied, the dissociation of nucleotide from actin is predominantly via the metal-nucleotide complex. The Mg-nucleotide complex dissociates about 2-3 times faster than the Ca-nucleotide complex. At low free [metal], dissociation of nucleotide from Ca-actin predominantly follows, and is limited by, dissociation of the tightly-bound Ca^{++}; dissociation of nucleotide from Mg-actin occurs about half through such a sequential mechanism and about half through dissociation of the Mg-nucleotide complex. At low [metal], nucleotide dissociation from Ca-actin is 3-4 times faster than from Mg-actin, reflecting the relatively faster dissociation of Ca^{++}, compared with Mg^{++}, from the high affinity site. The range of [metal] over which the mechanism of nucleotide exchange changes from dissociation of the metal-nucleotide complex to predominantly sequential dissociation is about 100-fold higher for Mg^{++} than for Ca^{++}. This is consistent with the slower association of Mg^{++} to actin resulting from the kinetic characteristics of the Mg^{++} aquo ion. Thus, the difference in nucleotide dissociation kinetics between Ca-actin and Mg-actin reflects the difference in the kinetics of dissociation of Ca^{++} and Mg^{++} from the high affinity site and the relatively higher stability of the Mg-nucleotide complex compared to the Ca-nucleotide complex. Supported by the Veterans Administration and NIH grant GM-32007.

M-Pos34

INFLUENCE OF THE TIGHTLY-BOUND DIVALENT CATION AND NUCLEOTIDE ON THE THERMODYNAMICS OF ACTIN POLYMERIZATION. H.J. Kinosian, L.A. Selden, J.E. Estes, L.C. Gershman. Research and Medical Services, VA Medical Center, Albany, and Departments of Physiology & Cell Biology and Medicine, Albany Medical College, Albany, NY 12208.

In earlier work, we reported that the tightly-bound divalent cation has a marked effect on the enthalpy and entropy changes for the polymerization of ATP-actin (Selden et al., J. Muscle Res Cell Motility 7:215-224, 1986). In this current study, measurements of the temperature dependence of the polymerization of Mg-actin and Ca-actin containing ADP as bound nucleotide revealed little effect of the tightly-bound cation on these thermodynamic parameters. Arrhenius and van't Hoff plots for the polymerization of Ca-ATP-, Mg-ADP- and Ca-ADP-actin were found to be non-linear. Values of the thermodynamic parameters for polymerization were obtained from analysis of free energy data for the polymerization of these actins as a second-order function of absolute temperature (Osborne et al., Biochemistry 15:317-320, 1976). The enthalpy changes (ΔH) and activation enthalpy changes (ΔH^*) for Ca-ATP, Mg-ADP and Ca-ADP-actin were found to be temperature dependent. In contrast, the ΔH and ΔH^* values for the polymerization of Mg-ATP-actin were lower and essentially constant over the temperature range studied. These results suggest that polymerization of actin which does not contain Mg^{++} and ATP may be a multi-step reaction which has a rate-limiting step different from that for polymerization of Mg-ATP-actin. Conceivably, Mg-ATP-actin has a unique conformation which enhances its ability to polymerize. Supported by the Veterans Administration and NIH grant GM-32007.

M-Pos35

CYTOCHALASIN D ACTIVATION OF MG-ATP-ACTIN ATPASE ACTIVITY. L.A. Selden, H.J. Kinosian, L.C. Gershman, J.E. Estes. Research and Medical Services, VA Medical Center, Albany, and Departments of Physiology & Cell Biology and Medicine, Albany Medical College, Albany, NY 12208.

Previously, we reported that the addition of cytochalasin D (CD) to Mg-ATP-actin results in a rapid burst in the hydrolysis of actin-bound ATP. We have measured both the CD-induced burst in ATPase activity and the steady-state ATP hydrolysis with $AT^{32}P$ at low ionic strength. The double reciprocal plot for the ATPase burst as a function of [CD] is linear and yields V_{max} about 0.13 $\mu M\ Pi \cdot sec^{-1} \cdot \mu M^{-1}$ of actin and K_m = 3.3 μM. The double reciprocal plot for steady-state ATPase activity vs. [actin] at low CD (0.02 μM) is linear and gives V_{max} about 0.29 $\mu M\ Pi \cdot sec^{-1} \cdot \mu M^{-1}$ of CD and K_m = 2.4 μM. The steady-state ATPase activity appears to be a complicated function of [CD]. At high [CD] (100 μM) the rate appears to be limited by the ADP off-rate from actin, but at lower [CD] (less than 100 μM) the steady-state rate is significantly lower than the ADP off-rate from actin. This may be related to the presence of oligomers containing actin subunits that have reduced ability to exchange nucleotide. The presence of oligomers would be facilitated by the other known actions of CD: barbed-end capping and fragmentation of actin polymers. Analysis of the actin ATPase activity at low [CD] and by the CD-induced ATPase burst indicate that CD is capable of activating the actin ATPase activity by a factor of about 3000. Supported by the Veterans Administration and NIH grant GM-32007.

M-Pos36

CONFORMATION AND ORIENTATION OF ACTIN PROBED BY SPIN-LABELED ANALOGS OF ATP. N. Naber and R. Cooke. Dept. of Biochemistry and CVRI, Univ.Calif. San Francisco.

We have incorporated two spin label analogs of ATP into F-actin and observed the mobility of the spin labels as well as their orientation. Both spin labels were connected to the 6 position of the adenine ring. Both these labels have some degree of mobility relative to the actin protein structure. Because the actin structure is now known at atomic resolution, we can determine the approximate position of these probes. They would be located in the deep cleft of the molecule which separates the two major domains. Thus the mobility of the probes would reflect changes in the conformation of this cleft region. Addition of myosin subfragment-1 restricted the mobility of the probes slightly. It is known that addition of phosphate will result in an ADP-Pi complex at the actin nucleotide site. Addition of phosphate also restricted the mobility of the probes. Addition of DNAse, which depolymerized the actin, resulted in very little change in the mobility of the spin probes. When actin was oriented either by flow into capillaries or by incorporation of the label into ghost fibers, the spin labels attached to the bound nucleotide were both highly oriented with respect to the axis of the actin filament. The spectra show that, although the probes have some mobility, the average angle of each probe is the same. This average angle was 64-68 degrees for both probes. Addition of subfragment-1 or phosphate to actin caused no discernable change in the angle of either probe. We conclude that the binding of either phosphate or S-1 to the actin filament causes some alteration in the structure of the cleft region, which does not involve appreciable rotations of the actin. Supported by a grant from the USPHS AM30868

M-Pos37

SPIN-PROBE STUDIES OF THE CYS-374 REGION OF ACTIN.
N.Naber and R.Cooke. Dept. of Biochemistry and CVRI, Univ.Calif. San Francisco.

Labels attached to the Cys-374 of actin were highly immobilized on the actin surface. The actin was oriented by smearing on glass plates, by incorporation into ghost fibers, or by forming threads after extrusion through a syringe. The label showed some degree of orientation in all three systems but was best oriented in the threads. The degree of orientation was much less than that observed for the nucleotide spin labels, discussed in another abstract at this meeting. The binding of myosin subfragment-1 to actin oriented on glass plates or in threads caused the spectrum to become disoriented. This result is similar to that reported previously by Belagyi et al (Acta Biochem Hung Acad 1980). However, addition of pyrophosphate which removed the myosin subfragment-1 did not regain the orientation of the label, suggesting that the label was disoriented because the subfragment had disoriented actin filaments instead of causing a conformational change within the actin. This conclusion was supported by the observation that the addition of subfragment-1 to actin that had been incorporated into ghost fibers did not change the orientation distribution of this label. The Cys-374 is known to be located in a region of actin that is near the surface of the actin filament and is thought to be adjacent to the site where myosin binds (Holmes et.al. Nature, 1990). Thus our results suggest that the orientation of this site is not altered by the binding of myosin. Supported by grants from the NIH AM30868.

M-Pos38

ORIENTATIONAL DISTRIBUTION OF SPIN-LABELED ACTIN ORIENTED BY FLOW.
E. Michael Ostap, Toshio Yanagida, and David D. Thomas. Dept. Biochemistry, Univ. of Minnesota Medical School. Minneapolis, MN 55455

We have previously used ST-EPR to demonstrate that actin spin-labeled at cys-374 (MSL-actin) undergoes microsecond rotational motions, and that these motions are restricted by the binding of myosin subfragments. We have also demonstrated that during the active interaction of S1, actin, and ATP, μsec rotational motions of actin remained unchanged despite increased rotational motion of S1. To determine whether the binding of S1, and the interaction with ATP, induce changes in actin conformation, we are using EPR to study the orientational distribution of MSL-actin oriented parallel to the magnetic field by flow. We are determining the orientational distribution of the spin label relative to the magnetic field (filament axis) by comparing the experimental spectra corresponding to known orientational distributions, using the Amoeba method (Fajer et al., 1990). Spectra acquired during flow indicate a narrow orientational distribution of probes. The angle between the actin filament axis and the nitroxide Z axis is centered between 30° and 35° while the nitroxide X axis lies almost precisely in the plane of the nitroxide Z axis and the filament axis. Knowing the angle of the spin label relative to the filament axis, we can determine the effects of actin-binding proteins on actin conformation. Upon binding of S1, less than a 10° change is apparent for either axis. Further refinement using the Amoeba method should yield more detailed information about the orientational disorder, providing essential data for the quantitative analysis of actin dynamics from ST-EPR spectra using this spin label.

M-Pos39

ORIENTATIONAL SELF-ORGANIZATION OF ACTIN FILAMENTS
Chris M. Coppin and Paul C. Leavis
Dept. of Physiology, Tufts Univ. School of Medicine
Dept. of Muscle Research, Boston Biomed. Res. Inst.
20 Staniford St., Boston, MA 02114

Actin filaments (F-actin) are thought to play an important role in generating movements in eukariotic cells. Numerous filaments act in concert to contribute to a localized deformation of the plasma membrane. Electron micrographs reveal that the cytoskeleton is highly anisotropic in these regions of the cell. It is usually assumed that that filaments are forced to align with one another by various actin binding proteins.

We have studied the spontaneous orientational organization of actin filaments in vitro. In our hands purified actin at concentrations greater than 1.2 mg/ml left undisturbed after polymerization in the presence of either ATP or ADP formed a liquid crystal at room temperature. Using a polarizing microscope we did not observe any coexistence of isotropic and anisotropic domains. The filament nucleating protein gelsolin was used in some cases to prepare filaments with a chosen average length. The temperature dependence of the birefringence and of the intensity of scattered light revealed that at constant actin concentration long filaments formed more highly ordered structures than short ones, and that the phase transition from the isotropic to the anisotropic state is continuous. Results of polarization of fluorescence measurements made with 3.5 mg/ml acrylodan-labeled actin were consistent with a nematic liquid crystal whose order parameter was about 0.75. However some specimens observed with the polarizing microscope had a texture reminiscent of a cholesteric liquid crystal with a screw axis pitch of about 10 μm. With these specimens there appeared to be some dispersion in the circular differential light scattering, which was also consistent with a cholesteric liquid crystal with a left handed screw axis. Cells may take advantage of this self-organizing behavior of actin filaments and modulate it with actin binding proteins to impart the desired architecture to the cytoskeleton.

M-Pos40

FORMATION OF ACTIN PARACRYSTALS ON PHOSPHOLIPID MONOLAYERS MIXED WITH QUATERNARY AMMONIUM SURFACTANTS.
Kenneth A. Taylor and Dianne W. Taylor. Dept. of Cell Biology, Duke Univ. Medical Center, Durham, NC 27710.

Paracrystals of F-actin can be formed in solution under a variety of conditions that usually involve use of polycations or high concentrations of magnesium. Paracrystals formed under these conditions are usually 3-D in character. Single-layered paracrystals of F-actin have been formed on egg yolk phosphatidylcholine (EY-PC) monolayers mixed with stearylamine (SA) up to concentrations of 30% by weight (Ward et al. *J. Elect. Microsc. Tech.* 14, 335-341 (1990)). We have experimented with several quaternary ammonium surfactants as substitutes for SA to see if they offer any improvement for the production of 2-D arrays of F-actin on the lipid monolayer. For these trials we used G-actin obtained from rabbit muscle acetone powder and purified by Superose 12 chromatography. Of the various surfactants examined as alternatives, the best ordered paracrystals were obtained using C_{12} acyl chain lipids such as dilaurylphosphatidylcholine (DLPC) mixed with didodecyldimethylammonium bromide (DDMA). Paracrystals were also more frequent on this C_{12} monolayer system than with EYPC-SA system. Concentrations of DDMA up to 30% by weight were used. Despite its saturated acyl chain, the DDMA-DLPC monolayer appears fluid down to temperatures of 4°C. The chemically similar monolayer formed using dipalmitoyl PC and dihexadecyldimethyl ammonium bromide is a much poorer substrate for crystal formation presumably because it is not fluid at room temperature. We used both F-actin and G-actin as starting materials. Well ordered single-layer rafts of F-actin up to 30 filaments wide and several micrometers long are formed on monolayers composed of DDMA-DLPC. G-actin injected under the monolayer into a polymerization solution of 20-50 mM KCl, 1.0 mM ATP and 2.0 mM Mg produces much better paracrystals than similar concentrations of F-actin in the same buffer. Optical and computed diffraction patterns taken from images of negatively stained paracrystals reveal sharp spots that index on a unit cell of dimensions a=70Å, b=770Å and gamma=90°. These spacings are indicative of parallel filaments packed tightly to form a 2-D crystalline phase. Support by a grant from the American Heart Association is gratefully acknowledged.

M-Pos41

SIZE DISTRIBUTION OF ACTIN FILAMENTS MEASURED FROM LIGHT MISCROSCOPIC IMAGES OF PHALLOIDIN-ACTIN. S. Burlacu and J. Borejdo, Baylor Research Foundation, Baylor University Medical Center, 3812 Elm St., Dallas, TX 75226.

The effect of ionic strength, pH, Mg^{2+} ion concentration and actin binding proteins on the length distribution of actin filaments was studied by fluorescence microscopy of rhodamine-phalloidin labeled actin. To study the effect of polymerizing conditions, G-actin was first polymerized in appropriate solvents, and resulting filaments were stained with phalloidin. When G-actin was polymerized using standard buffer (50 mM K-Acetate, 2 mM $MgSO_4$, 10 mM TRIS-Acetate pH 8) the number average length of filaments (L_n) was 5.55 μm. The ratio (ρ) of the weight average length to the number average length was 1.3. When Mg^{2+} ion concentration was kept fixed at 2 mM and K^+ ion concentration was increased from 0 to 100 mM, L_n increased from 4.43 μm to 5.23 μm and ρ increased from 1.17 to 1.3. When Mg^{2+} ion concentration was 0 and K^+ ion concentration increased from 0 to 100 mM, L_n increased from 3.80 μm to 5.62 μm and ρ did not change. Decreasing pH from 9 to 6 did not significantly change L_n but increased the number of very long filaments. To study the effect of actin binding proteins on length distribution of actin filaments, different molar ratios of HMM, gelsolin and tropomyosin were added to G- or F-actin before adding rhodamine-phalloidin. Adding saturating amounts of HMM to F-actin decreased L_n from 5.38 μm to 2.66 μm without changing ρ. Adding increasing amounts of gelsolin to G-actin and polymerizing actin with standard buffer, progressively decreased the size of filaments. When molar ratio gelsolin:actin became larger than 1:500, L_n became smaller than 0.5 μm. Gelsolin had similar effect when added to F-actin. Tropomyosin had no effect on the distribution when added to F-actin. These results demonstrate that rapid determination of the distribution of filament lengths by optical methods offers a convenient way to supplement mechanical measurements of physical properties of actin filaments. Supported by NIH RO1 AR40095-01.

M-Pos42

STRUCTURE OF ACTIN IN ZEBRA FISH EMBRYOS STUDIED BY CONFOCAL MICROSCOPY. Donald C. Chang, Dept. of Mol. Physiol. and Biophysics, Baylor Coll. of Med., Houston, TX 77030

When an embryonic cell divides, the properties of the two daughter cells are often not the same; each may develop into different cell types at later stages. This change of cell fate is not due to differences in genomic DNA, instead, it is probably caused by an asymmetrical distribution of cytoplasmic factors that regulate the expression of genes. These cell-fate determinant factors could be mRNA or transcription factor proteins. We think the localization of these factors is accomplished by their interactions with the cytoskeleton. To search for a cytoskeletal structure that may provide a basis for localization of cell-fate factors, we used a confocal microscope to study the actin structure of zebra fish embryos, which were fixed at different development stages and stained with rhodamine-conjugated phalloidin. By scanning the fluorescent signal of F-actin point by point, one can reconstruct a three dimensional image of F-actin in the embryo. Our results showed that there is a dense layer of F-actin at the cell surface, roughly resembling the microvilli structure. Underneath the surface membrane, we found another actin network approximately 20 μm thick; this network was different from the usual actin structures associated with cell motility and was more similar to the microtrabaculae..This sub-membrane actin network may provide the structural basis for the localization of cell-fate determinant factors.

M-Pos43

Identification of Two Actin Binding Sites on Actobindin by Covalent Crosslinking. Bubb, M.R., *Vancompernolle, K., Van Damme, J., *Vandekerckhove J., and Korn E.D. Laboratory of Cell Biology, NHLBI, NIH, Bethesda MD 20892 and *Laboratory of Genetics, State Univ. of Ghent, Ghent, Belgium.

Actobindin, an 88-amino acid polypeptide from *Acanthamoeba castellanii*, has been shown to bind two actin monomers simultaneously (Bubb, Lewis, & Korn, JBC, in press). We have now identified two actin-binding sites on actobindin using 1-ethyl-3-(3-dimethylaminopropyl)-carbodiimide (EDC) as a covalent crosslinking agent. The residues of actobindin that are crosslinked with EDC are Lys-16 and Lys-52, with a higher yield of crosslink at the first lysine. Lys-16 of actobindin was found to crosslink to rabbit skeletal muscle actin at one or more of the acidic residues in positions 1,2 and 3 and at Glu-100. The latter may be the primary site of interaction. These results are consistent with the crystal structure of actin (Kabsch et al. (1990) Nature 347, 44). Lys-52 crosslinked to the same amino acid(s) at actin's amino-terminus. The crosslinked lysine residues of actobindin are in the two nearly identically repeated regions of 33 amino acids, within the hexapeptide L K H A E T previously noted to be similar to sequences in tropomyosin, muscle myosin heavy chain, paramyosin and *Dictyostelium* α-actinin (Vandekerckhove et al. (1990) JBC 265, 12802). Additionally, a synthetic peptide corresponding to the first 29 amino-acid residues of actobindin, including the first L K H A E T repeat, was found to reduce the steady-state level of F-actin by an amount corresponding to binding between the peptide and G-actin with a K_D of approximately 40 μM. Consistent with the peptide containing only a single actin-binding site, the peptide decreased the rate of actin polymerization less than did native actobindin, which has two actin-binding sites.

M-Pos44

BRIEF PERTURBATION OF THE ENVIRONMENT PRODUCES PROLONGED CHANGES IN GENE EXPRESSION OF RAT HEARTS

S. Winegrad*, C. Wisnewsky#, P. Bouveret# and K. Schwartz#. *Dept. of Physiology, School of Medicine, University of Pennsylvania, Phila., and #I.N.S.E.R.M. U127, Hospital Lariboisiere, Paris, France

The effect of brief, controlled perturbation of the environment on genetic expression in the hearts of conscious rats has been measured. A technique originally used by Sassard and co-workers has been adapted to produce mild, noninvasive stress. A focused jet of air is activated in a metabolic cage, and animals move within 15 seconds to a part of the cage to avoid the jet. During the period of the air jet, animal's blood pressure rises about 5 mm Hg and then recovers within 15-20 minutes after the termination of the air jet. Two and 6 hours following perturbations, which lasted 2 or 15 minutes, total RNA, polyadenylated RNA and the accumulation of mRNA for alpha skeletal and alpha cardiac actin were measured in order to determine the changes produced in the overall expression of genes and in the expression of two genes specifically related to the function of cardiac cells. The 15 minute perturbation produced declines in total RNA at 6 hours even through the mild hemodynamic response to the perturbation was over within 20 minutes of the cessation of the perturbation. Accumulation of transcripts for both alpha actins was decreased at 2 hours, more in the case of alpha skeletal than alpha cardiac actin, with essentially total recovery of both by 6 hours. The response to the 2 minute signal was borderline. These results show that a brief environmental perturbation can produce a prolonged response in genetic expression that appears to have both general and specific focus and that is graded with the duration of the signal.

M-Pos45

THE EFFECT OF PROTEIN KINASE C - PHOSPHORYLATED CALDESMON ON THE DEPOLYMERIZATION OF ACTIN BY GELSOLIN. LP Adam*, N Margolin#, C Vlahos# and DR Hathaway*. *Krannert Institute of Cardiology, Indiana University, and #Lilly Research Laboratories, Indianapolis, IN.

Caldesmon is an actin binding protein that can be phosphorylated in intact tissue as well as in vitro by protein kinase C (PKC) and calcium and calmodulin dependent type II kinase (Cam II). Although phosphorylation of caldesmon by PKC has been found to alter its ability to interact with actin, the mechanisms underlying caldesmon-actin and phosphocaldesmon-actin interactions are unknown. To study these processes, we have labeled actin with N-(1-pyrenyl) iodoacetamide and monitored, by fluorescence, the effect of caldesmon on the conversion of F-actin to G-actin by gelsolin. Gelsolin alone caused a rapid depolymerization of F-actin in the presence of 1 mM calcium that was unaffected by either saturating amounts of caldesmon or tropomyosin. In the presence of both tropomyosin and caldesmon at actin: caldesmon ratios of 4:1, 2:1, 1:1, and 1:2, the initial rate of actin depolymerization was decreased by 53, 58, 70 and 76%, respectively. Caldesmon, phosphorylated by PKC (0.35 mol phosphate/mol caldesmon), inhibited depolymerization to a lesser extent than non-phosphoylated caldesmon - 39 and 53% at actin: caldesmon ratios of 1:2 and 1:4, respectively. Cam II-phosphorylated caldesmon also inhibited depolymerization to a lesser extent than non-phosphoylated caldesmon consistent with the observations that there is overlap among the sites phosphorylated by both kinases and that phosphorylation at a particular site may be responsible for the effects. In additional experiments, we found that PKC-phosphorylated caldesmon could directly block the ability of non-phosphorylated caldesmon to inhibit gelsolin. These results suggest that caldesmon protects actin from depolymerization by gelsolin via a complex interaction with tropomyosin. This protection can be inhibited by PKC-phosphorylated caldesmon suggesting that phosphorylated caldesmon and non-phosphorylated caldesmon may directly compete for a site responsible for the interaction with actin/tropomyosin.

M-Pos46

COMPARATIVE STUDIES ON THE EFFECTS OF CALPONIN AND CALDESMON ON THE INTERACTION OF SMOOTH MUSCLE MYOSIN TO ACTIN AND ACTIN-ACTIVATED MYOSIN ATPase. Kurumi Y. Horiuchi & Samuel Chacko, Department of Pathobiology, University of Pennsylvania, Philadelphia, PA 19104.

Both calponin, a troponin T-like protein, and caldesmon bind to actin and calmodulin. Caldesmon and calponin extracted from chicken gizzard were found to be unphosphorylated. The effect of these actin-binding proteins on heavy meromyosin (HMM) binding to actin and actin-activated ATPase were compared. Myosin, HMM, actin, and tropomyosin were isolated from gizzard smooth muscle. Calponin inhibited actin-activated ATPase of phosphorylated myosin and HMM in the presence or the absence of tropomyosin. The maximum inhibition required a calponin:actin molar ratio of 1:2, whereas with caldesmon, it was achieved at a caldesmon:actin molar ratio of 1:6. As evident from an increase in turbidity, calponin caused aggregation of actin filaments at high concentrations, as did caldesmon. Furthermore, calponin also inhibited HMM binding to actin, similar to the actin-binding fragment of caldesmon. Calponin also inhibited the cooperative turning-on of tropomyosin-actin by rigor complexes, but it required a 1:2 molar ratio of calponin to actin, compared to a 1:6 molar ratio of caldesmon to actin. Hence, the effects of calponin and the actin-binding fragment of caldesmon on the actin-myosin interaction and ATPase are similar although calponin is three to four-fold less effective. Supported by HL 22264 and DK 39740.

M-Pos47

PROTEOLYTIC SEPARATION OF THE ACTIN AND CALMODULIN-BINDING SITES WITHIN THE C-TERMINAL 10 KDA SEGMENT OF CALDESMON
A. Bartegi, A. Fattoum, J. Derancourt and R. Kassab
Centre de Recherche de Biochimie Macromoléculaire CNRS-INSERM, Montpellier, France

Recently we have isolated the 10 kDa CNBr fragment encompassing the C-terminal region of residues 659-756 in gizzard caldesmon and we have shown it to contain major structural determinants for the inhibitory binding to F-actin and for the specific regulatory interaction with Ca^{2+}-calmodulin (*J. Biol. Chem.* **265**, 15231, 1990). As the binding of the peptide to Ca^{2+}-calmodulin induces a red shift of the peptide tryptophan fluorescence quite similar to that observed with native caldesmon, we investigated its limited digestion with chymotrypsin in the aim to acheive the proteolytic dissociation of the two functions and to probe further their respective location on the active peptide. Under optimal conditions (protease : substrate ratio = 1:50, pH 7.5, 1 h, 25°C) the fragment was selectively split at Phe-665 and at the three tryp residues at positions 659, 692 and 722 as assessed by HPLC separation of the resulting peptides and N-terminal amino acid sequencing. Binding of Ca^{2+}-calmodulin abolished the chymotryptic susceptibility whereas the binding of F-actin or F-actin-tropomyosin was without effect. The proteolysis was followed by determining the inhibitory influence of the digested fragment on the skeletal acto-S-1 ATPase activity measured in the absence and presence of Ca^{2+}-calmodulin. During the entire course of the reaction, the extent of the ATPase inhibition did not change, but, in contrast, the release of the inhibition by Ca^{2+}-calmodulin was progressively aboslished. No peptide material of the final digest was retained by immobilized calmodulin. The data indicate that the actin and calmoduline sites lie on distinct portions of the 10 kDa fragment and that the intergrity of at least one trypophanyl peptide bond is required for calmodulin binding. (Supported by grants from CNRS, INSERM and Association Française contre les Myopathies).

M-Pos48

THE INTERACTION OF CALDESMON WITH THE COOH-TERMINUS OF ACTIN
R.Crosbie, S.B.Adams, L.Velaz*, J.M.Chalovich* and E. Reisler, Dept. of Chem. and Biochem. and the Mol. Biol. Inst., Univ. of Calif., Los Angeles, CA 90024; *E.Carolina Univ. School of Medicine, Greenville, N.Carolina 27858

The binding of caldesmon to the NH_2-terminal segment of actin is supported by several lines of evidence from crosslinking, immunochemical and H^1 n.m.r. studies. Since the N-terminus and the C-terminus of actin are in close proximity (Kabsch et al. Nature 347:37-44, 1990), we examined the carboxy-terminus of actin for potential caldesmon binding sites. The binding of caldesmon to actin labelled with pyrene-iodoacetamide at cysteine 374 was measured by using fluorescence and co-sedimentation methods. We report a reduction of fluorescence of up to 10% as the molar ratio of caldesmon to actin is increased to 4:1. Titrations with nitromethane did not reveal any caldesmon induced changes in the accessibility of the pyrene probe. In co-sedimentation experiments caldesmon binding to modified actin was reduced several fold relative to its binding to the unmodified actin. These results implicate the C-terminus of actin either as a part of the binding site for caldesmon or as a modulator of caldesmon's binding to the N-terminus of actin.

M-Pos49

BINDING OF CALDESMON TO MYOSIN: EFFECT OF PHOSPHORYLATION AND CALCIUM-CALMODULIN. M.E. Hemric*, J.O. Carey‡, R. Lu, and J.M. Chalovich. *Department of Physiology and Biophysics, University of Vermont, Burlington, VT 05405 and Department of Biochemistry, East Carolina University School of Medicine, Greenville, NC 27858.

We have shown previously that the binding of caldesmon to myosin is saturable, reversible and nucleotide dependent (Hemric and Chalovich, 1990; J. Biol. Chem.) It has been reported that calcium-calmodulin as well as caldesmon phosphorylation affect the binding of caldesmon to actin and to myosin. Because of the effect of ATP on the binding of caldesmon to myosin, we examined in more detail, the effect of phosphorylation of both myosin and caldesmon on their mutual interaction. We also studied the effect of calcium-calmodulin on the binding of caldesmon to myosin. Our results now show that phosphorylation of smooth muscle myosin, by myosin light chain kinase, has no effect on the binding of caldesmon to myosin in either the presence or absence of ATP. Phosphorylation of caldesmon, by the kinase that co-purifies with caldesmon, does weaken the binding of caldesmon to myosin. However, the incorporation of a single phosphate group into caldesmon is not sufficient to totally inhibit the binding. Rather, the interaction of caldesmon and myosin appears to become weaker as the number of phosphate groups incorporated into caldesmon increases. This result was confirmed using myosin affinity chromatography to select for the most highly phosphorylated caldesmon species. Changes in the level of phosphorylation affect the association constant but do not appear to affect the stoichiometry of binding. Calcium-calmodulin also inhibits the binding of caldesmon to myosin in a concentration dependent manner. However, analysis of the binding data suggest that the effect of calcium-calmodulin is rather complex.

M-Pos50

ELECTRON MICROSCOPIC STUDIES OF CALDESMON AND ITS COMPLEX WITH CALMODULIN OR F-ACTIN. Katsuhide Mabuchi, Jim J.-C. Lin[1] and C.-L. Albert Wang, [1]Dept. of Biology, University of Iowa, Iowa City, IA 52242, and Dept. of Muscle Research, Boston Biomedical Research Institute, Boston, MA 02114

An improved rotary shadowing technique has enabled us to visualize chicken gizzard caldesmon (CaD) and its complex with one or two covalently linked calmodulin (CaM) by electron microscopy (Mabuchi and Wang, J. Muscle Res. Cell Motility, 1990, in press). In this method, samples are mounted on a stage rotating about a horizontal axis and the shadowing angle is kept at 2-3°. More recently, we have obtained electron microscopic images of CaD-containing samples incubated with specific monoclonal antibodies against epitopes in the N- or the C-terminal region of CaD. With the aid of these antibodies, the polarity of the CaD molecule becomes readily identifiable. Images of the CaM-CaD complex, crosslinked by benzophenone-maleimide attached to the two cysteine residues of CaD, clearly demonstrate that the two bound CaM molecules are indeed attached to the two ends of the rod-shaped CaD molecule. CaM associated with the C-terminal end of CaD appears more frequently than that bound to the N-terminal end, suggesting that the affinity for CaM is higher at the C-terminal binding site near Cys^{580} than the one near Cys^{153}. Binding of CaD to F-actin results in an image where only one end of CaD appears to be attached to the filament. It is presumably the C-terminal end of CaD that is involved in the actin-binding. We can now use the monoclonal antibodies to ascertain this assignment. (Supported by grants from NIH and AHA)

M-Pos51

CHEMICAL MODIFICATION OF THE SOLE HISTIDINE RESIDUE OF SMOOTH MUSCLE CALDESMON. Armelle A. Bonet-Kerrache and Michael P. Walsh, Department of Medical Biochemistry, University of Calgary, Calgary, Alberta, Canada T2N 4N1

Caldesmon is a major actin-, myosin-, tropomyosin- and calmodulin-binding protein which has been implicated in the regulation of actin-myosin interaction and therefore the contractile state of smooth muscle. The sites of interaction between caldesmon and its binding proteins have been loosely defined largely by study of the binding properties of defined proteolytic fragments of caldesmon. The calmodulin-binding site is conserved in the C-terminal peptide (Cys595-Pro771) generated by specific cleavage at cysteine residues. This peptide contains a basic amphiphilic α-helix-forming sequence (Arg 608-His 625) which may represent the calmodulin-binding site. This sequence contains the only histidine residue in caldesmon. Specific chemical modification of His 625 was achieved by carbethoxylation with diethylpyrocarbonate: one mol histidine was modified/mol caldesmon. The 35 kDa C-terminal thrombin fragment of caldesmon (Ser 498-Pro771) was also specifically carbethoxylated at His 625. No significant modification of tyrosine occurred. The modification was completely reversed by treatment with 0.1M hydroxylamine. Modified and unmodified caldesmon (intact and C-terminal thrombin fragment) bound to calmodulin-Sepharose in a Ca^{2+}-dependent manner. Ca^{2+}/calmodulin was equally effective in releasing modified and unmodified caldesmon from F-actin. The affinities of F-actin for modified (K_d=1.3 x 10^{-6}M) and unmodified caldesmons (K_d=8.8 x 10^{-7}M) were comparable. Modified and unmodified caldesmons bound to tropomyosin-Sepharose and were eluted with 0.4M NaCl. Modified and unmodified caldesmons were equally potent in inhibition of skeletal muscle actin-activated myosin MgATPase activity. These results indicate that the properties of the C-terminal domain of caldesmon (calmodulin-, actin- and tropomyosin-binding, and ATPase inhibition) are unaffected by incorporation of a bulky substituent into His 625. They also suggest that this histidine residue, located at the C-terminal end of the putative calmodulin-binding site, is not essential for calmodulin binding.

M-Pos52

REGULATION OF THE SMOOTH MUSCLE ACTOMYOSIN MgATPase BY REVERSIBLE PHOSPHORYLATION OF CALPONIN: PURIFICATION AND CHARACTERISATION OF A CALPONIN PHOSPHATASE. Steven J. Winder & Michael P. Walsh, Department of Medical Biochemistry, University of Calgary, Calgary, Alberta, Canada T2N 4N1.

In reconstituted smooth muscle systems physiological concentrations of calponin inhibit the actin-activated MgATPase of myosin by ~ 80%. The inhibition by calponin is due to its interaction with actin thus preventing actin-activation of the myosin MgATPase. Phosphorylation of calponin by either protein kinase C (PKC) or Ca^{2+}/calmodulin-dependent kinase II (CaMKII) reverses its inhibitory effect by preventing calponin binding to actin. For the phosphorylation of calponin to be of physiological significance, a phosphatase must be present in order to regenerate unphosphorylated calponin. Using PKC-phosphorylated calponin to follow activity, we have purified a calponin phosphatase from chicken gizzard by ammonium sulfate fractionation, ion-exchange, hydroxylapatite and aminopropyl-agarose chromatography. 80% of the resultant phosphatase preparation consists of two polypeptides of M_r 38 and 49 kDa. Calponin phosphatase was classified as a type 2A phosphatase by the following criteria: 1. Inhibition by okadaic acid (IC_{50}=0.6 nM); 2. Lack of inhibition by inhibitor 1 or inhibitor 2, the heat-stable inhibitors of type 1 phosphatase; 3. Lack of metal ion dependency. This phosphatase is somewhat unusual in that, unlike other type 2 phosphatases, it does not dephosphorylate the β subunit of phosphorylase kinase. Calponin phosphatase exhibits a degree of substrate specificity: it is inactive towards phosphorylase kinase α or β subunits or histone IIA phosphorylated by cAMP-dependent protein kinase, caldesmon phosphorylated by PKC or CaMKII, or the 20 kDa light chain (LC_{20}) of intact myosin phosphorylated by myosin light chain kinase (MLCK); it is active towards isolated LC_{20} phosphorylated by MLCK, histone IIIS phosphorylated by PKC, and calponin phosphorylated by PKC or CaMKII. Calponin is the best substrate observed to date: K_m=5.7μM; V_{max}=0.1 μmol. $min^{-1}.mg^{-1}$. Calponin phosphatase is an important component of the enzymatic machinery required for reversible regulation of calponin-mediated control of smooth muscle contraction.

M-Pos53

CALPONIN AND CALDESMON PHOSPHORYLATION IN CANINE TRACHEAL SMOOTH MUSCLE. J. Pohl, *M.P. Walsh and W.T. Gerthoffer
Dept. Pharm. Univ. Nevada School of Med., Reno, NV 89557
and *Dept. of Medical Biochem., Univ. of Calgary, Alberta.

We tested the hypothesis that the thin filament proteins calponin and caldesmon are phosphorylated and dephosphorylated in intact smooth muscle at a rate sufficient to indicate a role in contraction and relaxation. Canine tracheal smooth muscle strips were labelled with ^{32}P and stimulated with $10^{-6}M$ carbachol to induce contraction. Strips were then incubated in 0 Ca PSS +1 mM EGTA + $10^{-6}M$ carbachol to induce relaxation. Caldesmon and calponin phosphorylation was measured for each strip at various times and expressed as cpm/ug protein. Carbachol stimulation increased caldesmon phosphorylation in 30 sec to 7.9 +/- 4.8 (n=4) fold greater than basal levels of 934.3 +/- 386 cpm/ug. At 5 and 15 min caldesmon phosphorylation remained elevated at 2.8 +/- 0.6 and 2.4 +/- 0.2 fold greater than basal levels, respectively. Treatment with 0 Ca PSS + EGTA + carbachol induced relaxation and reduced caldesmon phosphorylation to 1.2 +/- 0.28 fold basal in 2 min. After 5 and 15 min caldesmon phosphorylation was 1.2 +/- 0.2 and 1.5 +/- 0.3 fold over basal, respectively. Calponin phosphorylation increased to 5.0 +/- 1.8 (n=4) fold greater than basal levels of 287 +/- 9.9 cpm/ug at 30 sec in response to carbachol and decreased to 2.2 +/- 0.6 and 2.4 +/- 0.6 fold greater than basal levels at 5 and 15 min, respectively. After treatment with 0 Ca PSS + EGTA + carbachol, calponin phosphorylation decreased to 2.1 +/- 0.8 fold basal levels in 30 sec. and then to 1.6 +/- 0.4 and 1.6 +/- 0.8 fold basal levels at 5 and 15 min. Therefore, caldesmon and calponin phosphorylation increased rapidly in response to carbachol, within 30 sec, remained elevated at steady state, and decreased in response to calcium removal. The time course of caldesmon and calponin phosphorylation is similar to the time course of changes in myosin phosphorylation and shortening velocity in this tissue (Gerthoffer, Am. J. Physiol. 250: C597, 1986). Supported by NIH DK41315 (WTG), The PMA Foundation (JP) and MRC Canada (MPW).

M-VCR1

Caldesmon-Dependent Regulation of Thin Filament Motility

[1]Joe R. Haeberle, [2]Kathleen M. Trybus, and [1]David M. Warshaw, [1]Department of Physiology and Biophysics, University of Vermont and [2]Rosenstiel Basic Medical Sciences Research Center, Brandeis University

Caldesmon has been implicated as a thin-filament linked regulatory protein in smooth muscle. Caldesmon binds to actin and tropomyosin and inhibits actin-activated myosin-ATPase activity by competitively blocking the binding of myosin to actin; caldesmon also binds specifically to the S1/S2 region of myosin (Chalovich et al.,1988,J.Biol.Chem.263:1878). We have reported that the caldesmon content (mol caldesmon monomer:mol actin monomer) of phasic smooth muscles is 1:18 compared to 1:164 in large tonic arteries (Haeberle et al.,Biophys.J. 57:166a, 1990). In the present study we have utilized an *in vitro* motility assay (Warshaw et al., J.Cell Biol. 111:453, 1990) to investigate the effects of caldesmon on the movement of unloaded actin filaments over a surface of thiophosphorylated smooth muscle myosin. Rhodamine-phalloidin-labeled actin filaments were applied to a myosin-coated glass cover-slip in the absence of ATP. Motility was initiated by the addition of MgATP at 30°C. Under conditions of high ionic strength (80mM KCl), actin filaments bound weakly to the myosin surface and did not demonstrate myosin-activated motility. Addition of a C-terminal, actin-binding chymotryptic fragment of caldesmon (34kDa) completely displaced the filaments from myosin. The addition of saturating tropomyosin, increased the binding of actin filaments which moved at a velocity of 0.75 um/sec. The increased binding seen with tropomyosin was reversed by the simultaneous addition of up to 0.1 uM intact caldesmon, however, caldesmon concentrations above 0.1 uM promoted filament binding. At a concentration of 0.2 uM caldesmon, filaments bound transiently and moved with a velocity of 1.9 um/sec. At higher concentrations of caldesmon, binding progressively increased and velocity decreased (0.5 um/sec at 20 uM caldesmon). If methyl cellulose was included in the ATP solution to promote the binding of actin under high salt conditions, unregulated actin-filaments bound and moved with a velocity of 1.5 um/sec. In the presence of methylcellulose and concentrations of caldesmon from 20 nM to 2 uM, filaments moved at a velocity $\geq$ 1.4 um/sec; peak velocity was 1.9 uM/sec at a caldesmon concentration of 100 nM. Concentrations > 2 uM rapidly inhibited velocity with complete inhibition occurring at 10 uM. Taken together these findings demonstrate that 1. the C-teminal region of caldesmon weakens the binding of actin filaments to myosin, 2. low concentrations (<0.1 uM) of intact caldesmon also weaken binding, 3. intermediate concentrations of caldesmon promote both filament binding and high velocity filament movement, and 4. high concentrations of caldesmon promote tight binding and inhibit velocity. These findings support the suggestion of Hemric et al. (J.Biol.Chem. 263:1878, 1988) that caldesmon tethers actin filaments to myosin by forming an actin-caldesmon-myosin complex. In addition they suggest that formation of this complex promotes the productive interaction of actin with myosin to produce filament movement. It remains to be determined whether this effect of caldesmon is of physiologic importance or if it contributes to the different mechanical properties of phasic vs tonic smooth muscles.

M-Pos54

OBSERVATIONS ON MICROTUBULE RING INVOLVEMENT IN CHICKEN ERYTHROCYTE AND HUMAN PLATELET SHAPE CHANGES

Michael J. Stevenson and Wray H. Huestis
Department of Chemistry, Stanford University, Stanford, CA

A peripheral ring of microtubules is found in the elliptical chicken erythrocyte and the discoidal human platelet. Amphipath-induced shape changes in these cell systems have been investigated and the involvement of the microtubule ring examined through a simultaneous fixation/extraction procedure and electron microscopy. Addition of dimyristoylphosphatidylcholine (DMPC) induces slight and severe spiculation followed by sphering in the elliptical llama erythrocyte and the biconcave discoidal human erythrocyte, respectively; both cell types lack a microtubule ring. Chicken erythrocytes treated with DMPC spiculate slightly, then form a spindle shape before sphering. Pretreatment with colchicine, which depolymerizes the microtubule ring, abolishes this intermediate spindle shape. Exposure of human platelets to dilauroylphosphatidylcholine (DLPC) often produces holes in the platelet center with filopodia along the periphery, while the boundary where the microtubule ring lies remains intact and uncollapsed. Dissolution of the microtubule ring by exposure to cold causes resting platelets to become irregular and ruffled in shape. During rewarming, many platelets become elongated before regaining their discoidal shape. Treatment of platelets with colchicine before cold exposure inhibits both elongation and discoidal shape recovery. The involvement of the microtubule ring in these shape changes is discussed. (Supported by NIH grant HL 23787.)

M-Pos55

Q–BAND EPR AND ELECTRON SPIN ECHO STUDIES ON THE INTERACTION OF Mn^{+2} WITH THE E–SITE AND THE N–SITE OF $\alpha\beta$–TUBULIN.

John J. Correia*, Albert H. Beth†, Marcelino Bernardo‡ and Hans Thomann‡. *Department of Biochemistry, Univ. of Mississippi Medical Center, 2500 North State St., Jackson, MS., †Department of Molecular Physiology and Biophysics, Vanderbilt Univ., Nashville, TN., ‡Exxon Research and Engineering Co., Route 22E, Annandale, N.J.

Preliminary EPR studies (J.J. Correia and A.H. Beth 1989 Biophys. J. 57, 348a) demonstrated that the GTPMn–occupied E–site and N–site of the tubulin heterodimer have nearly identical Q–band EPR spectra. At 4–8 °C the N–site and the composite N–site–E–site spectra reflect fully rhombic, octahedral symmetry and can be simulated with zero field splitting parameters of D = 375 G and E/D = 0.333. The N–site spectra are broadened, apparently reflecting zero field splitting heterogeneity, ie. a 20% distribution of zero–field splitting parameters D and E. The composite N–site–E–site spectra can be simulated with the same parameters and an additional 10% heterogeneity in D and E. This result is consistent with cooperativity between the metal–nucleotide sites. In frozen samples at –12 °C the spectra for bound Mn^{+2} at the E– and the N–site are identical to one another and to the unfrozen N–site spectra reflecting the similarity of these GTP binding sites. Pulsed electron spin echo (ESE) modulation spectra were collected on samples of tubulin–bound Mn^{+2} with GTP or GDP bound at the E–site to investigate the role of water in Mn^{+2} coordination. D_2O exchange experiments reveal the presence of water molecules in the first coordination sphere of Mn^{+2} at both the E– and the N–site. The data are consistent with the water acting as a bridge to other H–accepters. The ESE data are also consistent with ^{31}P at the β and/or γ positions of the triphosphate coupled through an oxygen to Mn^{+2}. This result confirms that the divalent cation is coordinated to the guanine triphosphate at both the N– and the E–site of tubulin. Experiments are in progress to count the number of H_2O molecules in the first coordination sphere and verify the number of PO ands in the first coordination sphere. Future experiments will ›be the conformational changes, as viewed from the metal site, ‹t occur upon microtubule formation and during microtubule namics.

M-Pos56

STUDIES OF CRYSTALLIZATION CONDITIONS FOR NATIVE AND SUBTILISIN-CLEAVED TUBULIN

Sharon Lobert* and John J. Correia+, *School of Nursing and +Department of Biochemistry, University of Mississippi Medical Center, Jackson, MS 39216

A survey of crystallization conditions for pig brain tubulin, using standard vapor diffusion techniques in sitting drops or capillaries, has resulted in irregular, fragile needles or plates with their largest dimension .5mm. They occur in 2.5% PEG (MW 3350), .1 M Pipes, pH 6.2 and 6.4, 2-16 mM $MgSO_4$ and .1 mM GDP at 8°C. When GTP replaces GDP these aggregates do not form under any of the conditions surveyed (ie. temperature: 8-10°C, $MgSO_4$: 2-16 mM, pH: 6-7, PEG MW 3350: 1.25-12.5%). EM observations demonstrated that sheets of rings appear in crystal solutions in the presence of GDP or GTP. These results are consistent with the experiments of Howard and Timasheff (1986, Biochemistry, 25, 8292-8300), where it was found that tubulin double rings form more readily in the presence of GDP than in GTP. Tubulin crystallization experiments are hampered by its high degree of heterogeneity. Much of the variability lies in the carboxyl terminal region. Conditions for limited digestion of the heterodimer by subtilisin, removing only the carboxyl terminus, were determined. Reduction of heterogeneity was demonstrated by isoelectric focussing. The solubilities of native and subtilisin-cleaved tubulin in $MgSO_4$, $(NH_4)_2SO_4$, PEG (MW1450,3350,10000), DMSO, MPD were compared. Subtilisin-cleaved tubulin precipitates more readily than native tubulin, consistent with the fact that the carboxyl terminus is highly acidic. Vapor diffusion experiments using subtilisin-cleaved tubulin under conditions where native tubulin forms needles or plates resulted in similar aggregates.

M-Pos57

ATP AND THE DYNAMIC INSTABILITY OF MICROTUBULES.

Alan R. Cross and Robley C. Williams, Jr., Department of Molecular Biology, Vanderbilt University, Nashville, TN 37235.

Previous reports [e.g., O'Brien & Erickson (1989), Biochemistry 28, 1413] have shown that ATP, under certain conditions, may stabilize microtubules against disassembly. To see if this is a general effect, we have employed video-enhanced DIC microscopy to measure the dynamics of individual microtubules nucleated by pieces of flagellar axonemes in the presence and absence of ATP. Control measurements were made in 0.1 M Pipes, 2 mM EGTA, 1 mM DTE, pH 6.9, at 37°, at a tubulin concentration of 11 µM, in presence of 1 mM GTP and 1 mM $MgSO_4$. In the experimental measurements, both ATP and additional $MgSO_4$ were added, to maintain the concentration of free Mg^{2+} at 0.34 mM, equivalent to that in the controls. In the results shown below, where rates for (+) and (-) ends are averaged together, the dynamic properties of the microtubules appear virtually unaffected by ATP.

Addition	Growth rate (µm/min)	Shortening rate (µm/min)	Catastrophe frequency (min^{-1})	Rescue frequency (min^{-1})
None	1.2	-37	.29	5.6
2 mM GTP	1.6	-38	.19	3.8
2 mM ATP	1.2	-35	.24	4.4
4 mM ATP	1.3	-40	.25	4.4

We conclude that ATP, when its Mg^{2+}-binding capacity is compensated for, has little effect on dynamic instability. (Supported by NIH GM 25638.)

M-Pos58

TUBULIN CONFORMATIONAL STATE DETERMINATION OF ORGANIZATION OF MICROTUBULE NETWORKS: A COMPUTATIONAL INTERPRETATION.

R Lahoz-Beltra(1,2), S Rasmussen(3), S Hameroff(2), (1) Fulbright Scholar, Complutense Univ. of Madrid, Madrid-28040, Spain (2) Adv. Biotech. Lab., Dept. of Anesth., Univ. of Az. HSC, Tucson, AZ 85724, (3) CNLS, LANL, MS-258, Los Alamos, NM 87545.

Spatial and temporal assembly/disassembly of microtubules (MT) determine cell shape and function. Evidence for multiple conformational states of free tubulin, and GTP hydrolysis-induced conformational changes of tubulin within MT allow us to consider the importance of tubulin conformational states in dynamic behavior of MT and the cytoskeleton. Previously (Rasmussen et al., Physica D 42,428-449, 1990) we have modelled MT assembly/disassembly using a 5-state automaton and were able to simulate MT "dynamic instability" (Kirschner & Mitchison, Cell 45, 329-342, 1986). In the present work, we use MT conformational and energy states as the basis for a "mobile finite automaton" model (Thompson & Goel, J Theor Biol 131, 351-385, 1988) of MT assembly/disassembly. Our simulations suggest cytoskeletal activities and cellular functions can be organized by coordinated conformational changes among tubulins. The molecular logic underlying such conformational changes can be considered as a natural programming language within cells.

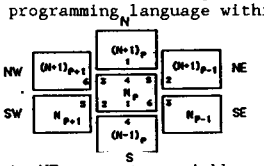

A. MT automaton neighbor hood and bond site relationship (p=protofilament, n=dimer number) Sites 3, 4 and 5 are on alpha monomer, 2,1 and 6 on beta.

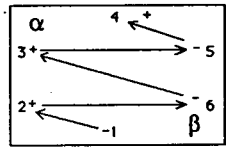

B. Conformational change in tubulin simulated as coordinated changes in value of each bond site.

Supported by Fulbright/MEC.

M-Pos59

STIMULUS-RESPONSE COUPLING IN HUMAN RESPIRATORY CILIATED CELLS IN VITRO.

M.Villalón, T. R. Hinds* and P. Verdugo. Ctr. for Bioengineering and Dept of Pharmacology*, University of Washington, Seattle, WA 98195, USA.

Previous investigations have shown that in epitheliary ciliated cells both prostaglandins and purinergic stimulation are coupled by an increase in cytosolic [Ca^{++}]. While stimulation by prostaglandin $F_{2\alpha}$ releases Ca^{++} from intracellular stores, stimulation by ATP induces inflow of Ca^{++} from the extracellular space (Nature 283,764, 1980; Biophys. J. 56,1255,1989). Beta-adrenergic agonists can also stimulate ciliary activity (AJP 48, 868, 1980; Cell Motil 1, 5, 1982), however the role of Ca^{++} in the coupling of β-adrenergic cilio-stimulation has not been investigated. The experiments presented here were designed to study the effect of purinergic and β-adrenergic stimulation in human ciliated cells, and the effect of these agonists on cytosolic [Ca^{++}].

Monolayers of ciliated cells of human airway were grown in primary culture (J.Appl Physiol 48,868,1980). The frequency of ciliary beat was monitored by laser-Doppler spectroscopy (Biophys. J. 16,1115,1976) Cytosolic [Ca^{++}] was measured by fluorescence emission of Fura 2 (JBC 260, 3440,1985).

Preliminary results are consistent with our previous findings in rabbit epitheliary ciliated cell that both ATP (100 μM) and isoproterenol (100 μM) can stimulate ciliary movement. Cytosolic [Ca^{++}] was found to transiently increase from about 100 nM to about 700 nM immediately following stimulation with 100 μM ATP. Although cytosolic [Ca^{++}] did not vary following stimulation of human ciliated cells with isoproterenol, more observations will be needed to verify the role of this cation in the cilio-stimulating effect of of β–adrenergic agonists.

Supported by grants HL-38494 and HL 24136 from NIH, and R 010-701 from the CCF. M.Villalón was supported by a fellowship from the CFF.

M-Pos60

THE EFFECTS OF SODIUM WITHDRAWAL ON K^+ CONTRACTURES AND CHARGE MOVEMENT IN FROG SKELETAL MUSCLE FIBERS. A.F. Díaz*, M.C. García** and J.A. Sánchez*. *Department of Pharmacology CINVESTAV-IPN, A. Postal 14-740, México 07000, D.F. and **Department of Biophysics, ENCB-IPN. Mexico City, Mexico.

The effects of Na^+ withdrawal on K^+ contractures and charge movement were investigated in single muscle fibers of Rana montezumae at T = 22-25°C. Methods: Isometric tension recording in intact fibers, and the triple vaseline gap voltage clamp technique (Hille & Campbell, J. Gen. Physiol. (1976) 67: 265-293) for charge movement experiments. Charge movement solutions were (mM): External: Ca^{2+} = 1, Co^{2+} = 10, Na or TEA = 81. TTX = 0.1, pH = 7.2 and $SO_4^=$ as anion. Internal: $MgCl_2$ = 1.5, EGTA = 1, Cs glutamate = 110, Na_2ATP = 2, pH = 7.2. Solutions for mechanical experiments were as in Hodgkin & Horowicz (J. Physiol. (1959) 148: 127-160). Na^+ was replaced by NMG. Results: K^+ contractures were potentiated in the absence of Na^+. With $[K^+]_o$ = 30 mM, tension doubled with a time constant of ca. 8 min. Potentiation was less pronounced for higher values. Time to half the peak value of K^+ contracture in $[K^+]_o$ = 30 mM decreased by 50% and spontaneous decay of tension became faster in NMG. Steady steady inactivation of K^+ contracture measured with double pulse experiments was shifted to lower $[K^+]_o$. Caffeine (2 mM) contractures increased 300% in the absence of Na^+. Movement of charge 1 did not depend on $[Na^+]_o$. However the mechanical threshold decreased by ca 10 mV at all pulse durations and the threshold charge increased by ca 50% in the presence of Na^+. Intracellular heparin (40 mg/ml) shifted the strength duration curve of the mechanical threshold by ca 20 mV towards more positive potentials but did not affect charge movement.
It is concluded that Na^+ withdrawal potentiates tension at a location beyond the voltage sensor.

Supported by CONACyT # DIII-904647

M-Pos61

EFFECTS OF CHOLESTEROL CONTENT ON CALCIUM CHANNEL BLOCKERS' PARTITIONING AND LOCATION IN MODEL AND NATIVE MEMBRANES.

R.P. Mason, L. Shajenko, and J. Hazard. The Travelers' Center on Aging and Biomolecular Structure Analysis Center, University of Connecticut Health Center, Farmington, CT. 06032

The effect of membrane cholesterol content on the interactions of 1,4-dihydropyridine and phenylalkylamine Ca^{+2} channel blockers was examined using small angle x-ray diffraction and radioligand binding assays. Several lines of experimental evidence suggest that certain Ca^{+2} channel blockers bind to hydrophobic, intramembrane receptor sites following partitioning and diffusion through the membrane bilayer. Thus, an understanding of drug interaction with the membrane bilayer may be essential to describing these drugs' molecular pharmacology.

Electron density profiles generated from the diffraction data showed that the addition of cholesterol produced a substantial increase in electron density within the membrane hydrocarbon core in a region approximately 11 Å in width, approximately the length of cholesterol's steroid nucleus. The resolution of these experiments was 8 Å. The presence of cholesterol in cardiac lipid multilayers altered the time-averaged location of the phenylalkylamine verapamil by approximately 17 Å from near the membrane bilayer center in the absence of cholesterol to near the hydrocarbon core/water interface in the presence of 25 mol% cholesterol. The location of the DHP amlodipine did not change as a function of cholesterol content. Correlating with structure data, the rate of verapmil's membrane dissociation was 2 fold longer in the absence of cholesterol versus 25 mol% cholesterol. By contrast, the dissociation of amlodipine was not significantly affected by cholesterol content. The partition coefficient ($K_{P[mem]}$) of these drugs into model and native membranes was highly influenced by membrane cholesterol content. The $K_{P[mem]}$ s for nimodipine, verapamil and amlodipine were reduced 11, 5 and 3 fold, respectively, between 0 and 37.5 mol% cholesterol in cardiac lipid extracts. These data showed that membrane composition can dramatically affect drug interactions with the membrane bilayer. (Supported by AHA, CT Affiliate; John A. Hartford Foundation and Pfizer Laboratories, New York).

M-Pos62

CAFFEINE BLOCKS Ca^{2+} CHANNEL INDEPENDENT OF ITS Ca^{2+} RELEASING PROPERTIES.

J.S.K. Sham, L. Cleemann, and M. Morad. Department of Physiology, University of Pennsylvania, Philadelphia, PA 19104.

Caffeine, which releases Ca^{2+} from sarcoplasmic reticulum, has been found to attenuate Ca^{2+} current (I_{Ca}) in purkinje fibers, guinea-pig atrial cardioballs and rat ventricular myocytes. The inhibition of I_{Ca} by caffeine could be ascribed either to Ca^{2+} induced inactivation resulted from the elevated intracellular Ca^{2+} concentration, and/or to a direct effect of caffeine on Ca^{2+} channels. In this study, we examined the latter possibility in ventricular myocytes perfused intracellularly with high Ca^{2+} buffer (mM): 120 CsCl, 5 MgATP, 14 EGTA, 20 HEPES, 0.01 cAMP. Caffeine at concentration between 1 to 10 mM was found to inhibit I_{Ca} in a concentration-dependent manner at various membrane potentials without shifting its voltage-dependence. The inhibition was fast and complete within 3-5 sec. The steady-state inactivation curve was suppressed but not significantly shifted by caffeine at holding potentials between -60 to -20 mV. The suppressive effect of caffeine on I_{Ca} was reversible, with complete recovery occuring within 20 sec of washout. When Ca^{2+} was replaced by Ba^{2+}, caffeine continued to inhibit I_{Ba} in a similar manner. The inhibitory effect of caffeine on I_{Ca} persisted even in the presence of 10 μM ryanodine, which suppresses Ca^{2+} release from the SR. Simultaneous measurement of I_{Ca} and Ca^{2+} transient in myocytes perfused with 0.4 mM fura-2 but without any other Ca^{2+} buffer showed that the inhibition of I_{Ca} by caffeine occurred even when the resting intracellular Ca^{2+} concentration was unchange and the Ca^{2+} transients induced by depolarizing pulses were greatly reduced. The data suggest that caffeine has a direct inhibitory effect on L-type calcium channels irrespective of the Ca^{2+} induced inactivation mechanism. (Supported by NIH grant HL16152)

M-Pos63

A ROLE FOR SODIUM-CALCIUM EXCHANGE IN RELEASE OF CALCIUM FROM SARCOPLASMIC RETICULUM IN GUINEA-PIG VENTRICULAR MYOCYTES. Paul C. Levesque, Normand Leblanc, and Joseph R. Hume, Department of Physiology, University of Nevada School of Medicine, Reno, Nevada, 89557.

Previously, we have reported that Na^+ influx through tetrodotoxin-sensitive Na^+ channels induces release of Ca^{2+} from cardiac SR. To test more directly whether Na^+-Ca^{2+} exchange mediates the Na^+ current-induced release of Ca^{2+} from SR, we used the Ca^{2+} indicator, indo-1, in whole cell voltage clamped myocytes to measure Ca^{2+} transients elicited via Na^+ current activation before and after inhibiting the exchanger. Typically, following a conditioning protocol (10-500 ms voltage clamp pulses from -80 to +60 mV at 0.2 Hz) to load Ca^{2+} stores, activation of Na^+ current during a test pulse to -50 mV from a holding potential of -80 mV elicited a Ca^{2+} transient in cesium-loaded myocytes superfused with solutions containing 2.5 mM Ca^{2+} and 5 μM nisoldipine. Intracellular Ca^{2+} rose to over 300 nM during the depolarizing test pulses before slowly returning to resting levels of about 150 nM. When extracellular Na^+ was replaced with equimolar lithium, which carries current through Na^+ channels but does not readily substitute for Na^+ on the Na^+-Ca^+ exchanger, or when Ni^{2+} (5 mM) or dichlorobenzamil (10 μM), which block the exchanger, were added to superfusion solutions, activation of Na^+ currents failed to elicit Ca^{2+} transients. These results provide further evidence in support of the hypothesis that depolarization induced Na^+ influx can trigger sarcoplasmic Ca^{2+} release in cardiac myocytes by activating Ca^{2+} entry through reverse-mode Na^+-Ca^{2+} exchange. (Supported by NIH grant HL 30143 and grants from AHA)

M-Pos64

KINETICS OF RYANODINE BINDING TO HEAVY SARCOPLASMIC RETICULUM VESICLES.

CHAUNAVEL, A., RONJAT, M and DUPONT, Y. Lab B.M.C, B.P 85 X, DBMS / CEN.G 38041 Grenoble, FRANCE.

Ryanodine (rya) is one of the best available probe to study direct binding of effectors to the Ca-channel of sarcoplasmic reticulum (SR). We have determined the kinetics of association and dissociation of rya with its receptor on SR vesicles. In our hands the time course of association of rya consistenly followed a simple pseudo-first-order kinetic. Moreover only one type of rya binding site was observe and the site concentration (Bmax) reliably equaled 30 nmoles/mg. We measured the apparent association rate constant of rya at different different rya concentration and pCa. A wide range of rya (2.5 to 700 nM) and Ca (pCa2 to 7) concentrations was explored. At each pCa we obtained a set of absolute association and dissociation rate constants that satisfied the rya concentration dependence of the apparent "on" and "off" rate constants as well as the observed equilibrium constant. We show that the association rate constant and the equilibrium constant vary as a function of pCa while the "off" rate constant does not. From these data we propose that the rya binding mechanism involves the existence of at least two cooperatively interacting activating Ca sites (Ka = 2-3 uM) and one inhibitory low affinity Ca site (Ki = 1.2 mM).

The effects of Ca on Ca-channel activity suggest that the Ca binding sites interacting with the ryanodine binding sites are the same as those involved in the activation and the inhibition of the SR Ca channel.

M-Pos65

EFFECTS OF PROCAINE ON CALCIUM RELEASE IN SKELETAL MUSCLE FIBERS.

S. González, G. Brum and G. Pizarro. Department of Biophysics, School of Medicine, Montevideo, Uruguay.

Procaine is an inhibitor of calcium induced calcium release (CICR) in skinned fibers and sarcoplasmic reticulum (SR) vesicles. The effect of this drug was studied in single cut fibers of the frog in a double vaseline gap voltage clamp. Charge movement and myoplasmic calcium transients were measured simultaneously. The effect of extracellularly applied procaine depends dramatically on external pH. at pH = 7, 1 mM procaine reduced the amplitude of the calcium transient elicited by a depolarizing pulse from -85 to 0 mV by 10 to 30 %. With the same concentration at pH = 8.5, the reduction was 70 %. In both cases charge movement was not affected. With a pKa of 8.9, at pH = 7 only 1 % of the drug is in its uncharged membrane permeable form, while at pH = 8.5 , 24 % is in this form. This pH dependence suggests an hydrophobic pathway to the site of action. The lack of effects on charge movement would imply a direct interaction with the SR calcium release channel. These results suggest: i) there is a CICR component operating under physiological conditions or ii) the drug inhibits calcium release independently of the triggering mechanism.

Supported with funds of PEDECIBA and Fundación Manuel Pérez.

M-Pos66

Ca FLUXES RELATED TO E-C COUPLING IN FROG FAST FIBERS.

B.A.Curtis, University of Illinois College of Medicine at Peoria, Peoria, IL 61656

^{45}Ca applied to small bundles of twitch muscle fibers during the mechanically refractory period following a potassium contracture enters a Ca pool with a rapid (5-15 min) time constant of efflux, Ca_{fast}. ^{45}Ca uptake increases with exposure during recovery; 4.7 pmolCa/30 sec to 10.6 pmolCa/120 sec. This ^{45}Ca uptake appears to be refilling a Ca compartment emptied during the preceding contracture. When a fiber with Ca_{fast} loaded with ^{45}Ca undergoes a second contracture (without ^{45}Ca in the solution) the efflux is then from a long (>100 min) time constant compartment, Ca_{slow}. Ca_{fast} no longer contains ^{45}Ca; it completely emptied during contraction and refills with non-radioactive Ca. The ^{45}Ca uptake into Ca_{slow} associated with this second contracture is 0.5 pmolCa; and must have transferred there from Ca_{fast}. If the bundle undergoes a caffeine contracture after Ca_{fast} is loaded with ^{45}Ca during recovery, the ^{45}Ca remains in Ca_{fast}. If a second K^+ contracture is blocked by 0.5 mM tetracaine applied after recovery, the ^{45}Ca which entered Ca_{fast} during recovery remains there in spite of the depolarization. ^{45}Ca loss from Ca_{fast} and ^{45}Ca uptake into Ca_{slow} appear related to E-C coupling rather than either depolarization or contraction alone. Supported by The Illinois Affiliate, American Heart Association.

M-Pos67

INTERNAL AND EXTERNAL BLOCKING SITES FOR DIVALENT CATIONS IN THE RYANODINE RECEPTOR OF SKELETAL MUSCLE.

Cheol Joo Lee and Roberto Coronado Department of Physiology, University of Wisconsin Medical School, Madison WI 53706

Ryanodine receptor channels of rabbit skeletal muscle heavy SR were recorded in planar bilayers using Cs^+ as charge carrier. The (Po) ranged from 0.05 to 0.15 at a free myoplasmic and lumenal (internal space of the SR) Ca^{2+} of 3.5 μM. Following activation of the channel by 3.5 μM myoplasmic Ca^{2+}, we studied the inhibition of activity produced by divalent cations added to the myoplasmic or lumeal solutions. The inhibitory potency of cations added to the myoplasmic side was Mg^{2+} (Kd=6.2 nM)> Mn^{2+} > Ca^{2+} > Cd^{2+}, Ba^{2+}, Ni^{2+}, Zn^{2+} > Co^{2+} > Sr^{2+} (Kd=1.1 mM). For cations added to the lumenal side, the ranking order was Ni^{2+} (Kd=6.4 μM), Zn^{2+} > Mn^{2+} > Cd^{2+}, Ca^{2+} > Sr^{2+} > Ba^{2+} > Co^{2+} > Mg^{2+} (Kd=2.7 mM). The myoplasmic inhibition was unrelated to atomic size but the lumenal inhibition varied inversely with the atomic size of blocking cations (except for Co^{2+} and Mg^{2+}). Hill coefficients were less than 1.0 in most cases. The activation by myoplasmic Ca^{2+} could thus be blocked at a cytosolic site and independently at a lumenal site. Since lumenal Ca^{2+} inhibited myoplasmic activation by Ca^{2+}, we studied the effect of lumenal Ca^{2+} on the Po vs myoplasmic pCa curve. At constant 3.5 μM lumenal Ca^{2+}, myoplasmic Ca^{2+} increased the Po at pCa<8 and decreased the Po at pCa<4 resulting in a bell-shaped Ca^{2+}-dependence centered at pCa 6. At constant 2 mM lumenal Ca^{2+}, the Po was depressed 10-fold at all myoplasmic pCa. The curve was bell-shaped but centered at pCa 3. From these results we concluded that millimolar levels of lumenal free Ca^{2+} severely inactivated the channel and shifted the myoplasmic Ca^{2+} dependence towards higher concentrations. The lumenal divalent binding site therefore appears to control the sensitivy the ryanodine receptor towards myoplasmic activation by Ca^{2+}. Supported by NIH, MDA, and AHA.

M-Pos68

TOXINS OF EXCITATION-CONTRACTION COUPLING: B. HOTTENTOTA SCORPION VENOM ENHANCES [3H]RYANODINE BINDING AND OPENS CALCIUM RELEASE CHANNELS OF SKELETAL MUSCLE. Hector H. Valdivia and Roberto Coronado. Department of Physiology, University of Wisconsin, Madison, WI 53706. (Introduced by Henry A. Kubinski).

Scorpion venoms have traditionally represented a rich source of toxins specific for Na^+ and K^+ channels. Using the binding of [3H]ryanodine as an indicator of activity, we screened 10 venoms in search of toxins specific for SR Ca^{2+} channels. In a standard assay containing 0.2 M KCl, 10 μM Ca^{2+}, pH 7.2, [3H]ryanodine binds to heavy SR vesicles of skeletal muscle with a K_d = 8 nM and Bmax = 4.2 pmoles/mg protein. At 80 μg/ml, the venom of the african scorpion *B. hottentota* increased the K_d to 3.4 nM and increased the Bmax to 7.8 pmoles/mg. In a plot of [3H]ryanodine binding activity as a function of [Ca^{2+}], the effect of *B. hottentota* was seen at all [Ca^{2+}]. The mechanism of action was different from that of caffeine, which increased [3H]ryanodine binding only at low [Ca^{2+}]. At low [Ca^{2+}] (10 nM), there was a dramatic synergism when both agonists were combined. Calcium release channels recorded after fusion of SR to planar bilayers averaged a Po of 0.24 at +20 mV and ~3 μM cis (cytoplasmic) [Ca^{2+}]. Addition of 100 μg/ml of *B. hottentota* venom increased Po to 0.89 and induced the appearence of a subconductance state with a kinetics and amplitude similar to the subconductance state produced by ryanodine. These results confirmed a direct channel-toxin interaction. The isolation of this novel ligand of the ryanodine receptor will help to establish the functional role of Ca release channels in excitation-contraction coupling. Supported by AHA, NIH and CFF.

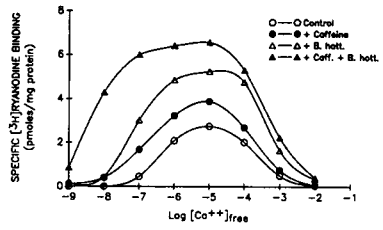

M-Pos69

RYANODINE RECEPTORS OF SARCOPLASMIC RETICULUM IN PIG AND HUMAN MALIGNANT HYPERTHERMIA ARE HIGLY SENSITIVE TO Ca AND CAFFEINE. Hector H. Valdivia, Oscar Fuentes, Jeffery Morrissette, Roque El-Hayek*, Kurk Hogan* and Roberto Coronado. Department of Physiology, and *Department of Anesthesiology, University of Wisconsin, Madison, WI, 53706. (Introduced by Lea Ziskind-Coinham).

Malignant hyperthermia (MH) is an inherited disorder in which sustained muscle contraction and elevation in body temperature are triggered by commonly used inhalational anesthetics and muscle relaxants. A defect in intracellular Ca homeostasis, due to a malfunction of ryanodine receptors (RyR)-Ca release channels in the SR, has been suspected to underlie the hypercatabolic state characteristic of MH. To determine which properties of the RyR were selectively affected in MH, and to determine how these anomalies would be revealed at the functional level, we performed binding experiments of [3H]Ryanodine to the receptor of normal and MH human skeletal muscle. Parallel studies were conducted in a pig animal model of MH. Normal (N) and MH human receptors solubilized with CHAPS bind [3H]Ryanodine in a Ca-dependent manner with an affinity constant for Ca (K_d[Ca]) of 250 ± 80 nM (N) and 120 ± 50 nM (MH). In N receptors, caffeine (10 mM) decreased K_d[Ca] to 40 ± 20 nM and reduced the minimum free Ca threshold necessary to detect [3H]Ryanodine binding to pCa 8. In MH, 10 mM caffeine reduced K_d[Ca] to 7 ± 4 nM and decreased the Ca threshold for [3H]Ryanodine binding to pCa 9. Similar results were obtained in N and MH pig receptors. Ca release channels recorded after fusion of SR to planar bilayers did not differ significantly in slope conductance and channel kinetics between N and MH populations. However, the caffeine sensitivity of MH channels was significantly increased. At +20 mV and 0.1 μM cytoplasmic [Ca^{++}], Po was 0.013 in N and 0.020 in MH. Following addition of 10 mM caffeine, Po increased to 0.38 in N and to 0.083 in MH. We conclude that an abnormal RyR, highly sensitive to Ca and caffeine, is present in MH skeletal muscle and suggest that the molecular pathology of MH resides in an abnormal Ca binding site in the RyR protein. Supported by NIH and AHA.

M-Pos70

CARDIAC AND SKELETAL RYANODINE RECEPTOR ISOFORMS IN FROG FAST-TWITCH SKELETAL MUSCLE IDENTIFIED BY ANTIBODIES. F. Anthony Lai, Qi-Yi Liu, Anita El-Hashem and Gerhard Meissner. Department of Biochemistry and Biophysics, University of North Carolina, Chapel Hill, NC 27599-7260.

The ryanodine receptor(RyR)-Ca^{2+} release channels of mammalian skeletal and cardiac muscle sarcoplasmic reticulum have been purified as homotetrameric 30S protein complexes of M_r ~560,000 polypeptides. The skeletal and cardiac RyR are homologous channels, but have been shown to be distinct proteins with respect to their Ca^{2+} activation, mobility on SDS gels and amino acid sequence. Using an identical isolation procedure for purifying the frog fast-twitch skeletal muscle RyR also resulted in identification of a 30S ryanodine-binding protein complex, but which comprised two distinct high molecular weight polypeptides, as has been found for the chicken pectoral muscle RyR (Airey *et al.*, *JBC* 265, 14187). The mobility of the upper and lower frog RyR doublet in SDS gels corresponded to that of the mammalian skeletal and cardiac RyR polypeptides, respectively. Immunoblot analysis showed that a polyclonal antiserumto the rat skeletal RyR cross-reacted with the upper, but not the lower, band of the frog receptor doublet. Conversely, monoclonal antibodies to canine cardiac RyR cross-reacted preferentially with the lower band of the frog receptor. This suggests the possible coexpression of skeletal- and cardiac-like RyR isoforms in amphibian fast-twitch skeletal muscle. Preliminary single channel recordings of the purified frog 30S receptor indicated a single main conductance of ~600 pS in 500 mM Na^+. Further characterization of ryanodine binding to, and $^{45}Ca^{2+}$ efflux from, isolated frog heavy SR vesicles is currently being performed to clarify the function of these two isoforms in frog skeletal muscle. Supported by USPHS and MDA grants.

M-Pos71

ACTIVATION OF A G-PROTEIN CAUSES CONTRACTION OF SKINNED FROG SKELETAL MUSCLE VIA THE DHP-SENSITIVE Ca^{++} CHANNELS OF SEALED T-TUBULES. B SOMASUNDARAM*, R T TREGEAR* & D R TRENTHAM@
*Institute of Animal Physiology, Babraham, Cambridge CB2 4AT, U.K. @NIMR, Mill Hill, London NW7 1AA, U.K. (Intro. by J.C.Kentish).

We have investigated the involvement of G-proteins in excitation-contraction coupling of fast twitch skeletal muscle, using a fibre preparation designed to retain intact T-tubules and sarcoplasmic reticulum. Single sartorius fibres were mechanically skinned in a relaxing solution ([mM] 110, K-propionate; 4, Mg acetate; 4, Na_2ATP; 1, NaN_3; 0.1-5, EGTA; 20, MOPS; pH 7.0) loaded with calcium (pCa 6.6) for 60s and rinsed in a relaxing solution containing 50-100μM EGTA, 5 mM creatine phosphate; 100u/ml creatine kinase. $GTP_\gamma S$ (114±23μM) and GMPPNP (647±44μM), nonhydrolysable analogues of GTP which activate G-proteins, caused a strong, transient isometric contraction in this preparation. Reduction of the calcium buffering of the sealed T-tubules by altering the EGTA concentration from 5mM to 0.1mM lowered the threshold to $GTP_\gamma S$. Sustained T-tubule depolarisation (avoiding Na^+ in the skinning and subsequent solutions) reversibly raised the threshold to $GTP_\gamma S$-induced contraction. The dihydropyridine (DHP) calcium channel antagonists nicardipine (10μM) and nifedipine (10μM) allowed a first contraction and then blocked subsequent $GTP_\gamma S$ action. The phenylalkylamine D600 (10-100μM) did likewise reversibly at 10°C. $GDP_\beta S$ and procaine reversibly blocked the action of $GTP_\gamma S$; pertussis toxin also blocked it. Photolytic release of 68 ±9μM, (n=20) $GTP_\gamma S$ within 0.1 s from S-caged $GTP_\gamma S$ caused contraction after a latent period of 0.3-20 s. Photolysis of S-caged $ATP_\gamma S$ in the same experiments did not cause contraction. We conclude that $GTP_\gamma S$ can activate contraction in frog skeletal muscle via a route requiring both the integrity of the T-tubular DHP sensitive calcium channel (DHPr) and the presence of Na^+ in the sealed T-tubules. We propose that in this preparation $GTP_\gamma S$ activates a G-protein, which in turn activates the DHPr as a calcium channel and releases stored calcium from within the sealed T-tubule.

M-Pos72

THE EFFECTS OF TAURINE DEPLETION ON EXCITATION-CONTRACTION COUPLING IN RAT CARDIAC TRABECULAE. N. Lake, D.W. Eley, H.E.D.J. ter Keurs, Department of Physiology, McGill University, Montreal, and Departments of Medicine and Medical Physiology, University of Calgary, Calgary.

The sulfur-containing amino acid taurine is the major free amino acid within mammalian myocardium. Taurine deficiency has been associated with reduced active tension and prolonged relaxation [Lake *et al*, Can J Physiol Pharmacol 68:800, 1990], and may cause heart failure [Pion *et al*, Science 237:764, 1987].. We have studied rat myocardium to investigate mechanisms underlying abnormal excitation-contraction coupling due to taurine depletion. Rats were treated with the taurine transport antagonist guanidinoethane sulfonate (GES), which specifically depletes myocardial taurine by 70-80% [Lake *et al*. Life Sci 40:997, 1987]. Free-running right ventricular trabeculae (n=5) were dissected from the right ventricle after 6 weeks of GES treatment, and compared with 6 muscles (C) from rats fed a normal diet. Twitch force (Fo) was measured with a silicon strain gauge, and sarcomere length (SL) with laser diffraction techniques. The muscles were stimulated from 0.2-3.2 Hz in modified Krebs Henseleit solution (pH 7.4, T=26 C) with varying [Ca^{2+}]; resting SL=2.15 μm. Fo in both taurine depleted muscles and in controls increased by 30% with increase of stimulus frequency from 0.2 Hz and 3 Hz ([Ca^{2+}] = 0.7mM). Time to peak force, the Fo - [Ca^{2+}] and the Fo - SL relationships of the groups were similar. Time to 50% of Fo during relaxation of the twitch and rest potentiation were increased by 20% in taurine depleted muscles. The decay-constant of Fo during decay of post extra-systolic potentiation (B_f) was reduced in taurine depleted muscles compared to controls (B_f control = 0.78 ± 0.02; B_f taurine deficient = 0.67 ± 0.05; mean ± s.e.m.; $p<0.05$).

Our observations suggest that taurine deficiency may reduce Ca^{2+} uptake by the SR. Secondary enhancement of sarcolemmal Ca^{2+} extrusion through Na^+/Ca^{2+} exchange could explain prolongation of late repolarization of the rat cardiac action potential [Lake *et al*., 1987].

Supported by the MRC and the Heart and Stroke Foundations of Canada.

M-Pos73

PHENYLGLYOXAL EFFECTS ON CALCIUM CURRENTS AND CHARGE MOVEMENT.
P. Bolaños. CBB, IVIC, Caracas, Venezuela.

Charge movement and excitacion-contraction coupling (EEC) are diminished by phenylglyoxal (PGO) treatment (Etter, J. Physiol. 421:441, 1990). As proposed by Ríos and Brum (1987), there is now increasing evidence favouring a dual function for dihydropyridine receptors (DHPR) acting both as voltage sensors for excitation-contraction coupling and voltage dependent L-type calcium channels. Therefore we studied the effect of PGO on both functions using the three vaseline gap voltage clamp technique with cut skeletal muscle fibers from tropical toad L.insularis (Caputo and Bolaños, 1989). Beside inhibiting 37% of the charge movement (n=6)(Etter, 1990), PGO 5 mM (pH 7.5-8) also inhibited 55% (n=6) of the peak calcium current with a similar exponential time course decay. PGO also slowed the open and closed time kinetics of calcium channels and the ON and OFF falling phase of charge movement. The charge distribution curve was shifted by 4 ± 1 mV toward more negative potentials and the potential dependence of ICa did not appear to be affected. The similarity of action of PGO on charge movement and calcium current is compatible with the idea of the same molecular entity serving for both functions. (Supported by Muscular Dystrophy Association, MDA).

M-Pos74

RYANODINE DEPRESSION WAS POTENTIATED BY HALOTHANE IN SKINNED MYOCARDIAL FIBERS OF THE RABBIT. **J.Y. Su, Department of Anesthesiology, RN-10, University of Washington, Seattle, WA 98195 USA**

Ryanodine (RYA), a sarcoplasmic reticulum (SR) Ca^{2+} channel blocker, causes dose-related depression of the second control caffeine-induced tension transient in skinned myocardial fibers (Pflügers Arch 411:132,1988). Halothane (HAL), an anesthetic, enhances the submaximum caffeine-induced tension transient (Pflügers Arch 380:29,1979). The purpose of this study was to examine whether HAL would cause an additive RYA depression if increased Ca^{2+} release from the SR by HAL is by direct activation of the SR Ca^{2+} channel. Accordingly, I studied the interaction between HAL, submaximum caffeine, and RYA on the tension transient in skinned rabbit muscle fibers. Right ventricular papillary muscles were skinned by homogenization (J Appl Physiol 39:1052, 1975). Fiber bundles were dissected from the homogenate and one end was attached to a tension transducer with the other end fixed. A load-release cycle was performed by immersing the fiber bundle in solutions to load Ca^{2+} and then to release Ca^{2+} from the SR with 25 mM caffeine, resulting in a tension transient (Pflügers Arch 380:29,1979). The area of the tension transient (TT) was used as an estimate of the amount of Ca^{2+} released from the SR. Three cycles were carried out in each preparation: a control (C1, no HAL or RYA), followed by a test (T, release solution containing 2 mM caffeine + [HAL] + 0.1 μM RYA), and finally a second control (C2). C2/TT was expressed as a percent of C1/TT. C2/TT was not significantly changed when any two of RYA, caffeine, or [HAL] were combined in the test solution. However, when the test solution contained 2 mM caffeine, 0.1 μM RYA, and [HAL], there was a significant decrease in C2/TT. The C2/TT depression was a function of HAL concentrations (65%, 73%, 79%, 95%, and 100% for 0.25%, 0.5%, 1%, 2%, & 3% HAL, respectively). Thus, HAL potentiated the submaximum activation of the SR Ca^{2+} channels by caffeine. It is concluded that HAL may at least partly cause a nonspecific SR Ca^{2+} release which potentiates the caffeine-activated specific SR Ca^{2+} channels containing ryanodine receptors. **(Supported by NIH HL 20754)**

M-Pos75

THE ACTIVATION TIME COURSE OF CALCIUM RELEASE IN FROG SKELETAL MUSCLE FOLLOWS THE FOURTH POWER OF CHARGE MOVEMENT
Bruce Simon and David Hill. Dept. Physiology and Biophysics, UTMB, Galveston, TX 77550

Charge movement and calcium release were measured in frog skeletal muscle at 8° C using the double vaseline gap voltage clamp with 1 mM AP III to monitor Δ[Ca^{2+}]. Fibers were stretched to >3.8 μm/sarcomere to inhibit contraction. The time course of the integral of charge movement (Q(t)) and the rate of SR calcium release (RREL) were calculated for 100 ms duration test pulses to membrane potentials ranging from -30 to +20 mV. Each test pulse was preceded by a 40 ms prepulse to +50 mV to remove the inactivating component of RREL. The time course of the remaining non-inactivating component of RREL was then compared with Q(t) at each test potential. RREL turned on more slowly than Q(t) during the depolarizing step but turned off more rapidly when the fiber was repolarized. However, at each test pulse potential, the time course of RREL during both the on and off steps closely followed $Q^n(t)$ where n ranged from 3 to 4 (7 fibers). Furthermore, if the steady-state Q vs V curve was fit with the equation for a Boltzmann two-state model, RREL vs V could be fit with the same equation raised to the 4th power. These results suggest that SR calcium release is controlled by a voltage sensor in the T-tubular membrane with four identical gating subunits.

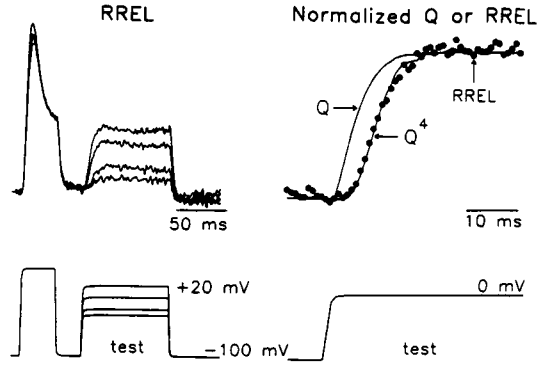

M-Pos76

$[Ca^{2+}]_i$ RELEASE IN GUINEA PIG VENTRICULAR MYOCYTES IS MODULATED BY I_{Ca} AND NOT BY MEMBRANE POTENTIAL.

Joshua I. Goldhaber and James N. Weiss, Division of Cardiology, UCLA School of Medicine, Los Angeles, CA. 90024

In cardiac muscle, transsarcolemmal Ca^{2+} entry is required for release of Ca^{2+} from intracellular stores, but the extent to which membrane voltage may modulate Ca^{2+} release is uncertain. We examined the relationship between I_{Ca} and the amplitude of the $[Ca^{2+}]_i$ transient in patch clamped guinea pig ventricular myocytes loaded with the pentapotassium salt of FURA-2 (0.1 mM). I_{Ca} was modulated by a) varying the test potential during successive 300 msec voltage clamps from a holding potential of -40 mV, or by b) rapidly altering $[Ca^{2+}]_o$ immediately prior to a voltage clamp from -40 mV to 0 mV. The relationship between the size of I_{Ca} and the magnitude of the Ca^{2+} transient (normalized to values obtained during a control voltage clamp from -40 to 0 mV in 1.8 mM $[Ca^{2+}]_o$) was the same (see figure) whether I_{Ca} was modulated by voltage (open circles) or $[Ca^{2+}]_o$ (closed circles). Thus membrane potential did not modulate Ca^{2+} release from intracellular stores independently of its effects on I_{Ca}, consistent with a Ca^{2+}-induced Ca^{2+} release mechanism of excitation-contraction coupling. However our experimental conditions would have minimized a (voltage-dependent) contribution of Na^+-Ca^{2+} exchange to the $[Ca^{2+}]_i$ transient.

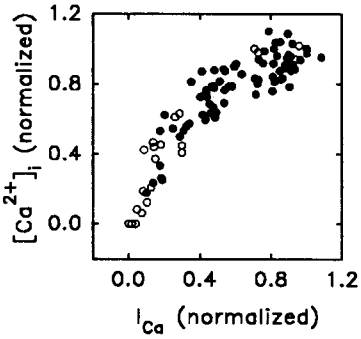

M-Pos77

CALCIUM CURRENT (I_{Ca}) IN DENERVATED SINGLE MAMMALIAN SKELETAL MUSCLE FIBERS. O. Delbono, J. García & E. Stefani. Dept. of Molecular Physiology and Biophysics. Baylor College of Medicine. Houston, Texas.

Denervation of the extensor digitorum longus (edl) muscle of the rat was performed by removing 5-8 mm of the sciatic nerve at the sciatic notch level. Single fibers from the edl muscle were dissected at different denervation stages (4-15 days). We studied the I_{Ca} with the double Vaseline gap technique. At 0 mV the peak I_{Ca} amplitude of normal fibers was: -4.79 ± 0.29 A/F (mean ± sem; n = 51). Within the first 5 days of denervation this value was: -5.96 ± 0.48 A/F (n = 10 fibers, $p < 0.001$); on the day 7: -4.72 ± 0.56 A/F (n = 10, p = 0.34); between the days 8-13: -3.29 ± 0.45 A/F (n = 9, $p < 0.001$); and between days 14-15: -2.87 ± 0.35 A/F (n = 11, $p < 0.001$). The calculated Q_{10} (17-27°C) for the peak I_{Ca} was: 2.47 ± 0.21 (n = 6) and 2.24 ± 0.22 (n = 10, p = 0.24) in normal and at day 14 of denervation, respectively. In innervated fibers the maximum I_{Ca} amplitude was reached at 0 mV (17°C) and at -16 ± 2.45 mV (27°C), while in denervated fibers it was reached at 10 mV (17°C) and at -1.66 ± 2.45 mV (27°C, $p < 0.001$). Nifedipine sensitivity was also tested at the cell level. The action of 1 and 10 μM nifedipine upon the 1-(peak I_{Ca} amplitude/control) relationship was: in control, 0.25 ± 0.022 and 0.74 ± 0.032 (n = 10 fibers); at the 7th day of denervation, 0.27 ± 0.061 and 0.75 ± 0.1 (n = 10); and at the 14th day, 0.24 ± 0.12 and 0.76 ± 0.08 (n = 8). This indicates that the sensitivity to nifedipine was not modified upon denervation.

These data closely parallel the changes in denervated muscle wet weight and relative increase of intracellular Ca^{2+} concentration (Kirby et al., Comp. Biochem. Physiol. 70A:583, 1981). This study may explain the disappearance of the Ca^{2+} action potential (Ca^{2+} AP) caused by denervation and the reappearance of the Ca^{2+} AP by increasing the Ca^{2+} driving force or by blocking the Ca^{2+} activated-K current with apamin, and finally the maintained nifedipine blocking effect upon denervation (Delbono and Kotsias, unpublished). Supported by NIH and MDA.

M-Pos78

IMMUNOGLOBULINS G (IgG) FROM PATIENTS WITH AMYOTROPHIC LATERAL SCLEROSIS (ALS) AFFECT DYHIDROPYRIDINE SENSITIVE CALCIUM CHANNELS OF SKELETAL MUSCLE. O. Delbono, J. García, S. H. Appel & E. Stefani. Dept. of Molecular Physiology and Biophysics and Dept. of Neurology. Baylor College of Medicine. Houston, Texas.

We studied the action of the IgG from ALS and disease control patients on dyhidropyridine-sensitive Ca^{2+} channels. Single fibers were dissected from the extensor digitorum longus muscle of the rat and were voltage-clamped with the double Vaseline gap technique. The control peak I_{Ca} was (mean ± sem): -4.7 ± 0.29 A/F (at 0 mV) and after 40 min incubation in ALS IgG: -2.52 ± 0.04 and the I-V curve was shifted 10 mV toward more positive potentials. The peak I_{Ca} in test IgG/control relationship in normal and disease control was measured. This parameter in normal patients was: 0.97 ± 0.013 (n = 15 fibers), ALS: 0.77 ± 0.013 (n = 25), Myasthenia Gravis: 1.07 ± 0.097 (n = 7), Guillain Barré Syndrome: 0.87 ± 0.04 (n = 5), Multiple Sclerosis: 0.97 ± 0.21 (n = 4), Lambert-Eaton Syndrome: 0.75 ± 0.1 (n = 3, 1 patient) and 0.97 ± 0.08 (n = 3, other patient), Chronic Relapsing Inflammatory Polyneuritis: 0.98 ± 0.13 (n = 4). The charge movement (CM) was reduced in the presence of ALS IgG. Neither the effect on I_{Ca} nor on the CM was verified when the ALS Ig was boiled or adsorbed to muscle tissue overnight. The kinetic studies demonstrated that ALS IgG acts on I_{Ca} modifying the alpha and beta parameters of activation. The effect of ALS IgG and nifedipine was additive. The n parameter of the Hill equation was 1.4 in nifedipine and 1.49 in nifedipine plus ALS IgG.

Since: 1) the action of ALS IgG on I_{Ca} is voltage dependent, 2) ALS IgG affect CM, 3) ALS IgG has an additive interaction with nifedipine on I_{Ca}, we suggest that IgG from ALS patients react with the skeletal muscle DHP sensitive Ca^{2+} channels. These observations suggest that DHP receptors may be an antigenic target for an autoimmune response in ALS. Supported by NIH and MDA.

M-Pos79

BLOCKADE OF CHARGE MOVEMENT FROM SKELETAL MUSCLE BY RYANODINE AND TETRACAINE. J. García, A.J. Avila-Sakar & E. Stefani. Department of Molecular Physiology and Biophysics, Baylor College of Medicine, Houston, Texas.

Charge movement and myoplasmic calcium transients were simultaneously recorded from frog skeletal muscle fibres by using the Vaseline gap technique. Calcium transients were monitored with the fluorescent indicator Rhod-2. The extracellular application of 100 μM ryanodine elicited a temporary initial increase of Q_γ and the calcium transient. Both phenomena were later blocked with the same temporal course and to the same extent. The blockade of Q_γ and the calcium transient was also observed with ryanodine concentrations of 1-10 μM. For membrane potentials positive to -10 mV, the Q_{on} measured was larger in the presence of ryanodine; Q_{off} was not modified. Tetracaine (400-500 μM) blocked a delayed component of Q_{on}, identified as Q_γ, as well as the calcium transient monitored simultaneously. This effect was observed in the first minutes after the addition of tetracaine to the extracellular solution. Tetracaine blocked a faster initial component of Q_{on} for voltages positive to -10 mV, corresponding to the voltage range of activation of the calcium current (I_{Ca}). At these same membrane potentials, Q_{off} was also reduced to a similar extent than the Q_{on}. Ryanodine and tetracaine showed different effects on I_{Ca}. Whereas the slow I_{Ca} was not apparently modified upon the addition of ryanodine, it was completely blocked in the presence of tetracaine. The effects of tetracaine on the charge movement, the calcium transient and the slow I_{Ca} were reversible. These results suggest that ryanodine and tetracaine may act at different sites. Ryanodine exerts its effect on the sarcoplasmic reticulum ryanodine receptor blocking calcium release and Q_γ, while tetracaine at these concentrations may affect the release channel and the dihydropyridine receptor causing a blockade of the charge movement, calcium transient, and I_{Ca}. Furthermore, the experiments with ryanodine indicate that calcium release from the sarcoplasmic reticulum may play a role in the generation of Q_γ. Supported by NIH and MDA.

M-Pos80

LOCALIZED BLOCK OF SARCOPLASMIC RETICULUM Ca^{2+} RELEASE IN SKELETAL MUSCLE FIBERS STAINED WITH AN INDODICARBOCYANINE DYE AND EXPOSED TO LIGHT. Jinhong Fan and S. M. Baylor, Department of Physiology, University of Pennsylvania Medical Center, Philadelphia, PA.

$DiIC_1(5)$ (Molecular Probes, Inc.) is a fluorescent dye previously used in axons as an optical probe of membrane potential (dye 122 of Cohen et al., J. Membr. Biol. 19:1-36, 1974). If a frog single muscle fiber is stained for 1-2 min with 5 μg/ml of this dye and subsequently stimulated by a single action potential, a large fluorescence decrease (ΔF) is normally observed (cf. Oetliker et al., Nature 157:693-696, 1975). Because the time course of ΔF slightly lags that of the myoplasmic Ca^{2+} transient but precedes that of the twitch response, ΔF has been assumed to reflect Ca^{2+} release from the sarcoplasmic reticulum (SR).

We now report that if a region of a $DiIC_1(5)$-stained fiber is focally illuminated for 2-3 min with a narrow bar (e.g. 50 μm width) of 630 nm light oriented transversely to the fiber axis, ΔF is irreversibly reduced in the region of illumination to about 5-15% of normal size; in the immediately-adjacent fiber regions, ΔF is of normal size. Since the exposure to light does not bleach the dye, SR Ca^{2+} release appears to be locally blocked by the combination of dye and light, a conclusion confirmed by the finding that the myoplasmic Ca^{2+} transient (measured with the Ca^{2+}-indicator furaptra) is also greatly reduced in the illuminated fiber region. Since the action potential itself propagates across the region of the block, a step relating T-tubular depolarization to SR Ca^{2+} release appears to be affected. The mechanism of the block may be non-specific and involve "photodynamic damage" (cf. Cohen et al., 1974), since somewhat longer exposures to light (e.g. 8-10 min) can cause macroscopically-visible structural changes at the illumination site. (No such changes, however, are detected for long periods following a 2-3 min exposure to light.) Irrespective of the mechanism of the block, the ability to produce a focal lesion in SR Ca^{2+} release may prove useful in future studies of muscle function. Supported by NIH 17620.

M-Pos81

HEPARIN BLOCKS EXCITATION-CONTRACTION (EC) COUPLING AND TT DEPOLARIZATION-INDUCED SR CA^{2+} RELEASE IN MECHANICALLY SKINNED RABBIT SKELETAL MUSCLE FIBERS. Sue K. Donaldson and Daniel A. Huetteman, University of Minnesota, Minneapolis, MN 55455

Since single mechanically skinned (sarcolemma peeled) skeletal fibers (rabbit adductor magnus muscle) demonstrate transverse tubule (TT) to sarcoplasmic reticulum (SR) coupling stimulated via TT depolarization, their responses were studied in the presence and absence of bath heparin (100μg/ml). Bath constituents equilibrate within the peeled fibers. All experiments were performed on halves of single fibers to allow comparison of paired responses. Procaine (10mM) was used in all bathing solutions, except those for Ca^{2+} loading, to eliminate Ca^{2+}-induced Ca^{2+} release. Heparin is a competitive inhibitor of IP_3 for the IP_3 receptor (IP_3R) in a variety of cell types. Heparin completely blocked the tension transients induced by TT depolarization and by a saturating concentration (1.0μM) IP_3 (polarized TTs). Since heparin blocks both exogenous IP_3 and TT depolarization-induced tension transients, without altering caffeine contractures, its effects appear IP_3R specific and IP_3 is likely to participate in the TT depolarization to SR Ca^{2+} release step of EC coupling. Heparin also significantly reduced net ^{45}Ca release by these same stimuli. Comparison of ^{45}Ca release responses of paired fiber halves (net ^{45}Ca released normalized as a percent of total releasable ^{45}Ca from IP_3 and caffeine stimulation) revealed that heparin blocked IP_3-induced Ca^{2+} release to a greater extent under bathing solution conditions for depolarized TTs, independent of anion/cation composition of the bathing solutions. For paired fiber halves, heparin was a less effective inhibitor of IP_3-induced ^{45}Ca release in the: 1) 66mM Cl^- (4mM K^+) versus the 4mM Cl^- (66mM K^+) bathing solution and 2) 4mM Cl^- following preskinning presoak in 1mM ouabain versus 4mM Cl^- with no ouabain presoak. The heparin block of the TT depolarization-induced $^{45}Ca^{2+}$ release and tension transient may be enabled in this preparation by the method of slow TT depolarization. Supported by USPHS, NIH grant (AR 35132).

M-Pos82

INHIBITORY AND EXCITATORY GTPγS EFFECTS IN MECHANICALLY SKINNED RABBIT SKELETAL MUSCLE FIBERS. Lisa Carney and Sue K. Donaldson. University of Minnesota, Minneapolis, MN 55455

G proteins in skeletal muscle transverse tubules (TTs) might be involved in the skeletal muscle excitation-contraction coupling mechanism working through IP_3 (DiVirglio et al., 1986, EMBO J. 5:239) or the DHP receptor (DHPR) (Somasundaram et al., 1990, J. Physiol. (Lond.) 427:55P). The effects of GTPγS, a G protein activator, were studied in single mechanically skinned (sarcolemma peeled) fibers. In this preparation, sealed TTs can be polarized or depolarized; TT depolarization causes a tension transient due to Ca^{2+} release from the sarcoplasmic reticulum (Donaldson, 1985, J. Gen. Physiol. 86:501). GTPγS (200μM) and GDPβS (500μM), a G protein inhibitor, were added to the peeled fiber bath. The polarization state of the TTs in the peeled fibers did not influence the excitatory effects of GTPγS. GTPγS elicited tension transients independent of TT polarity or a preceding depolarization-induced tension transient. The GTPγS excitatory responses were blocked by prior application of GDPβS, suggesting G protein site of action. Preliminary data demonstrate that GTPγS responses are not prevented by a use-dependent D600 (10μM) block of TT depolarization-induced tension transients. Thus the GTPγS-G protein excitatory mechanism is unlikely to involve the DHP receptor, either as the putative voltage sensor or as a TT Ca^{2+} channel. In addition to acting as a separate Ca^{2+} release stimulus, GTPγS enhanced the depolarization-induced tension transient, possibly through effects on DHPR (Gamboa-Aldeco et al., 1989, Biophys. J. 55:91A). The pattern of fiber responses to GTPγS was either excitatory or inhibitory. When GTPγS induced a tension transient in the TT polarized state, the subsequent depolarization-induced tension transient was unaltered or enhanced. If GTPγS was non-excitatory in the TT polarized state, the subsequent TT depolarization-induced response was inhibited. This suggests that excitatory and inhibitory G proteins may mediate GTPγS activation in skeletal muscle fibers. Supported by USPHS, NIH (AR 35132).

M-Pos83

INOSITOL 1,4,5-TRISPHOSPHATE PHOSPHATASE ACTIVITY IN MEMBRANES ISOLATED FROM AMPHIBIAN SKELETAL MUSCLE. Cecilia Hidalgo, Ximena Sánchez, M. Angélica Carrasco and Julio Vergara[1]. Centro de Estudios Científicos de Santiago and Dept. Fisiol. Biofís., Fac. Med., U. de Chile, Casilla 70055, Santiago, Chile. [1]Dept. Physiol. and Jerry Lewis Neuromuscular Res. Ctr, Sch. Med., U.C.L.A. Los Angeles, CA 90024, USA.

In analogy to its function in other cell systems, where inositol 1,4,5-trisphosphate (IP3) plays a role as intracellular messenger coupling external stimuli to calcium release from non-mitochondrial stores, IP3 has been postulated as a chemical messenger linking transverse-tubule (T-T) depolarization to calcium release from sarcoplasmic reticulum (SR). According to this hypothesis, relaxation of skeletal muscle is dependent on an IP3 phosphatase (IP3-ase) that would remove the IP3 released by electrical stimulation. In this work, we compared the rates of hydrolysis of IP3 in a soluble fraction and in purified T-T and SR membranes isolated from frog skeletal muscle. We found that T-T membranes displayed rates of hydrolysis several-fold higher than those of SR and soluble fraction; the activity of SR was so low that it might reflect residual contamination with T-T membranes. The T-T enzyme had an absolute requirement for Mg, was completely inhibited by 0.1 mM CdCl2, and had Km and Vmax of 25.2 uM and 44.1 nmol per mg per min, respectively. These results agree with those reported by Milani et al [1] who found both membrane bound and soluble IP3-ase activity in rabbit skeletal muscle, with the highest specific activity in a microsomal fraction enriched in T-T membranes. However, in contrast to their findings [1], we found that T-T membranes sequentially hydrolyzed IP3 to inositol bisphosphate, inositol 1-phosphate and inositol, indicating that T-T membranes have inositol bis and monophosphatases as well as IP3-ase. These results indicate that skeletal muscle has significant IP3-ase activity, and that this enzyme is predominantly localized in the T-T system. The IP3-ase activity may be directly involved in the mechanism of relaxation since it is high enough to account for the physiological relaxation rates. Supported by NIH GM-35981, by FONDECYT 972-88 and by DTI.

[1] Milani, D., Volpe, P. and Pozzan, T. (1988) Biochem. J. 254, 525-529.

M-Pos84

INOSITOL 1,4,5 TRISPHOSPHATE AND ALTERATIONS IN THE CONTRACTILITY OF THE PERFUSED RAT DIAPHRAGM. RC Kolbeck, N Guo, B Brown, S Sloop, J Ginsburg, & TM Nosek. Biophysics Research Group, Medical College of Georgia, Augusta, Georgia 30912.

Alterations in diaphragmatic contractile force are thought to be related to changes in the concentrations of a variety of intracellular agents, including Ins(1,4,5)P3. Isolated-perfused, contracting rat diaphragms were subjected to short term hypoxia (15 min without oxygen), ischemia (5 min without perfusion), and to fatiguing interventions, after which they were freeze-clamped and analyzed for Ins(1,4,5)P3. While hypoxia and ischemia caused significant diminishments in diaphragmatic contractility (38.5% and 17.0% of control, respectively), decreases in tissues levels of Ins(1,4,5)P3 were observed only in those diaphragms subjected to ischemia (a diminishment of 36.0%, n=8). Five min of low frequency fatiguing stimulation (20 Hz train-pulsing with a frequency of 1.5 Hz and a 50% duty cycle) caused diaphragmatic tension development to drop to 72.5% of control but did not alter Ins(1,4,5)P3 levels (n=32). Five min of high frequency fatiguing stimulation (80 Hz train-pulsing at a frequency of 2 Hz and a 20% duty cycle), on the other hand, caused a significant decrease in Ins(1,4,5)P3 levels by 39.0% (n=15). While the role of Ins(1,4,5)P3 in the EC coupling process of striated muscle remains poorly defined, our study indicates that it may be involved in the maintenance of diaphragmatic contractility. As we have shown previously, Ins(1,4,5)P3 may serve to increase the sensitivity of the contractile apparatus to calcium. (This work supported by Grants from the American Lung Assoc, Ga Affiliate; and NIH #HL/AR 37022)

M-Pos85

PERCHLORATE CAUSES CONVERSION OF Qβ INTO Qγ IN SKELETAL MUSCLE. A. González, I. Stavrovsky and E. Ríos. Rush University, Chicago, IL.

We extend results of Lüttgau et al. (Biophys. J. 43, 1983) and others on the potentiation of skeletal muscle EC coupling by ClO_4^-. In 6 frog twitch fibers voltage clamped in a 2-Vaseline gap, ClO_4^- (8mM) shifted to the left the distribution Q(V) of mobile charge and the threshold for Ca release measured optically. The central voltage V_T of a Boltzmann fitted to Q(V) was shifted by -23 mV (s.e.m.=2.4 mV). A visible hump (Iγ) and a high steepness region in the Q(V) appeared in ClO_4^- at potentials that elicited neither release nor Iγ in reference. The steepness parameter K of the Boltzmann fit, went from 10.1 mV (ref.) to 5.8 mV (ClO_4^-); the difference was significant. Capacitance in controls did not change.

A hump component in the charge movement current and a high steepness region in the Q(V) curve define charge movement of the γ type. Therefore ClO_4^- increased Qγ as judged by both criteria.

The maximum charge Q_{max}, however, did not change; it was 18 nC/μF (2.9) in reference and 18 nC/μF in ClO_4^-. One way of describing this increase of Qγ without change in Q_{max} is as a conversion of Qβ into Qγ.

ClO_4^- did not have these effects in fibers depleted of Ca^{2+} in the SR by repeated pulsing in high internal [EGTA]. This indicates that Ca release is necessary for these effects.

According to Csernoch et al. (Biophys. J. 1989; Pizarro et al., this meeting), Iγ arises as a consequence of Ca^{2+} release, as Ca^{2+} binds near the internal face of the voltage sensors of EC coupling. This model readily explains the present observations: ClO_4^- allows Ca^{2+} to be released at voltages that are subthreshold in reference; thus, the process of activation of Iγ occurs at lower voltages. As fewer sensors undergo the transition as Iβ at these voltages, more are available for delayed movement and Iγ is greater. Since Iβ and Iγ originate in the same population of voltage sensors, Q_{max} does not change.

In this view it is not necessary to invoke a primary agonist effect of ClO_4^- on the voltage sensors. It seems that only voltage sensors coupled to functional, releasing SR channels, are affected by ClO_4^-. The primary target of ClO_4^- could either be the release channel or a coupled voltage sensor–release channel complex (cf. Ríos et al., this meeting). Supported by NIH, AHA and MDA.

M-Pos86

MODELING Qγ AND POSITIVE FEEDBACK IN EC COUPLING OF SKELETAL MUSCLE. G. Pizarro‡, L. Csernoch* and E. Ríos. Rush University, Chicago, IL, ‡Univeristy of Montevideo and *University of Maryland.

We simulated quantitatively and compared with experimental results a probable mechanism of generation of the hump or Iγ component of intramembrane charge movement. In the model (Csernoch et al. Biophys. J. 1989) Iγ is a consequence of Ca^{2+} release: $[Ca^{2+}]_i$ increases upon release, and Ca^{2+} binds to sites on the myoplasmic face of the voltage sensors of EC coupling.

Charge movements and Ca release flux R(t) were derived from simultaneous measurements in frog skeletal fibers. The time course of myoplasmic $[Ca^{2+}]$ near the sensors was derived from R(t) by modeling diffusion, and used to compute Ca^{2+} binding and the consequent increase in local surface potential. This increase, operating on an ensemble of two-state voltage sensors, caused a hump-like charge movement. The model simulates well the recorded currents, provided that the rate constants of the population of sensors are $\simeq$ 3-fold faster than exponential rates measured by Hollingworth and Marshall (J.Physiol.321, 1981). This difference is explicable if the charging of the membrane is slowed by series resistance in the T tubules (Lamb, J. Physiol.376, 1986).

A second, more complete model includes positive feedback: Iγ is due to movement of more voltage sensors of EC coupling and results in opening of more release channels. The complete simulation with feedback starts from an applied pulse and computes the initial charge movement in an ensemble of sensors (Iβ). Ca release flux is computed assuming a simple transfer function between movement of sensors and opening of Ca release channels. The consequent increase in local $[Ca^{2+}]_i$ is calculated and used to generate Iγ, which in turn causes more channel opening. Inactivation of release by $[Ca^{2+}]_i$ (Schneider & Simon, J. Physiol. 1988) is included in the model and determines the decay after the peak in the release waveform.

This model successfully accounts for four observations: 1) the steepness of R *vs.* V is greatest at potentials near threshold, where Iγ is most prominent; 2) the decay after the peak of R(t) and 3) the reduction of R(t) by a conditioning pulse of fixed potential are maximum at test potentials near threshold; 4) perchlorate causes conversion of Qβ into Qγ (González et al., this meeting).

M-Pos87

EVIDENCE FOR A 30S RYANODINE RECEPTOR - Ca^{2+} RELEASE CHANNEL COMPLEX IN STOMACH SMOOTH MUSCLE OF TOAD. Le Xu, F. Anthony Lai, Elaine Etter*, Fredric S. Fay* and Gerhard Meissner. University of North Carolina, Chapel Hill, NC 27599, and *University of Massachusetts Medical Center, Worcester, MA 01605.

The ryanodine receptor - Ca^{2+} release channel complex of striated muscle sarcoplasmic reticulum has been purified as a homotetrameric 30S protein complex of M_r ~560,000 polypeptides. We now report that crude microsomal membranes prepared from the stomach muscle of toad *Bufo marinus* also bind [^{3}H]ryanodine with high affinity (K_D = 2 nM), although with a lower concentration than rabbit skeletal or canine cardiac crude microsomes (~0.3 vs. 5-10 pmol/mg protein). Toad membranes were solubilized with Chaps and a 30S ryanodine receptor protein fraction was obtained on sucrose gradients (Lai *et al.*, *Nature* 331, 335). SDS PAGE indicated the specific comigration of a high molecular weight polypeptide with the 30S receptor peak, which had a mobility similar to the cardiac ryanodine receptor. The 30S fraction, upon reconstitution into planar lipid bilayers, displayed a main single channel conductance (830 pS with 250 mM K^+ as the permeant ion) with a pharmacology similar to the skeletal and cardiac muscle Ca^{2+} release channels. The toad smooth muscle channel was activated by μM Ca^{2+}, mM ATP, inhibited by μM ruthenium red, and modified by ryanodine. Occasionally, a Ca^{2+}- and IP_3-activated channel was observed which could be inhibited by mM heparin. These results suggest that, in single channel recordings, a high-conductance channel from toad smooth muscle is sensitive to activation by Ca^{2+} and IP_3, and inhibition by ruthenium red and heparin. Supported by USPHS and MDA grants.

M-Pos88

IONIC CURRENTS IN A HUMAN SKELETAL MUSCLE CELL LINE. J. Hidalgo, K. Everett, R. Caviedes and E. Jaimovich. Dpto. Fisiología y Bioffsica, Universidad de Chile, Casilla 70005, Santiago, Chile and C.E.C.S.

We are in the process of characterizing the ionic conductances in a skeletal muscle cell line of human origin.
Using the whole-cell variation of the patch-clamp technique we have recorded macroscopic currents resulting from voltage clamp pulse protocols whith normal Ringer's solution in the bath and using either potassium or cesium as the major cationic component in the recording pipette.

With potassium in the pipette, outward currents are recorded. In some cells we find that these currents show a biphasic time course at strong depolarizing test pulses which could be attributed to either inactivation or blockade of a subclass of potassium channels.

With cesium in the pipette, we see net inward currents with no apparent inactivation. We believe this inward current to be primarily carried by calcium ions, supported by 2 observations. Firstly, the addition of 1 mM $BaCl_2$ to the bathing medium increases the current amplitude and secondly, a tail current present in the control situation is strongly diminished. The latter finding also suggests that the tail current is a conductance activated by the inward going calcium ions but not by barium. The absence of fast inactivating inward currents may reflect a degree of de-differentiation at which these cells are placed by the transformation procedure or continuous culture.

As these cells are capable of fusing into myotubes and of expressing differentiated markers, they appear as a good model for the study of ionic conductances expressed at different stages of differentiation.

Supported by:NIH GM35981, FONDECYT 896 and MDA.